Cenozoic mountain building and topographic evolution in Western Europe: impact of billion years lithosphere evolution and plate tectonics

Frederic Mouthereau, Paul Angrand, Anthony Jourdon, Sébastien Ternois, Charlotte Fillon, Sylvain Calassou, Sébastien Chevrot, Mary Ford, Laurent Jolivet, Gianreto Manatschal, et al.

BSGF - Earth Sciences Bulletin 2021, 192, 56

https://doi.org/10.1051/bsgf/2021040

BSGF Earth Sciences Bulletin

Available online at: www.bsgf.fr

Special Issue Orogen lifecycle: learnings and perspectives from Pyrenees, Western Mediterranean and analogues ed. O. Lacombe, S. Tavani, A. Teixell, D. Pedreira and S. Calassou (Guest editors)

OPEN ACCESS

Cenozoic mountain building and topographic evolution in Western Europe: impact of billions of years of lithosphere evolution and plate kinematics

Frédéric Mouthereau[1], Paul Angrand[1], Anthony Jourdon[2], Sébastien Ternois[3], Charlotte Fillon[2], Sylvain Calassou[2], Sébastien Chevrot[1], Mary Ford[4,*], Laurent Jolivet[5], Gianreto Manatschal[6], Emmanuel Masini[7], Isabelle Thinon[8], Olivier Vidal[9] and Thierry Baudin[8]

[1] GET-OMP, UMR 5563, Université Paul Sabatier, Toulouse, France
[2] Total EP, R&D Nexts, Avenue Larribau, 64018 Pau, France
[3] ISTO, Université d'Orléans, CNRS, 45000 Orléans, France
[4] CRPG, Université de Lorraine, Nancy, France
[5] Sorbonne Université, UMR 7193 CNRS-UPMC, Institut des Sciences de la Terre Paris, F-75005 Paris, France
[6] IPGS, EOST, Université de Strasbourg, Strasbourg, France
[7] M&U SAS, 3 Rue des Abattoirs, 38120 Saint-Egrève, France
[8] BRGM, GeoResources Division, Orléans, France
[9] ISTERRE, Université Grenoble Alpes, CNRS, Grenoble, France

Received: 21 May 2021 / Accepted: 24 September 2021 / Publishing online: 15 November 2021

Abstract – The architecture and tectono-magmatic evolution of the lithosphere of Europe are the result of a succession of subduction, rifting and inputs from plumes that have modified the lithospheric mantle since the Neoproterozoic (750–500 Ma). These events gave birth to contrasting crust-mantle and lithosphere-asthenosphere mechanical coupling between strong, viscous, thick, cold, depleted mantle of the Archean lithosphere of the West African Craton and the East European Craton, and the weak, low viscous, thin, hot and less depleted mantle of the Phanerozoic lithosphere of Central Europe. These differences were long-lived and explain the first-order present-day stresses and topography as well as the styles of orogenic deformation. The lack of thermal relaxation needed to maintain rheological contrasts over several hundreds of millions of years requires high mantle heat flux below Central Europe since at least the last 300 Ma. A combination of edge-driven convection on craton margins and asthenospheric flow triggered by rift propagation during the Atlantic and Tethys rifting is suggested to be the main source of heat. The topography of Central Europe remained in part dynamically supported during most of the Mesozoic thinning in line with the long-term stability of thermal-mechanical structure of the lithosphere. Timing and rates of exhumation recorded across Western Europe during convergence indicate that an additional control by the architecture of Mesozoic rifted margins is required. By 50 Ma the acceleration of orogenic exhumation, from the High Atlas to the Pyrenees, occurred synchronously with the onset of extension and magmatism in the West European Rift. Extension marks the onset of distinct orogenic evolution between Western Europe (Iberia) and the Alps (Adria) in the east, heralding the opening of the Western Mediterranean. A major kinematic re-organisation occurred triggering the involvement of more buoyant and thicker portions of rifted margins resulting in widespread orogenic growth. We conclude that conceptual models of collision require to better account for the thermo-magmatic evolution of the continental lithosphere, especially the original architecture and composition of its mantle, as well as the precise knowledge of the architecture of the rifted margins to explain the timing and rates of orogenic topography.

Keywords: lithosphere / topography / continent / mantle / geodynamics

*Corresponding author: frederic.mouthereau@get.omp.eu

Résumé – Construction orogénique et évolution topographique de l'Europe de l'Ouest au Cénozoïque : impact de l'évolution de la lithosphère sur des milliards d'années et de la cinématique des plaques. L'architecture et l'évolution tectono-magmatique de la lithosphère européenne sont le résultat d'une succession de périodes de subduction, d'amincissement et de la contribution de panaches mantelliques qui ont modifié le manteau lithosphérique depuis le Néoprotérozoïque (750–500 Ma). Ces événements ont donné naissance à des couplages mécaniques croûte-manteau et lithosphère-asthénosphère très différents entre le manteau résistant, très visqueux, épais, froid et appauvri de la lithosphère archéenne du craton ouest-africain et du craton est-européen, et le manteau faible, faiblement visqueux, mince, chaud et moins appauvri de la lithosphère phanérozoïque de l'Europe centrale. Ces différences qui ont persisté depuis reproduisent au premier ordre bien les contraintes et la topographie actuelles, ainsi que les styles de déformation orogénique. L'absence de relaxation thermique nécessaire au maintien des contrastes rhéologiques pendant plusieurs centaines de millions d'années nécessite un flux de chaleur mantélique élevé sous l'Europe centrale depuis au moins les 300 derniers Ma. Nous suggérons que le principal moteur soit la combinaison de la convection sur les bords des cratons et d'un flux asthénosphérique déclenché par l'ouverture de l'Atlantique et de la Téthys. La topographie de l'Europe centrale est restée en partie soutenue dynamiquement pendant la majeure partie de l'amincissement mésozoïque, en accord avec à la stabilité de la structure thermo-mécanique de la lithosphère. La chronologie et les taux d'exhumation enregistrés en Europe occidentale pendant la convergence indiquent qu'un contrôle supplémentaire par l'architecture des marges continentales mésozoïques est nécessaire. Vers 50 Ma, l'accélération de l'exhumation orogénique, du Haut Atlas aux Pyrénées, s'est produite de façon synchrone avec le début de l'extension et du magmatisme dans le rift ouest-européen. L'extension marque le début d'une évolution orogénique distincte entre l'Europe occidentale (Ibérie) et les Alpes (Adria) à l'est, annonçant l'ouverture de la Méditerranée occidentale. Une réorganisation cinématique majeure s'est produite, déclenchant l'implication de parties moins denses et plus épaisses des marges riftées, ce qui a entraîné une croissance orogénique généralisée. Nous concluons que les modèles conceptuels de collision doivent davantage tenir compte de l'évolution thermo-magmatique de la lithosphère continentale, en particulier de l'architecture et de la composition initiale de son manteau, ainsi que de la connaissance précise de l'architecture des marges continentales pour expliquer la chronologie et la vitesse de construction de la topographie orogénique.

Mots clés : lithosphère / topographie / continent / manteau / géodynamique

1 Introduction: inherited lithosphere properties or convection control on collisional orogeny?

Continental collision is seen as the tectonic process that occurs at convergent boundaries by the accretion of continental rocks, after the suturing of an ocean, and detachment from the underlying lithospheric levels. Collision zones form broad regions of continental deformation, which surface expression shapes the collisional orogenic systems (Dewey *et al.*, 1973; Molnar, 1988). Collision occupies a peculiar place in plate tectonics (Wilson, 1966; Morgan, 1968; Le Pichon, 1968) as diffuse zone of plate convergence that weakly applies to rigid plate approximation (Gordon, 1998). Although closely related during plate convergence, continental collision does not equal subduction that is defined by the loss of lithospheric materials into the asthenosphere and localized strain across the narrow plate interface. End-member types of collisional orogens can be defined based on the magnitudes of crustal thickening (*e.g.*, Alps and Pyrenees *versus* Himalayas and Andes). But there is no consensus as to whether these differences reflect the mechanical properties of the continental plates (strong *vs.* weak lithospheres; Mouthereau *et al.*, 2013) or the scale and type of mantle flow (large-scale/symmetric flow *vs.* small-scale/asymmetric flow) (Faccenna *et al.*, 2013a). In this respect, collision zones with small asymmetric mountain belts like the Alps or the Pyrenees, transiently evolving into subduction orogens in the Mediterranean region (Jolivet, 2003; Jolivet *et al.*, 2008; Royden and Faccenna, 2018) can reveal the deformation of weak continental lithospheres, accommodating convergence by distributed strain, or slab-pull type orogens (retreating subduction zones) related to small scale convection cells.

Despite obvious differences between collision zones they share a common element, the continental lithosphere. Due to its long-lasting tectono-magmatic evolution (> 1–0.5 Gyr), the continental lithosphere is buoyant, strongly anisotropic, both mechanically and compositionally, and structurally complex compared to the oceanic lithosphere. But these parameters, especially their interactions, are ill-defined in most orogenic belts.

Progress in modelling coupling processes between lithosphere dynamics and deep mantle flow have demonstrated that first-order indicators of plate tectonics, such as present-day surface motions, nature and magnitude of strain rates and deviatoric stresses, are best reproduced if lithospheric body forces (gravitational potential energy, GPE) arising from regional variations in topography, crustal and lithosphere thickness and upper mantle density are coupled with mantle flow (Ghosh *et al.*, 2013). It is therefore expected that the mechanical anisotropy represented by long-lived weakness and composition of the lithosphere at cratonic margins play a dominant role on orogenic deformation (Audet and Bürgmann, 2011; Mouthereau *et al.*, 2013), in addition to whole mantle conveyor belts and smaller scale slab-induced mantle flow (Faccenna and Becker, 2010; Becker and Faccenna, 2011).

The evolution of strain distribution, uplift and exhumation during mountain building should therefore theoretically reveal the first-order relationships between structure and inherited properties of the continents (*e.g.*, density, temperature, thickness and anisotropy), mantle convection and the

dynamics of subducted slabs. To best examine these relationships it is required to target collision domains that have well preserved the geological record of pre-convergence evolution. Only these domains can well resolve the impact of long-lasting thermal, tectonic and magmatic events on the rheology and architecture in collision zones. Here, we examine the case of Western Europe that is shaped by numerous orogenic segments of variable elevation made of Paleozoic Massifs, Mesozoic and Cenozoic Foreland and Rift Basins, bounded by low topography provinces of the Baltica and Africa shields (Figs. 1 and 2). The topographic and tectonic patterns appear to mirror the contrasting tectono-magmatic evolution between the Archean cratons and the Proterozoic and Paleozoic orogenic belts (Pan-African, Variscan and Caledonian orogenies) (Fig. 1). It has also been recently suggested from reconstructions of Iberia in the Western Mediterranean region (*e.g.*, Angrand and Mouthereau, 2021) and evidence for amagmatic closure in the Pyrenees and the Alps (McCarthy *et al.*, 2020) that the Alpine Tethys, which closed between Europe and Africa, was formed by rift basins overlying a strongly thinned continental lithosphere, including narrow oceanic basins instead of a single large oceanic domain.

Pioneering seismic surveys in the 90's imaged the deep crustal structure of Europe. Combined with numerical modelling, surface data have permitted linking topography and lithosphere strength with the tectonic evolution of sedimentary basins (Ziegler *et al.*, 1995, 1998; Cloetingh and Ziegler, 2007). Among regional studies, the tectonic reorganisation of the Alpine/Mediterranean region caused by Late Cenozoic slab retreat has received much attention (Jolivet and Faccenna, 2000; Faccenna *et al.*, 2001, 2014). The integration of regional and global seismic tomography with geodynamic models of lithospheric deformation have provided clues on the role of subducted slabs relative to large mantle convection on topography (Faccenna and Becker, 2010) as well as the role of absolute plate motions relative to slab dynamics on crustal deformation (Spakman *et al.*, 2018).

In comparison, although there is also an extensive body of studies on the long-term geological, geochronological and geochemical evolution of the continental crust and mantle, yet this knowledge is not exploited to resolve the temporal and spatial evolution of collisional orogeny. Improving our understanding of how properties of a continent interplay in time and space with kinematic boundary conditions to build mountain ranges was one of the main goal of the OROGEN project. This manuscript is intended to provide a review of the data and concepts on the rheology, tectono-magmatic and topographic evolution of Europe based in part on the results from the OROGEN project. It is organized in five main sections that can be read as independent analyses that together form a coherent ensemble to support our model.

In Section 2, we present the lithosphere architecture and topographic patterns of the Africa-Europe plate boundary based on geophysical constraints. In this part we make the link between the age of the lithosphere, its mechanical properties and composition of the mantle, and the topography. In Section 3, we review the long-term magmatic evolution of the European continental lithosphere through the exploitation of Re-Os and Sm-Nd depletion events. This provides us with constraints to examine further the relationships between the melting ages of the mantle and the overlying crust. This part is aimed to provide the necessary database for understanding the geodynamic processes that have modified the original structure and rheology of the cratons to build the lithosphere of Europe. Combined with geophysical constraints on the lithosphere-asthenosphere boundary (LAB) depth we establish a geological model for the architecture of the lithosphere and age-dependent composition of the mantle. This is done along a 4000 km-long transect stretching between the West African and East-European cratons. In Section 4, we analyze a large and relevant thermochronological dataset to infer spatial and temporal evolution of the Cenozoic orogenic topography. The results are then used to discuss the relationships between the formation of the orogenic topography and the tectonic and magmatic history of the lithosphere. The Section 5 aims to investigate the far-field drivers of plate motions based on a synthesis of the kinematic evolution of Africa-Europe convergence. In Section 6, we summarize the main results and present a dynamic model of the topographic evolution of Western Europe accounting for long-term interactions between lithosphere properties and plate kinematics.

2 Lithosphere and topography of Western Europe: fingerprints of long-term tectonic and thermal evolution?

2.1 Geophysical fingerprints of lithospheric evolution

The evolution of the continental lithosphere can be described by the variations of tectono-thermal or thermo-tectonic ages, which are known to be well correlated with the strength (or effective elastic thickness of the lithosphere, Te) of continents (Burov and Diament, 1995; Artemieva and Mooney, 2001; Mouthereau *et al.*, 2013). They are defined by the timing of the last main tectonic or magmatic events resetting the lithosphere both thermally and compositionally. In Europe and north Africa, the oldest lithospheres are represented by Archean to Early Neoproterozoic basement exposed in the regions of the East-European Craton (EEC) of Scandinavia, and the Western African Craton (WAC), south of Atlas mountains (Fig. 1). Stretching between the cratonic domains, the central part of Europe has recorded deformation, metamorphism or partial melting during the Caledonian and Variscan orogenies. This newly formed Paleozoic basement was then partially overprinted by deformation and magmatism during the subsequent Mesozoic rifting stages and Cenozoic plate convergence.

The spatial resolution of seismic tomographic imaging of the deep structure of Europe lithosphere has improved in the recent years with a special attention given to resolve 1) the geometry of high-velocity anomalies of the Mediterranean slabs (Spakman, 1990; Bijwaard *et al.*, 1998; Piromallo and Morelli, 2003; Spakman and Wortel, 2004; Meer *et al.*, 2018; El-Sharkawy *et al.*, 2020) and 2) temperature variations in the shallow continental mantle below geothermal fields of the Cenozoic Magmatic Province of Europe (Goes *et al.*, 2000; Heuer *et al.*, 2006; Geissler *et al.*, 2010; Legendre *et al.*, 2012; Meier *et al.*, 2016). We present below some of the main seismic and thermal-mechanical properties the European continental lithosphere inferred from those recent geophysical models.

Crustal thickness and depth of the Lithosphere-Asthenosphere Boundary (LAB) of Figures 2a and 2b are derived from

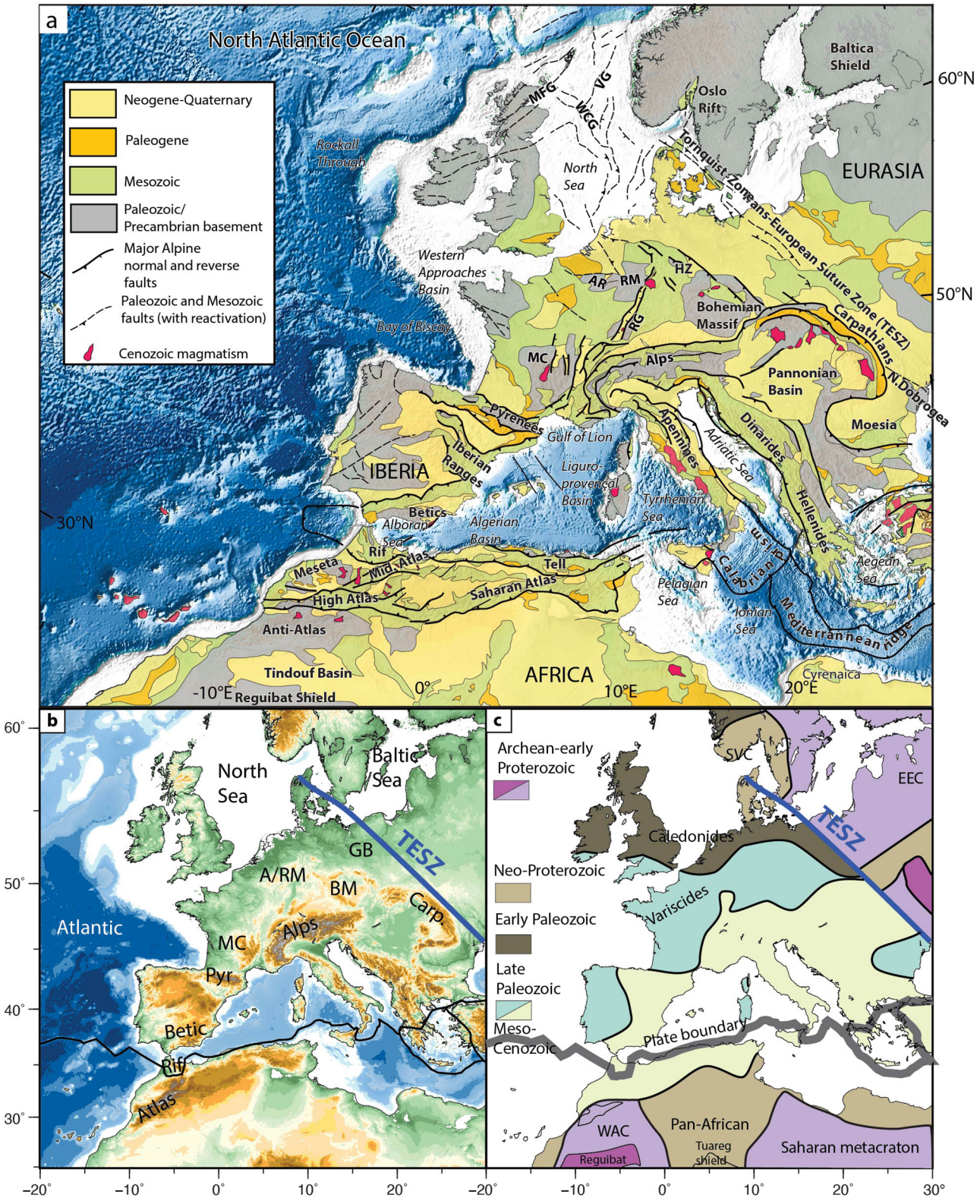

Fig. 1. Geology and basement structure of Europe. (a) Main Alpine tectonic elements and synthetic geology of Europe, redrawn after the 1:5 Million International Geological Map of Europe (CCGM). (a) Present-day topography and main geotectonic features of western Europe (A/RM: Ardennes/Rhenish Massif; GB: German Basin; BM: Bohemian Massif; MC: Massif Central; Carp.: Carpathian Mountains; Pyr.: Pyrenees). (b) Ages of the continental lithosphere defined by timing of the last main tectono-magmatic event. We also mapped within the so-called East European Craton (EEC) and Western African Craton (WAC), Neo-Proterozoic Belts, including the Sveconorwegian abbreviated SVC (1 Ga) and Pan-African (0.6 Ga) orogenies (Ennih and Liégeois, 2008; Artemieva and Meissner, 2012; Liégeois *et al.*, 2013).

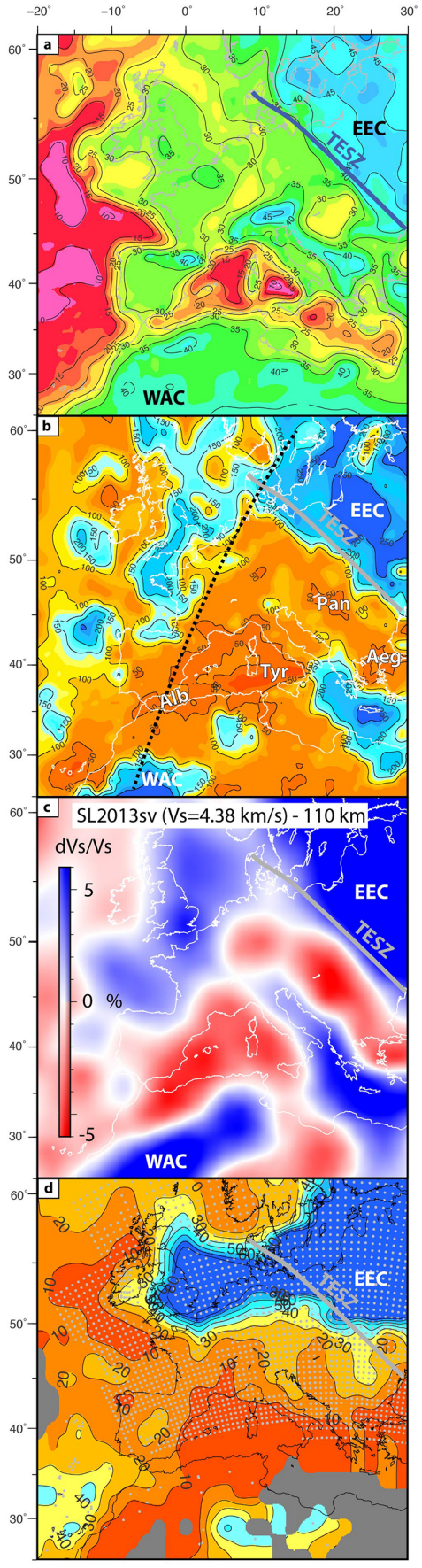

regional EPcrust model (Molinari and Morelli, 2011) and LITHO1.0 model based on global surface wave dispersion (Pasyanos *et al.*, 2014). LAB variations show a pattern that is generally consistent with the trend of lithosphere ages. Archean to early and Neoproterozoic lithosphere (Fig. 1c) is associated with lithosphere thickness above 200 km (Fig. 2b) and thick crust of 40–45 km (Fig. 2a) in the range of crustal roots of Cenozoic mobile belts like the Alps, Dinarides, Pyrenees, or the Atlas. The lithosphere thickness model of EEC inferred from LITHO1.0 is consistent with estimates based on regional surface-wave tomography (Meier *et al.*, 2016) and global models that assumed a direct correspondence between seismic tomography and temperature (Priestley and McKenzie, 2013; Steinberger and Becker, 2016; Hoggard *et al.*, 2020), or other models using joint inversion of multiple data sets (Afonso *et al.*, 2019).

South of the Hellenic trench (Ionian and Herodotus Basins) the LAB is remarkably deep, revealing an apparent lithosphere thickness up to 250 km, which is difficult to reconcile with a thermally-relaxed oceanic lithosphere. Subduction of the Tethys remnant in this domain potentially introduces biases, hence overestimating the LAB depth. Nevertheless, this domain characterized by high Vs anomalies (Fig. 2c) appears to extend below Adria, indicating a colder or/and depleted uppermost mantle and possibly more viscous sub-continental lithospheric mantle (SCLM) in agreement with the role of indenter played by Adria. The expected higher strength of Adria is however not reflected in Te values (Fig. 2d). The younger Phanerozoic lithosphere of central and southern Europe is much thinner, typically below 150 km, and has been thermally eroded, partly delaminated or mobilized during Paleozoic and Cenozoic orogenic evolution.

Differences between cratonic (*e.g.*, EEC and WAC) and Phanerozoic lithospheres are known to reflect different degrees of depletion of the SCLM in incompatible elements and associated minerals (clinopyroxene, garnet), which is particularly important below craton because of the high degree of magmatic extraction (Poudjom Djomani *et al.*, 2001; Carlson *et al.*, 2005; Lee *et al.*, 2011). Depletion of mantle lithosphere below cratons explains their buoyancy. They are also strong as indicated by high effective elastic thickness of the EEC (Te > 80 km in Fig. 2d) and cold, explaining the relatively higher shear velocities of EEC in Figure 2c. By contrast, the Phanerozoic lithosphere has denser SCLM due to

Fig. 2. Deep structure of the continental lithosphere of Europe. (a) Moho depth after EPcrust model (Molinari and Morelli, 2011). (b) Seismic lithosphere thickness (also LAB Lithosphere-Asthenosphere Boundary) after global model LITHO1.0 (Pasyanos *et al.*, 2014). Dashed black line depict location of profile shown in Figure 3. Alb: Alboran Basin; Aeg: Aegean Basin; Tyr: Tyrrhenian Basin; Pan: Pannonian Basin. (c) S-wave velocity anomalies at 110 km for velocities of reference Vs = 4.38 km/s after global Vs model SL2013sv obtained from inversion of surface and S-wave forms (Schaeffer and Lebedev, 2013). (d) Effective elastic thickness (Te) in km as obtained from combination of spectral admittance and coherence between Bouguer gravity anomaly data and forward modelling of the gravity anomalies and the present-day topography/bathymetry (Mouthereau *et al.*, 2013). Data points used in the model are indicated as small grey dots.

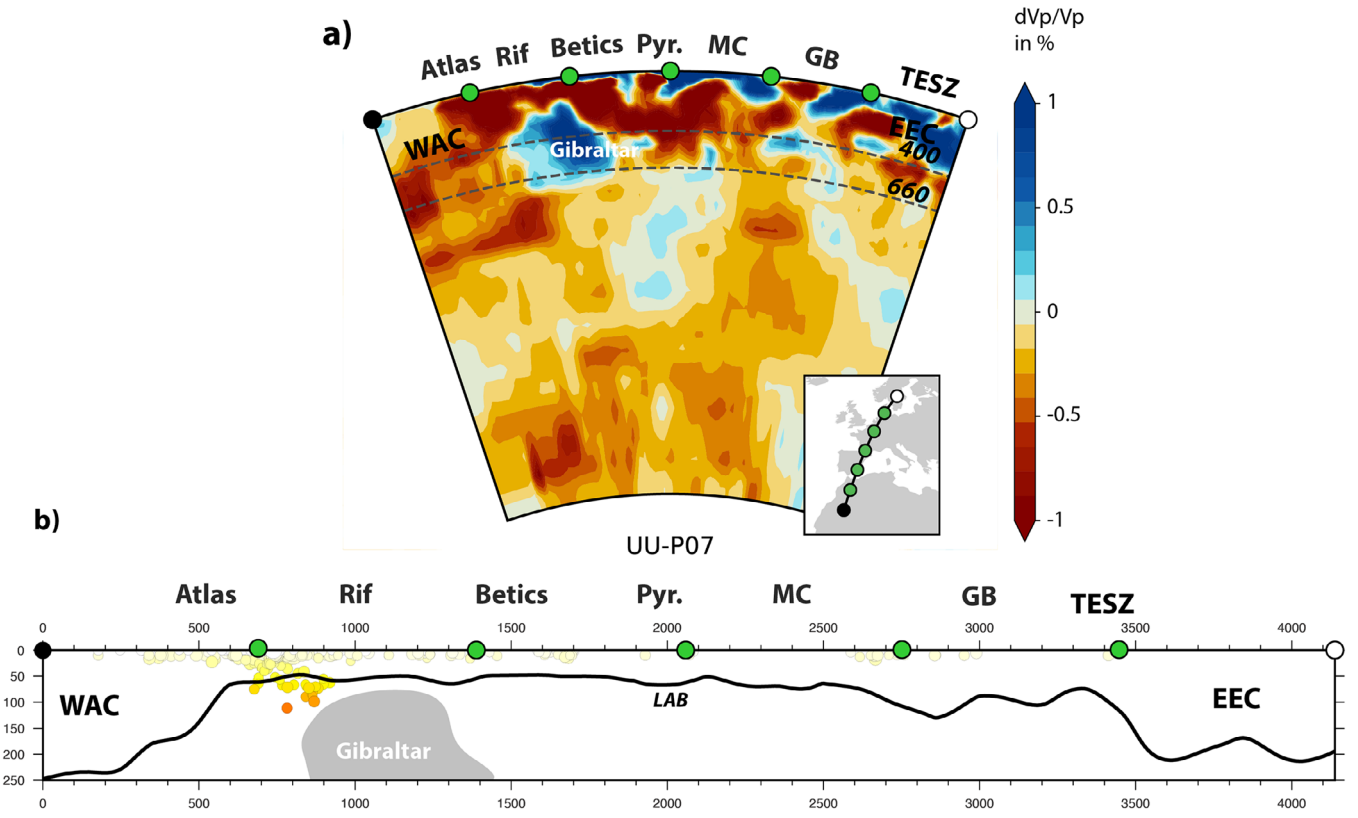

Fig. 3. P-wave seismic tomography and lithosphere thickness variations across Western Europe. (a) P-wave velocities anomalies from global model UU-P07 (Amaru, 2007) along a section stretching between the East European Craton (Sweden) and the Western African Craton (Morocco). (b) Seismic lithosphere thickness after model LITHO1.0 (Pasyanos *et al.*, 2014) along the same transect. Position of the high Vp anomaly corresponding to the Gibraltar slab in (a) is shown in grey. Hypocenters of major earthquakes are also shown. Abbreviations: Pyr.: Pyrenees; MC: Massif Central; GB: German Basin.

refertilization by fluids and melts mobilized during Proterozoic/Paleozoic subduction events (*e.g.*, Cadomian and Variscan subduction) and Mesozoic tectono-magmatic events during post-Variscan extension and opening of Tethys and Atlantic. They are also characterized by higher heat flow, thus limiting their maximum lithospheric thickness to about 150 km and are also much weaker (Te < 30 km). The transition between the different lithospheric provinces is well imaged in Central Europe (Fig. 2) by the abrupt reduction of LAB depth and S-wave velocities across the NW-SE-directed Trans-European Suture Zone (TESZ) (Geissler *et al.*, 2010; Legendre *et al.*, 2012; Schaeffer and Lebedev, 2013; Soomro *et al.*, 2015; Meier *et al.*, 2016).

Despite this general figure, we must distinguish the lithosphere below the Caledonides showing LAB depths close to 150–200 km, and both Vs anomalies and Te values (up to 80 km) that equate those of cratons (Figs. 2c and 2d). Low lithospheric thickness in the 50–100 km range is found in Central Europe (Pannonian Basin) and the Mediterranean Sea (Alboran, Algerian, Tyrrhenian and Aegean Basins). They are associated with attenuated crusts down to 15 km (Fig. 2a) related to back-arc thinning of the continental lithosphere (Faccenna *et al.*, 2014), involving retreating mantle delamination in the Alboran domain (Seber *et al.*, 1996; Calvert *et al.*, 2000; Thurner *et al.*, 2014; Mancilla *et al.*, 2015a; Daudet *et al.*, 2020), the Apennines (Chiarabba *et al.*, 2014; Agostinetti and Faccenna, 2018), and on the northern Africa margin (Roure *et al.*, 2012).

Regions with shallow LAB and thin crust are also found in the Neogene intracontinental magmatic provinces of the Bohemian Massif (Czech Republic, Poland and eastern Germany) in the Ohre Rift (or Eger Graben), in the Eifel volcanic field of the Rhenish Massif and Vogelsberg region emplaced on the Upper Rhine Rift (Goes *et al.*, 2000; Meier *et al.*, 2016) below which a plume has been inferred (Ritter *et al.*, 2001; Kreemer *et al.*, 2020). Similar plume-related volcanism accompanying uplift has been proposed based on teleseismic tomography in the Massif Central in close relationship with the Limagne Graben (Granet *et al.*, 1995). Other Neogene volcanic centers are found in Iberia stretching from the Eastern Betics (~ 34–2 Ma), Alboran domain (~ 12.1–6.1 Ma), Valencia Trough (~ 24–0.01 Ma), Calatrava Volcanic Province (~ 9–2 Ma) and Olot–Garrotxa (~ 10–0.01 Ma) that concentrate the most recent occurrence of alkaline lavas. They are interpreted to indicate mixing of partial melts from the lithospheric and asthenospheric mantle. The Late Cenozoic volcanic province temporally and spatially overlaps with the West European Rift system (Figs. 1 and 2).

Figure 3a presents the distribution of Vp anomalies in the deep mantle and the LAB geometry along a 4000 km-long

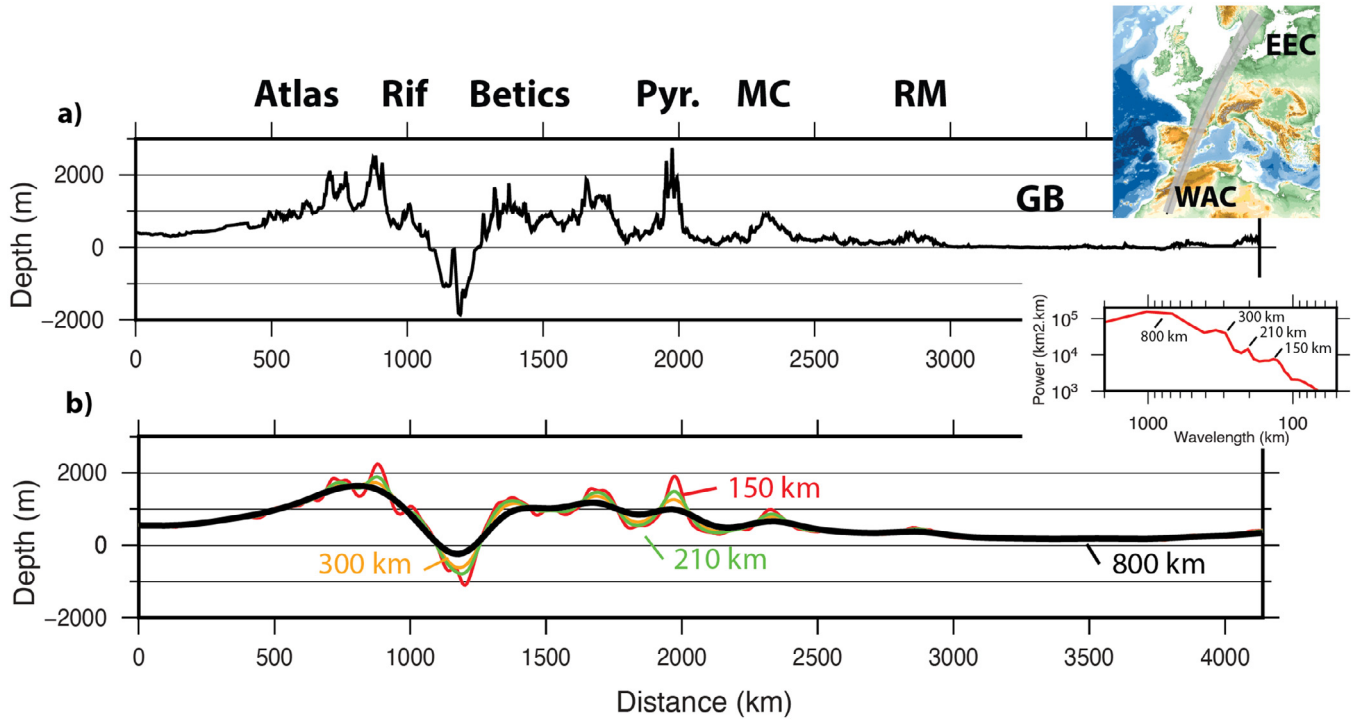

Fig. 4. Topography of Western Europe and filtered wavelengths of topography. A low-pass filter was applied on the total topographic (a) so the residual topography (b) contains only wavelengths larger than 150, 210, 300 and 800 km. Inset shows the dominant wavelengths obtained by the power spectral density analysis.

profile stretching from Morocco to Sweden. The Gibraltar anomaly is the only well identified slab along the transect. It is dipping eastwards and rests on the 660 km discontinuity. Based on regional geophysical experiments it is inferred the slab is detached from the surrounding Rif and Betic crustal roots (Mancilla *et al.*, 2015a). Because slab length also equals the size of the Alboran Sea, it is interpreted as part of delaminated Alboran SCLM. This is confirmed by recent geophysical studies (Thurner *et al.*, 2014; Petit *et al.*, 2015; Heit *et al.*, 2017; Molina-Aguilera *et al.*, 2019) and is indirectly supported by the uniform exhumation inferred from thermochronological study in the Flysch Complex of the western Betics (Daudet *et al.*, 2020) and cross-section balancing (Pedrera *et al.*, 2020a, 2020b) that argue for limited convergence between the Alboran basement and the Iberia paleomargin. The lithosphere thins gradually southward from 100–150 km below Germany to 50–100 km below Iberia (Pyrenees, Betics) and Alboran, and in northern Africa below the Rif and the Atlas (Fig. 3b). The boundaries with the thick cratonic roots of 200–250 km for the WAC and EEC are sharp, revealing localized tectono-magmatic reworking of the SCLM (Fig. 2; see discussion in Sect. 3).

It is apparent from these data that the lithosphere thickness and strength express a direct dependence on the age of the last tectonic and thermal events. The most evolved Archean cratonic (WAC and EEC) and their adjacent Proterozoic lithospheres (Figs. 1 and 2) are the strongest, whereas the Phanerozoic lithospheres modified by the succession of Variscan and Alpine orogenic cycles are the weakest.

2.2 Topographic fingerprints of European lithosphere thickness and composition

The topography of continents reflects the combined effects of 1) isostasy that results from the variation of age-dependent lithosphere thickness and densities and 2) a non-isostatic (dynamic) component caused by plate strength, subduction dynamics, or more broadly mantle flow that could also be driven by anomalously hot asthenosphere from the deeper mantle (*e.g.*, plume). Erosion and climate modulate these main mechanisms.

A topographic profile of Western Europe (Fig. 4a) parallel to the tomographic section of Figure 3 exhibits topographic variations at different wavelengths. The power spectral density analysis of the topography (inset in Fig. 4) reveals dominant wavelengths at 150, 210, 300 and 800 km. We then filter the topography using those selected wavelengths (Fig. 4b). Wavelengths in the range 150–300 km reveal topographic modulation associated with mountain belts (Pyrenees, Iberian Chain, Betic, Rif and Atlas), volcanic swells associated with the Cenozoic volcanic fields of Western Europe (Massif Central, Rhenish Massif), lithosphere thinning in the Alboran domain. The larger wavelength component of 800 km depicts the regional positive elevation changes ranging between 0 and 1700 m over Iberia and North Africa. Those wavelengths likely express the superposition of isostatic process in the lithosphere and dynamic topography arising from mantle flow and lithosphere strength (*e.g.*, regional isostatic support caused by plate flexure). It clearly appears that the highest elevations are associated with the younger Phanerozoic lithosphere that

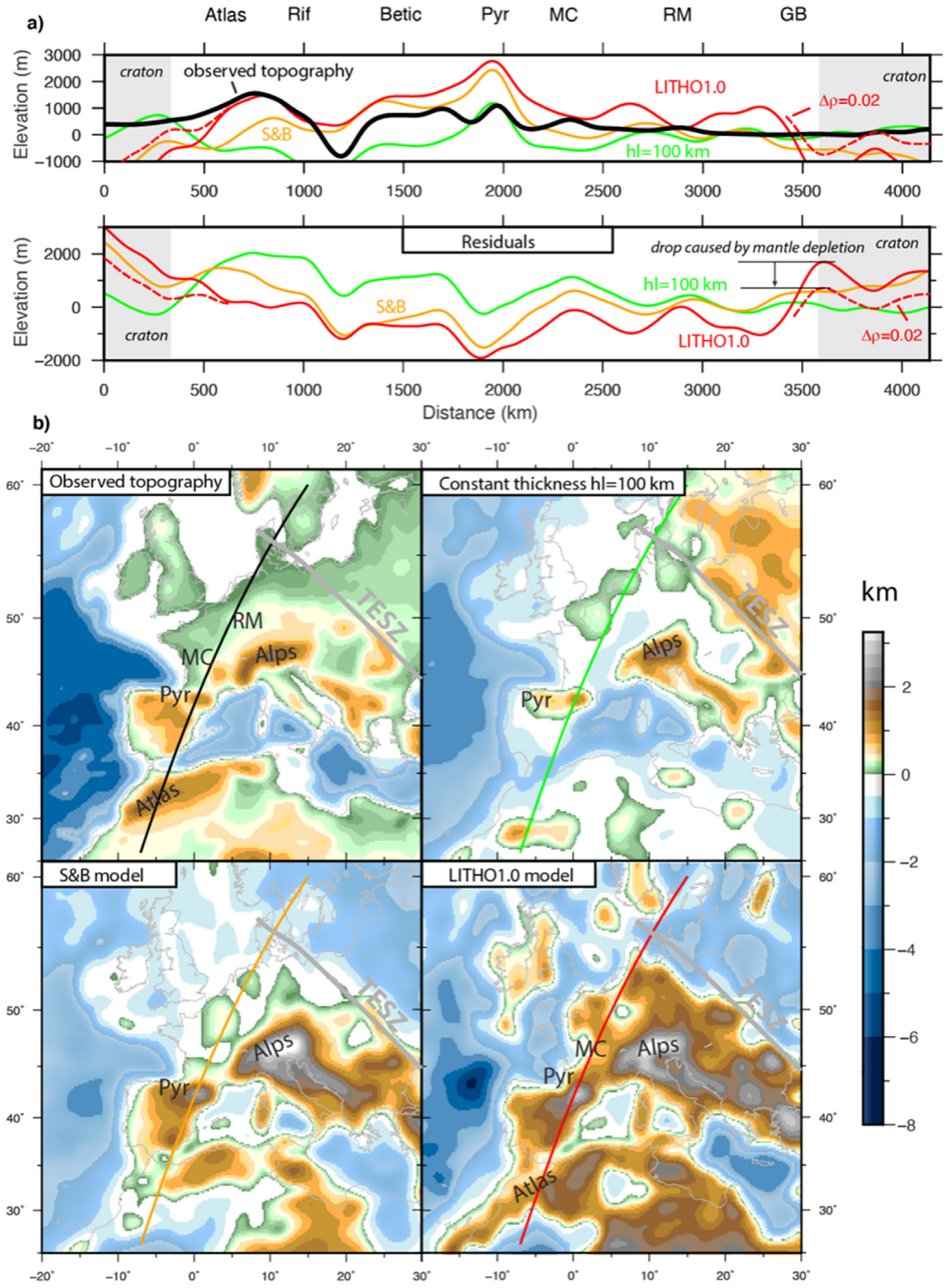

Fig. 5. Predicted topography for different lithosphere thickness models. (a) Profiles of predicted (top) and residuals (below) for constant lithosphere thickness of 100 km (green), lithosphere thickness model S&B (orange) after (Steinberger and Becker, 2016), and lithosphere thickness model LITHO1.0 (red) after (Pasyanos *et al.*, 2014). Red dashed line refers to the case in which the lithosphere density has been reduced by 0.02 kg/m^3 below cratons hence leading to drastic diminution of the topographic residuals in regions with thick lithosphere. (b) Maps depicting the predicted topography of Western Europe for each models in (a) and location of profiles (see text for explanation). Topography, LAB, crustal thickness and densities have been smoothed using gaussian filtering with a filter width of 300 km.

was tectonically and thermally reset during the Variscan and Alpine orogenic cycles (Fig. 1c).

The non-isostatic "anomalous" component of the topography can be approximated by the residual topography obtained by subtracting the observed topography from the predicted isostatic (Airy) component of the lithosphere. It theoretically requires the knowledge of the thickness and density variations of the crust and mantle lithosphere. In practice, because the thickness variations and composition (densities) of the lithosphere are poorly resolved it is common to fix both to constant values (Faccenna *et al.*, 2014). Assuming constant thickness of the lithosphere (115 km), constant crustal density and crustal thickness derived from updated CRUST1 model (Laske *et al.*, 2013), Faccenna and Becker (2020) estimated negative residual topography above subduction zones (Calabria, Hellenic trench, Ionian Sea, Rif) and positive residuals of 500–800 m for the Atlas, 400 m over Iberia, up to 1000 m in the Massif Central that they identify as dynamic topography driven by mantle flow. In the Mediterranean region, subduction dynamics has indeed been shown to be a major process explaining the main features of this anomalous topography (Faccenna *et al.*, 2014; Faccenna and Becker, 2020).

Below, we test the effect of lithosphere thickness variations on the topography of Western Europe. The approach is similar to Faccenna *et al.* (2014). First, we calculate the residuals using lithosphere model LITHO1.0 (Pasyanos *et al.*, 2014) shown in Figure 2b and compare with the LAB model of Steinberger and Becker (2016). The regional crustal thickness and density model are taken from EPcrust (Molinari and Morelli, 2011). The elevation of a buoyant lithospheric column in Airy isostatic equilibrium, with respect to the average ridge height of sea level $H_0 \approx 2.6$ km, is given by Lachenbruch and Morgan (1990):

$$e = \frac{h_c(\rho_a - \rho_c)}{\rho_a} + \frac{h_l(\rho_a - \rho_l)}{\rho_a} - H_0, \quad (1)$$

where h_c and ρ_c are the crustal thickness and density after EPcrust. h_l is the mantle lithosphere thickness, which is left to vary but its density is considered a constant $\rho_l = 3.3$ and the asthenosphere density is $\rho_a = 3.226$. The residuals are then calculated considering a smoothed topography required for interpolation purpose with crustal thickness, densities and LAB grids.

The predicted topography is presented in Figure 5 for models assuming constant and variable lithosphere thickness. For S&B and LITHO1.0 models that predict reduced lithosphere thickness for the Alpine-Variscan domain the elevation calculated is generally larger than the observed one. However, in many instances, in Iberia and North Africa (Betic, Rif and Atlas) these two models well reproduce the high elevation, as argued by the lower residuals than the model assuming constant thickness of 100 km (Fig. 5). The largest topographic residuals are found in the Pyrenees and in the cratonic areas, where both S&B and LITHO1.0 overestimate or underestimate the topography, respectively. In the Pyrenees, the elevation predicted by LITHO1.0 is indeed about 1 km higher than observed. In comparison, the constant lithosphere thickness model of 100 km appears more satisfactory for the central Pyrenees (Fig. 5). This result is consistent with the underthrusting of the Iberian lithosphere below Europe constrained by resistivity measurements, indicating lithosphere thickness of 110 km in the Pyrenees (Campanyà *et al.*, 2011; Mouthereau *et al.*, 2014). We also note for the Pyrenees that the averaged crustal density inferred from EPcrust of 2.75 (Supplementary Material Figure S1) is probably too low as it is not accounting for the exhumed dense mantle slices that are at the origin of large positive gravity Bouguer anomalies at crustal depths (Wang *et al.*, 2016; Chevrot *et al.*, 2018).

The large differences between observed (high) and predicted (low) topography of the WAC and EEC lithosphere for S&B and LITHO1.0 models indicate an excess of mass represented by a 200–250 km-thick lithosphere. Lower densities of stable Archean cratonic roots are expected due to their high degree of partial melting (Jordan, 1978). The assumption of constant ρ_l densities in the mantle is therefore certainly not valid. Assuming increasing melt depletion of the cratonic mantle such that its density decreases by $\Delta\rho_l = 0.02$ (54 kg/m^3 between lithosphere and asthenosphere) diminishes the residual topography up to 1 km where the lithosphere is the thickest (Fig. 5a). Based on these results, it appears that a careful adjustment of density contrasts in the crust and in the lithospheric mantle, informed by petrographic data and geochemical composition inferred from ophiolites, mafic rocks and xenoliths data, can provide, in addition to asthenospheric mantle flow, explanations for anomalous present-day elevation features of Western Europe. Below we provide some clues to a qualitative understanding of lateral variations of the European mantle composition based on a review of its long-term tectono-magmatic evolution.

3 Architecture and composition of the European-African lithosphere

We have seen in Section 2 that the understanding of the orogenic topography, and obviously its evolution over geological times, requires a better characterization of the architecture and the tectono-magmatic and thermal evolution of the continental lithosphere. A relevant approach for investigating the relationship between orogenic evolution, and the lithosphere rheology back in time is to focus on the evolution of the SCLM itself, as the latter is assumed to be the most resistant layer of the lithosphere (Burov and Watts, 2006). It is expected that tectonic and magmatic events that have previously acted on the lithosphere determine the mechanical coupling between crust and mantle but this is yet to be clearly established. While crustal evolution is directly accessible by studying the evolution of magmatic and sedimentary rocks at the surface, constraining the evolution of the SCLM relies on geochemical and petrographical constraints from ultramafic rocks in ophiolitic complexes, orogenic peridotites massifs, and mantle xenoliths.

In Western Europe, the lithosphere formed by a succession of continental assembly, orogenies and breakup since the Precambrian between two stable cratons, the West African Craton (Reguibat shield) and the East European Craton (Baltica shield) (Fig. 1). As it will be presented in details below, the European lithosphere has been amalgamated during a series of Proterozoic Cadomian and Fennoscandian orogenic events, Phanerozoic continent-continent collisions of Gondwana-derived terranes during the Caledonian and Variscan orogenies. Both the crust and mantle of the original EU cratonic lithosphere have been deeply remobilized during these successive tectonic and magmatic events, including magmatic arc formation and

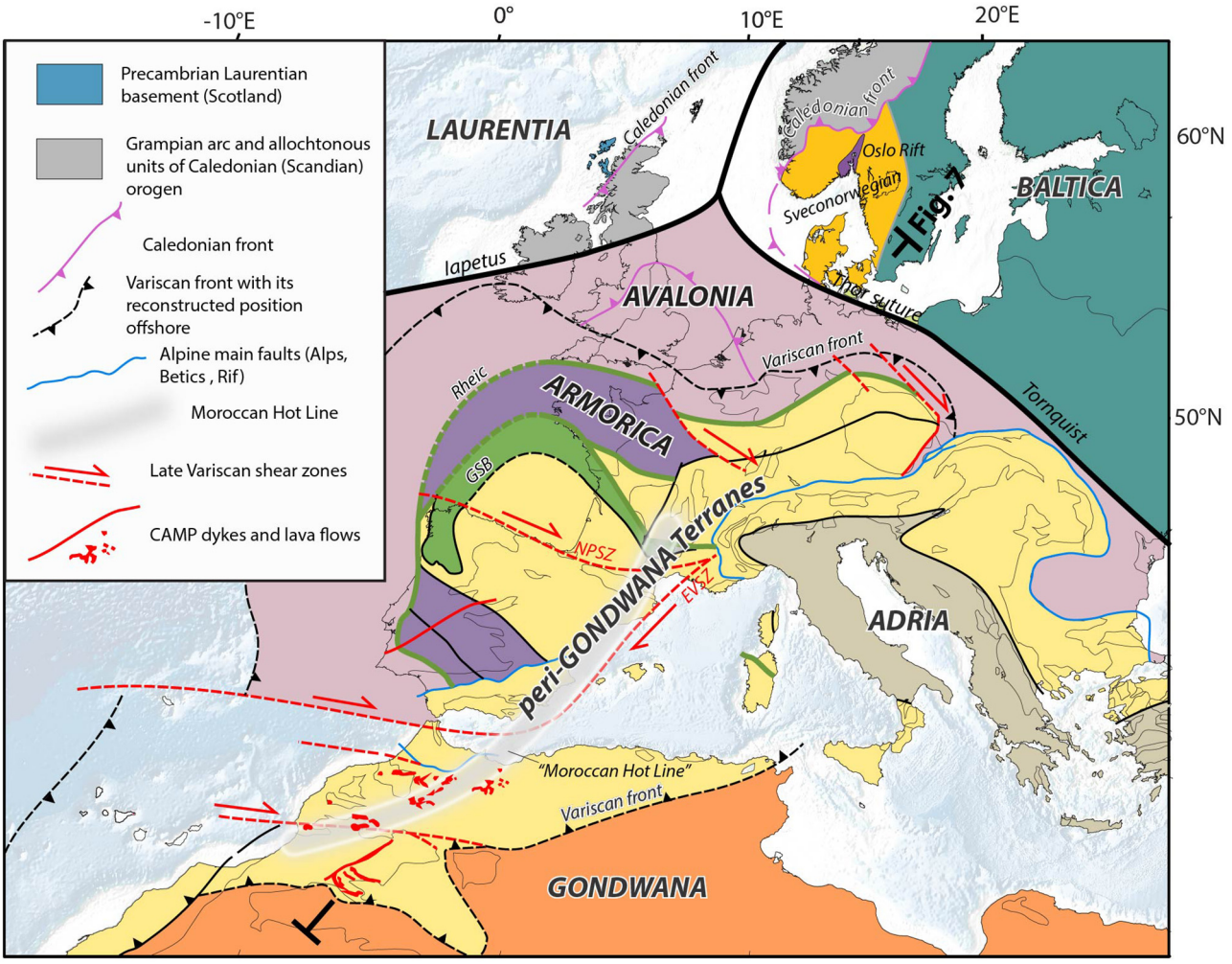

Fig. 6. Mapping of continental elements including stable cratons (Gondwana/Reguibat, Baltica, Laurentia) and Gondwanan terranes (Avalonia, Armorica, Adria) accreted during assembly of Gondwana (closure of Iapetus) and Pangea (closure of Rheic) leading to Caledonian and Variscan orogenies. AR: Ardennes; RM: Rhenish Massif; HZ: Harz Massif; RG: Rhine Graben; MGF: Moray Firth Graben; VK: Viking Graben; MC: Massif Central; WCG: West Central Graben; L.: Lizard Ophiolites; BM: Brabant Massif; GSB: Galicia-South Brittany Ocean. Although being another peri-Gondwanan terranes, ADRIA is distinguished north of Gondwana for its role as indentor for the Alpine orogeny. Late Variscan right-lateral shear zones formed during transition towards opening of the Neo-Tethys Ocean are also indicated.

accretion, partial melting in crust and mantle, rifting between Gondwana and Laurentia. These events define a structural and mechanical background of a layered crust and mantle that was reactivated during the Tethyan rifting in the Mesozoic and during the Cenozoic convergence. In the following, we present a synthesis based in part on Re-Os and Sm-Nd depletion events inferred from mantle rocks in ophiolites and xenoliths or mantle-derived magmatism in the crust. Constraints are presented from North to South, and for cratonic and phanerozoic lithospheres, and summarized along a 4000 km cross-section of W Europe.

3.1 Europe lithosphere evolution: East European Craton and Avalonia

3.1.1 East European Craton (Baltica) and Avalonia

The East European Craton (Baltica) forms a 250 km-thick lithosphere (Figs. 2 and 3) made of a coherent ensemble of Precambrian continental segments (Figs. 1 and 6). These segments include Fennoscandia, exposed in the Baltica Shield, Sarmatia, exposed in the Ukrainian Shield and Volga-Uralia that were assembled at ca. 1.8–1.7 Ga (Bogdanova *et al.*, 2008). The cratonic core of Fennoscandia is the Karelian and Kola craton (3.2–2.5 Ga) (Lahtinen *et al.*, 2005). Re-Os isotopic composition of mantle xenoliths sampled in 600 Ma kimberlite pipes confirms the main part of the Karelian lithospheric mantle, down to 180 km, is made of harzburgitic layer that derives from a 3.3 Ga magmatic event of the same age as the overlying crust (Peltonen and Brügmann, 2006) (Fig. 7). It overlies a basal, less depleted and metasomatized, garnet-lherzolitic/harzburgitic mantle between 180 and 250 km that formed at ca. 2 Ga during the earliest stages the Svecofennian orogeny (Peltonen and Brügmann, 2006) (Figs. 6 and 7). The western craton margin recorded partial melting of an enriched mantle that result from the rise of volatile-enriched magmas from the Svecofennian subduction

(1.95–1.86 Ga) at the origin of a volcanic arc that eventually collided with Fennoscandia and the Volgo-Samartian craton (Rutanen *et al.*, 2011). A subsequent post-collisional bimodal (mafic and felsic) magmatism from the Svecofennian domain emplaced at 1.82–1.79 Ga (Fig. 7). As EEC was amalgamated to Rodinia supercontinent, during collision with Amazonia, its western margin was involved in the Sveconorwegian-Grenvillian orogeny (1.15–0.9 Ga) (Torsvik *et al.*, 1996; Li *et al.*, 2008; Cawood and Pisarevsky, 2017; Bingen *et al.*, 2020). The Ediacaran-Cambrian Iapetus Ocean opened at 570 Ma by the separation of Baltica, Laurentia and Amazonia. Continental breakup was likely triggered by plume magmatism of the Central Iapetus Magmatic Province (CIMP) at 615–590 Ma on the NW margin of Baltica still preserved as dyke swarms (Fig. 7) in the overthrusted pre-Caledonian distal margin of Baltica (Svenningsen, 2001; Tegner *et al.*, 2019a).

Peridotite lenses from the HP and UHP terrains of the Western Gneiss Region of the Scandinavian Caledonides (420–380 Ma) provide constraints on the evolution of the continental mantle of the margin of Baltica shield. An ancient Archean depletion event at 3.2 Ga, at the origin of large lenses of harzbugites and dunites, is reported in garnet mantle peridotites that were later affected by a Mid-Proterozoic melt-related refertilization event at 1.6 Ga (Fig. 7) contemporaneous with Gothian orogeny (Brueckner *et al.*, 2002; Beyer *et al.*, 2004; Beyer *et al.*, 2006). Later crustal (and mantle) reworking is attested by metamorphism and magmatism during the Sveconorwegian-Grenvillian orogeny at 1.15–1.25 Ga (Lapen *et al.*, 2005) and after at 0.95–0.94 Ga (Söderlund *et al.*, 2002, 2005; Bogdanova *et al.*, 2008). A more recent tectonic event dated to ~ 600 Ma, likely related to Central Iapetus Magmatic Province (CIMP), is indicated by garnet kelyphite in mantle peridotites. It reflects decompression/exhumation to crustal depth associated with lithosphere thinning during the opening of the Iapetus (Lapen *et al.*, 2009).

The Caledonian orogeny that resulted from the closure of Iapetus Ocean between Laurentia and Baltica initiated in the Late Cambrian-Ordovician ca. 500 Ma (Roberts, 2003) with intra-oceanic subduction and the formation of the Grampian-Taconic arc (Cawood *et al.*, 2001; Chew and Strachan, 2014; Domeier, 2016). The final suturing in the Scandinavian Caledonides known as the Scandian phase ~ 420–380 Ma (Silurian-Devonian) is recorded by continental subduction and underthrusting of the Baltica margin (Roberts, 2003; Hacker and Gans, 2005; Kylander-Clark *et al.*, 2007; Corfu *et al.*, 2014).

Laterally, south-westwards, arc-continent collision occurred between the Grampian oceanic arc and Laurentia margin in the Late Ordovician (450 Ma) while subduction was ongoing below east Avalonia (SW Britain, Brabant Massif, N Germany and Poland) (Chew and Strachan, 2014). In Scotland, collision of the southern margin of Laurentia with Baltica is dated to mid-Silurian (430–440 Ma) coeval with the Scandian phase (Goodenough *et al.*, 2011; Domeier, 2016), but the final oblique collision of Laurentia with Avalonia is constrained by a Middle Devonian unconformity (Chew and Strachan, 2014). During the Early Ordovician, east Avalonia and Baltica margins were separated by the Tornquist Sea (Figs. 6 and 7), which then closed by subduction and collision in the Late Ordovician ~ 450 Ma (Torsvik and Rehnström, 2003; Domeier, 2016). This narrow suture now forms the Trans-European Suture Zone (TESZ), a marked geophysical transition between the EEC (Baltica) and Caledonian/Variscan Belt of Central Europe (Figs. 1 and 2). A Late Carboniferous (Late Variscan)-Permian extension (310–245 Ma) associated with voluminous magmatism occurred on the southern margin of Fennoscandia, forming the Oslo Rift (Heeremans *et al.*, 1996) (Figs. 1 and 6). This event is coeval with widespread post-Variscan alkaline magmatism observed elsewhere in Europe (see below). A source for these lavas is inferred to be represented by garnet-bearing peridotites that have been affected by partial melting at the lithosphere-asthenosphere boundary (Neumann *et al.*, 2002) possibly linked to a metasomatism of the lithospheric mantle associated with emplacement of carbonatite at 600 Ma (Neumann *et al.*, 2004) and contemporaneous with CIMP.

South of TESZ, detrital zircon from Cambrian-Silurian sediments of the Brabant Massif and Nd isotopic signature of magmatic rocks reveal the margin of East Avalonia is formed by a Pan-African (Neoproterozoic) basement recycling an older Mesoproterozoic juvenile crust (1.3–1.7 Ga), that was rifted from Gondwana during the Cambrian (Linnemann *et al.*, 2012). The evolution of West Avalonia (Nova Scotia) is concurrent with East Avalonia since it recorded the same main Cadomian continental arc magmatic event north of Gondwana during the Neoproterozoic (630–570 Ma). Isotopic composition of magmatic rocks from Avalonia basement show it derives from recycling and melting of 1.2–1.0 Ga juvenile crust (Murphy *et al.*, 2000; Nance *et al.*, 2002). Most rift-related mafic rocks that crystallized between 610 and 370 Ma were derived from the same mantle enriched at 0.8–1.1 Ga (Murphy and Dostal, 2007) (Fig. 7) possibly related to global-scale high-degree melting of the mantle during Rodinia assembly (Dijkstra *et al.*, 2016). Taken altogether these data confirm that Avalonia crust and lithospheric mantle remained coupled since rifting and drifting of Avalonia from Gondwana until collision with Laurentia.

3.1.2 West African Craton (Reguibat Shield) and Anti-Atlas

Positioned to the south of our transect, the West African craton (WAC) includes the Reguibat shield and the Anti-Atlas to the north, separated by the Tindouf Basin (Figs. 1, 6 and 7) where the lithosphere thickness is 200–250 km (Fig. 2). U-Pb and Sm-Nd ages from a granulitic pluton indicate the Reguibat shield formed by crustal growth events at 3.5 Ga followed by HT metamorphism between 2.98 Ga and 2.7 Ga and crustal melting at 2.7 Ga (Potrel *et al.*, 1998). An Re-Os age of ~ 3.4 Ga for eclogite xenolith from the Man shield, south of WAC, suggests the deep lithospheric mantle formed, or was amalgamated, during the Archean crustal growth stage (Barth *et al.*, 2002).

The Anti-Atlas consists of a 2 Ga Eburnean basement (Thomas *et al.*, 2002, 2004) that has been involved in the Pan-African/Cadomian, Variscan and Alpine orogenies (Ennih and Liégeois, 2001). This domain is segmented by a Neoproterozoic (686 Ma) Pan-African suture. The suture is represented by the Sirwa and Bou Azzer ophiolitic complexes dated to 759–762 Ma (Thomas *et al.*, 2002; Samson *et al.*, 2004; Hodel *et al.*, 2020) that were originally emplaced in back-arc setting as a result of the intra-oceanic subduction and closure of the Pan-African Ocean between the WAC and Cadomia-Avalonia terranes (Ennih and Liégeois, 2001).

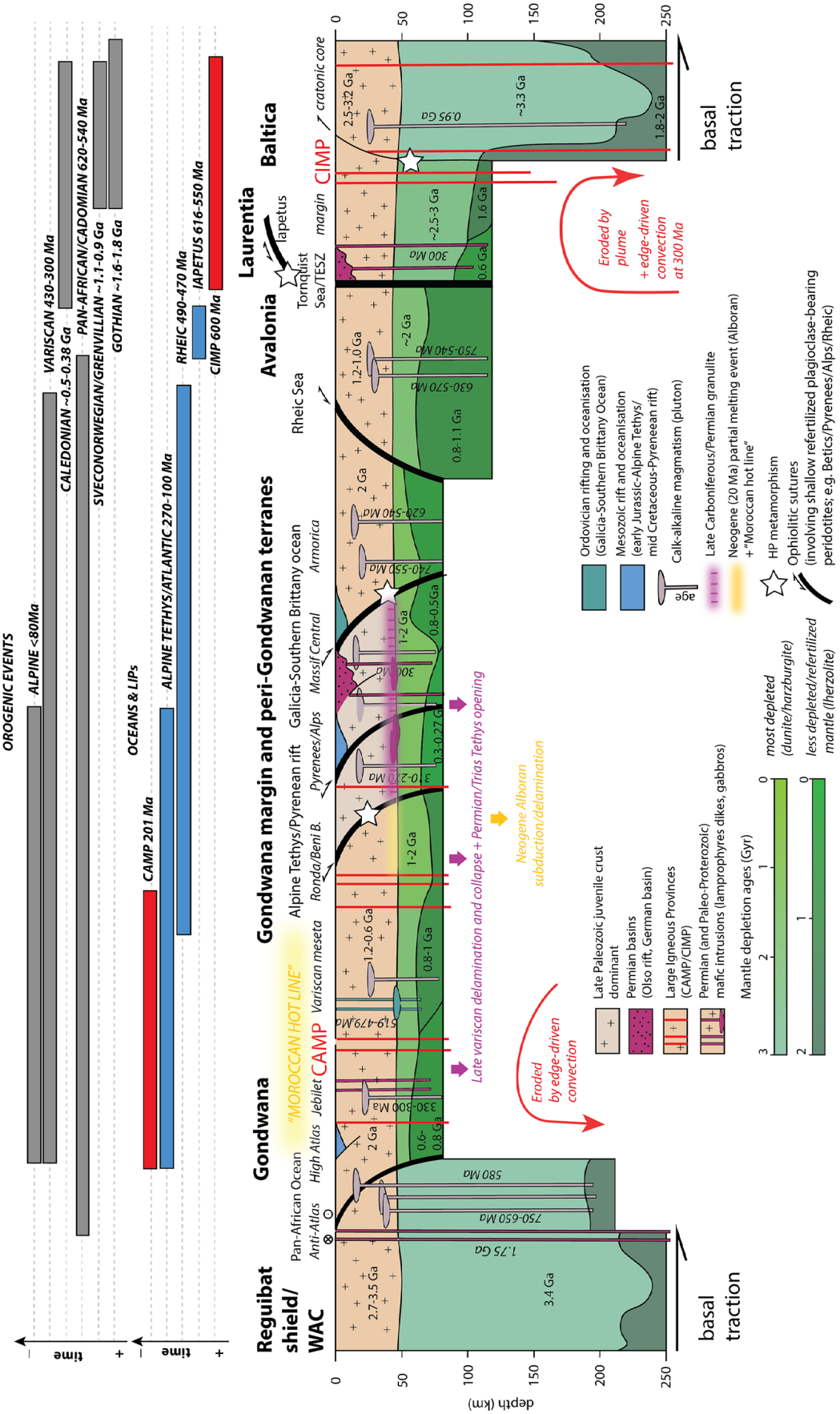

Fig. 7. Architecture of the European lithosphere showing the main magmatic events and depletion ages for the crust and mantle lithosphere. Those ages are inferred from Sm-Nd and Re-Os systematics that reflect variable composition and densities at the base of the lithosphere. Temporal and spatial relationships with orogenic events, oceanic and LIPs (CAMP, CIMP) are also indicated. Main tectono-magmatic events are related to Columbia, Rodinia, Gondwana and Pangea supercontinents assembly at ca. 1.8, 1.2, 0.5 and 0.3 Ga, respectively.

Arc magmatism resulting from this subduction was long-lived, ranging from 750 to 650 Ma, and characterized by episodic accretionary stages (Triantafyllou *et al.*, 2018). The final obduction of the back-basin and ophiolites is dated by the age of arc accretion on the northern wedge of the WAC at ~630–580 Ma (Thomas *et al.*, 2002; Gasquet *et al.*, 2008) before the intrusion of Late Pan-African granite dated to 580 Ma (Inglis *et al.*, 2004) possibly related to delamination and transtension (Fig. 7). To the north-east of the suture (*e.g.*, Sirwa and Sarho Massifs), the Eburnean basement is not exposed. It is covered by Cryogenian turbidites and basalts that were deposited on the rifted margin of the Eburnean crust. This is in agreement with the formation of a juvenile magmatic arc, similar to Cadomian magmatism recognized to the North, with Nd isotopic signature from the 750–700 Ma gneiss and other igneous rocks and intrusive of the Bou Azzer inlier (D'Lemos *et al.*, 2006; Triantafyllou *et al.*, 2020), indicating no substantial assimilation of the Eburnean basement. To the southwest, in contrast, the Eburnean basement is exposed and forms Precambrian inliers "boutonnières". They are positioned on the margin of the WAC that was affected by a 1.75 Ga magmatic event, likely reflecting a tentative initial breakup of the WAC lithosphere (Youbi *et al.*, 2013).

3.1.3 Summary: tectono-thermal events in EEC, WAC and Avalonia

From this brief review, it is apparent that both crust and mantle of the East European Craton (EEC) have remained coupled since the Archean. Large bodies of refractory (dunite/harzburgite) Archean mantle (Beyer *et al.*, 2006) are documented, indicating the core of Karelian craton resisted melt-related refertilization during Proterozoic Svecofennian magmatic event at 1.8 Ga and the subsequent Sveconorwegian-Grenvillian event. The western margin of Baltica, however, recorded two major magmatic and metamorphic events during plume metasomatism at 600 Ma and subduction at 500–380 Ma during opening and then closure of the Iapetus Ocean. The 600 Ma event thermally eroded and thinned the lithosphere to about 100 km (Fig. 7) as argued by geophysical data (Fig. 2). The rapid change in lithospheric thickness may have triggered small-scale edge-driven convection cells on the Baltica margin as suggested for the WAC (*e.g.*, Kaislaniemi and van Hunen, 2014). This event promoted inversion and subduction during the Scandian orogeny and later the Permo-Carboniferous rifting along the TESZ.

The lithosphere of Avalonia bears the imprints of an older Neoproterozoic (750–540 Ma) tectono-thermal event related to subduction north of Gondwana, which resulted, during the Cambrian-Early Ordovician in rifting and drifting of Avalonia from Gondwana and the opening of the Rheic Ocean (Murphy *et al.*, 2006; Domeier, 2016). The close genetic relationships between crustal growth and mantle depletion events since the Neoproterozoic suggests the sub-continental mantle of Avalonia remained coupled to the crust. We view Avalonia as an intermediate continental block characterized by a decratonized, relatively thin 100 km lithosphere with no significant crust-mantle decoupling (Fig. 7). Isotopic data from the Western African Craton (WAC) in the Reguibat and Man shields, although less abundant than for the EEC, indicate the crust and mantle are coupled since the Archean. The first evidence of magmatism on the margin of the WAC arguing for the removal of the cratonic root and potential decoupling between crust and mantle is dated to 1.75 Ga.

3.2 Variscan Europe and Northern Africa: a tectono-magmatic history of long-lasting lithospheric thinning

3.2.1 Prolonged tectono-magmatic reworking of peri-Gondwanan terranes

South of Avalonia, peri-Gondwana terranes have recorded the Cadomian/Pan-African orogeny (Fig. 6). They were then involved in the Late Paleozoic Variscan orogeny during closure of the Rheic Ocean (Martínez Catalán *et al.*, 2007; Kroner and Romer, 2013; Ballèvre *et al.*, 2014). These terranes include Armorica, Saxo-Thuringia, Bohemian Massif and NW Iberia (Galicia). The lithosphere with that thermal ages appears particularly thin (Figs. 2 and 3) characterized by lithospheric thickness below 100 km and weak ($Te < 30$ km). They are separated by Cambro-Ordovician and Devonian ophiolitic sutures (Fig. 7), with many overprinted by HP metamorphism (Berger *et al.*, 2006). Whether these ophiolites represent sutures of large oceanic domains between pre-Gondwanan Units or thin continental crusts is still controversial (Matte, 2001; Kroner and Romer, 2013; Franke *et al.*, 2017). They comprise the Rheic-Rheno-Hercynian suture between Avalonia and North Armorica devoid of HP metamorphism (Figs. 6 and 7), the Galicia-Southern-Brittany/Bohemia suture (also named Medio-European, Paleo-Tethys, Eo-Variscan suture or Central-Moldanubian) between Armorica and Gondwana (paleo-Adria), with an intermediate Saxo-Thuringia suture between North and South Armorica/Bohemia (Franke *et al.*, 2017).

North Armorica exhibits a juvenile 2.06 Ga crust (Icart Gneiss), having close affinity with the 2.1 Ga Eburnean basement of the West African craton (Samson and D'Lemos, 1998). This basement was then involved in the Cadomian cordilleran evolution (620–540 Ma) to form a large zone of deformation and magmatism (Chantraine *et al.*, 2001). Between Avalonia and Armorica, the Rheic Ocean opened by the reactivation of Neoproterozoic suture in the Late Cambrian–Early Ordovician during closure of the Iapetus Ocean (Murphy *et al.*, 2006, 2009). The Lizard ophiolite in SW Britain is commonly viewed as the Rheic oceanic suture. However, this ophiolite hosts sheared spinel lherzolite transformed before Early Devonian (397 Ma) into low-pressure plagioclase-bearing peridotites during exhumation to depth of 25 km in a magma-poor rifted margin (Cook *et al.*, 2000). This ophiolite therefore represents the rifted margin of short-lived Rheno-Hercynian Ocean rather than the Rheic Ocean that is inferred to be a wide oceanic domain based on paleobiogeography and paleomagnetism (Domeier, 2016; Franke *et al.*, 2017).

South Armorica and NW Iberia display widespread Cadomian magmatism (750–550 Ma) and Early Ordovician magmatism (Martínez Catalán *et al.*, 2007; Ballèvre *et al.*, 2014) (Fig. 7). Geochemistry and Nd isotopic analyses of Early Ordovician lavas, including basalts from NW Iberia, reveal a mixed magmatic signature ranging from a juvenile mantle to a sub-continental mantle enriched at 1 Ga during Cadomian subduction (Murphy *et al.*, 2008). These lavas are interpreted

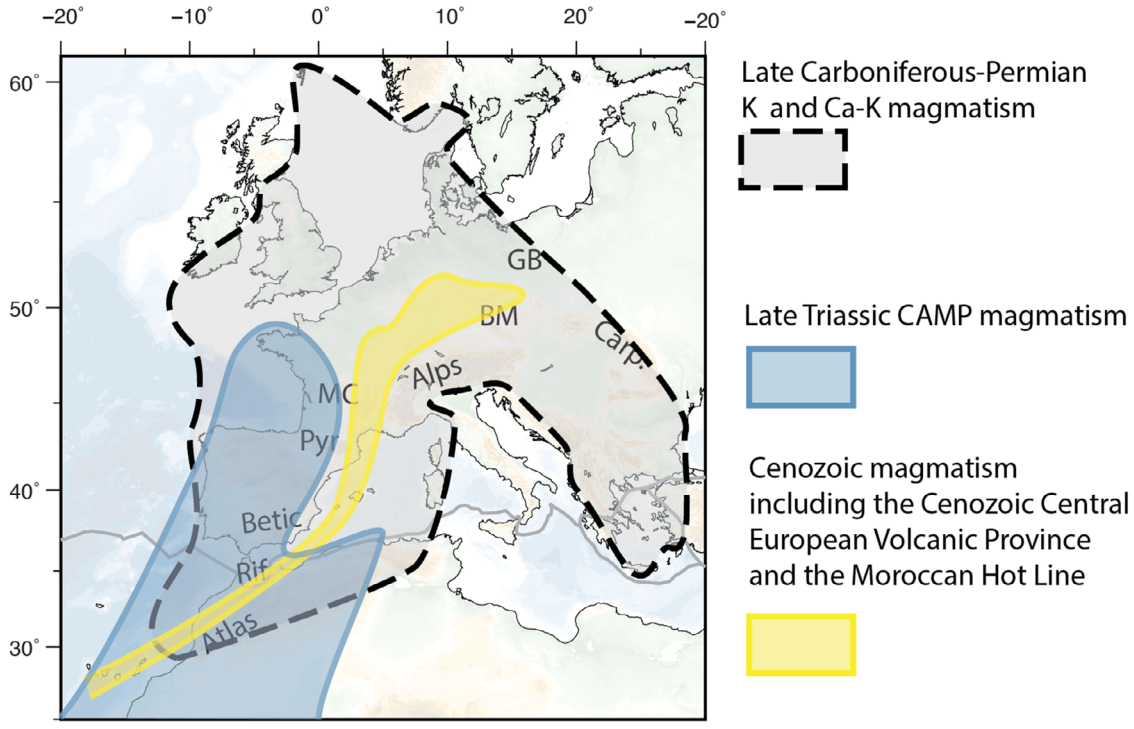

Fig. 8. Spatial distribution of main Late Paleozoic, Mesozoic and Cenozoic magmatic provinces of Europe and northern Africa. CAMP: Central Atlantic Magmatic Province.

to indicate a continent-ocean transition on the northern Gondwana margin that developed synchronous with the opening of the Rheic Ocean. The widespread Ordovician extension between Armorica and the northern margin of Gondwana (Fig. 7) formed slow spreading centers or hyper-extended crust (Berger *et al.*, 2006; Lardeaux, 2014). Paleobiogeographic and paleomagnetic data also indicate that the Massif Central and Gondwana were not separated by a large ocean, suggesting that these extended domains are distinct from the Rheic Ocean (Fortey and Cocks, 2003). It corresponds to the Galicia-Southern-Brittany suture (Fig. 6), south of Massif Central and in the Galicia-Cabo Ortegal complex, characterized by 495–469 Ma (Cambrian-Early Ordovician) MORB-type magmatic rocks that recorded UHP metamorphism at 412–390 Ma (Early Devonian) (Casado *et al.*, 2001; Berger *et al.*, 2010). Petrology and geochemistry of mantle pyroxenites within the harzburgitic massif from the Cabo Ortegal complex indicate they were produced by melt-rock reactions at the root of Cadomian arc during the Cambrian-Neoproterozoic (654 ± 72 Ma). This is before the terminal emplacement onto the rifted Gondwana margin during the Variscan orogeny (Tilhac *et al.*, 2016, 2017).

Geochemical and geochronological analyses of detrital zircons in orthogneiss from the Massif Central indicate the pre-Variscan crust is derived from sediments deposited on the northern Gondwana margin (Melleton *et al.*, 2010; Chelle-Michou *et al.*, 2017). Soon after deposition in backarc setting at 550–545 Ma partial melting of these sediments produced the S-type Cadomian granites (Couzinié *et al.*, 2017). This origin is also argued by Archean and Paleoproterozoic detrital zircons recovered from Paleoproterozoic gneissic rocks in eastern Europe that indicate the Cadomian "basement" reworked a thinned remnants of older cratonic crust (Linnemann *et al.*, 2007). A similar Gondwanan source of detrital zircon is documented in 630–385 Ma sediments from Bohemia Massif, indicating these terranes remained close to Gondwana margin until the Devonian (Drost *et al.*, 2011). In the Massif Central, the Early Ordovician (480 Ma) extension is attributed to the formation of peripheral marginal basins floored by thinned lithosphere with local oceanic affinity, now metamorphosed as amphibolite. A synthesis of Sm-Nd isotopic data from Neoproterozoic and Early Paleozoic mafic rocks (800–500 Ma) in the Bohemian Massif, Vosges, Armorica, Massif Central, and Pyrenees (Dostal *et al.*, 2019), further reveals they were extracted from a juvenile mantle (*i.e.*, depletion age of 800–500 Ma). This suggests melting during asthenospheric upwelling in a backarc basin and opening of the Rheic Ocean (Fig. 7).

3.2.2 Late- to post-Variscan transition: Late Carboniferous-Permian thermal event

The Variscan orogen terminates at the end of the Carboniferous-Early Permian with the transition towards extension associated with widespread volcano-sedimentary basins and mafic magmatism throughout Europe (Fig. 8; Wilson and Downes, 1992; Ménard and Molnar, 2004; Neumann *et al.*, 2004; Timmerman, 2004; Wilson *et al.*, 2004; McCann *et al.*, 2006). The accumulation of Permo-Carboniferous volcanic-derived sediments (Figs. 7 and 8) reaches 1–2 km kilometers in the North-German Basin (Timmerman, 2004), in the Pyrenees (Lago *et al.*, 2004a; Gretter *et al.*, 2015; Rodríguez-Méndez *et al.*, 2016; Espurt *et al.*, 2019), Iberian Ranges (Arche and López-Gómez, 2005),

Massif Central (Bruguier *et al.*, 2003; Michel *et al.*, 2015) and southern Alps (Cassinis *et al.*, 2011). Magmatic events were presumably triggered by a combination of right-lateral wrenching (Fig. 6) between Gondwana and Laurussia (Matte, 2001) closely connected to the opening of the Neo-Tethys and N-directed subduction of the Paleo-Tethys (Kroner and Romer, 2013). Latest Carboniferous and Permian plutonism is widespread in the southern, central and eastern Europe, including the Pyrenees (Michard-Vitrac *et al.*, 1980; Maurel *et al.*, 2004; Denèle *et al.*, 2007; Esteban *et al.*, 2015; Kilzi *et al.*, 2016; Vacherat *et al.*, 2017), the Massif Central (Faure, 1995), Spain and Portugal (Dias and Leterrier, 1994; Bea *et al.*, 1999; Fernández-Suárez *et al.*, 2000), Germany (Romer *et al.*, 2001), North-Sudetic Basin of Bohemian Massif (Awdankiewicz *et al.*, 2013), Poland near the TESZ (Zelaźniewicz *et al.*, 2016) and Dobrogea (Seghedi, 2012) (Fig. 8). The heat required by the Late Variscan magmatic event is interpreted to indicate post-collision mantle delamination (Fig. 7), which may have commenced before the latest Carboniferous, for instance, in Iberia (Fernández-Suárez *et al.*, 2000). Indeed, there are several indications of mantle-derived sources as old as 330 Ma that also reveal melting of an enriched mantle such as for the Central Massif (Laurent *et al.*, 2017), the Alps (Bussy *et al.*, 2000) and central Europe (Raumer *et al.*, 2013). Only in the external Hellenides of Crete (Zulauf *et al.*, 2015) and in the Menderes Massif (Candan *et al.*, 2016) the Late Carboniferous-Early Permian magmatism is related to arc magmatism that resulted from the subduction of the Paleo-Tethys.

Geochemical and petrographic data in central and southern Europe show evidence of a drastic change in the composition of the mantle. This is argued by negative Nd isotopic values and old depletion ages (1.8–0.8 Ga) from Late Carboniferous-Permian lamprophyre dykes and high Mg-K rocks (Dostal *et al.*, 2019). An interpretation is the partial melting during post-Variscan rifting of a mantle previously enriched during the Variscan subduction (Soder and Romer, 2018). Modification of the mantle source for the same crustal regions suggest crust and mantle were both decoupled during the Variscan orogeny (Dostal *et al.*, 2019). This is in line with inferences from the Massif Central that reveal a lack of autochthonous basement older than 550 Ma (*e.g.*, Cadomian basement) below Gondwanan-derived sediments (Chelle-Michou *et al.*, 2017). Mantle xenoliths (spinel lherzolites) associated with the Miocene Massif Central volcanism preserve a record of ancient depletion events at 313–377 Ma (Wittig *et al.*, 2006; Harvey *et al.*, 2010) in agreement with melt extraction in a spinel-facies mantle during the Variscan orogeny (Fig. 7). Despite intense metasomatic events during the Neoproterozoic (Cadomian arc), the Variscan and the Cenozoic, Re-Os isotopes reveal a 1.8 Ga depletion event, arguing for preservation of Proterozoic magmatic events (Harvey *et al.*, 2010). These data collectively point to the heterogeneity of the Late Variscan mantle, comprising a component of juvenile mantle depletion event (0.3 Ga) in an heterogeneous, mostly Proterozoic, mantle (0.8–1.8 Ga).

3.2.3 Post-Variscan rift-related lithosphere evolution

Permian post-orogenic HT metamorphism of the Variscan basement (*e.g.*, granulite) and mafic intrusions of mantle-derived magmas (gabbros, lamprophyre dykes, syenites, microdiorites) (Figs. 7 and 8) are recognized in Iberia (Orejana *et al.*, 2008, 2009, 2020; Gutierrez-Alonso *et al.*, 2011), in the Pyrenees (Debon and Zimmermann, 1993; Lago *et al.*, 2004b), in the Alps (Voshage *et al.*, 1990; Barth *et al.*, 1993; Vavra *et al.*, 1999; Hermann and Rubatto, 2003; Schaltegger and Brack, 2007; Schuster and Stüwe, 2008; Petri *et al.*, 2016) and Corsica (Paquette *et al.*, 2003; Martin *et al.*, 2011). The magmatic event spread over a region (Fig. 8) that is now defined by a thin lithosphere (50–100 km) and low S-wave velocities (Fig. 2). This event is also documented in garnet pyroxenites of Ronda Massif (Sánchez-Rodríguez and Gebauer, 2000) and by anatexis found associated to the initial emplacement of the Beni-Boussera peridotites during the Permo-Carboniferous (Rossetti *et al.*, 2020). Mafic-ultramafic xenoliths further argue for calc-alkaline Permian (ca. 257 Ma) magmatic underplating, for instance, in Massif Central (Féménias *et al.*, 2003).

Pressure-temperature estimates in Late Variscan gabbros or diorites and post-Variscan Permian alkaline magmatism (lamprophyre dykes) in Iberia reflect increasing depths of magma production from the garnet-spinel lherzolites field in the mantle lithosphere to the asthenospheric mantle (Orejana *et al.*, 2020). This late magmatic event could mark the transition towards the CAMP at ca. 200 Ma (Figs. 7 and 8) recognized in the same region of Spain (Cebriá *et al.*, 2003), announcing the onset of break-up of Pangea and the opening of the Central Atlantic at 190–175 Ma (Labails *et al.*, 2010; Olyphant *et al.*, 2017). The imprint of the Permian magmatic event in the mantle peridotites is particularly well recorded in the Alps and Apennines. Nd isotopic data in Ligurian ophiolites reveal a Permian 275–285 Ma depletion event in a Proterozoic (2–1 Ga) subcontinental mantle of Gondwanan (African) affinity (Rampone *et al.*, 1995, 1996; McCarthy and Müntener, 2015). The depleted Permian mantle formed in regions of partially melted asthenosphere, which after cooling became part of the Permian sub-continental mantle (McCarthy and Müntener, 2015; Picazo *et al.*, 2016). Asthenospheric upwelling related to extension and thinning during the Jurassic ca. 160 Ma is reflected in co-genetic gabbros and basalts with typical MORB composition (Kaczmarek *et al.*, 2007). A similar relationship is found in Corsica at ca. 162 Ma (Rampone *et al.*, 2009). In addition, the ascending melt can react with the old and Permian fertile spinel lherzolites, forming domains of refertilized plagioclase lherzolites (Müntener and Piccardo, 2003; Piccardo *et al.*, 2004). Grain-size reduction associated with melt-rock reaction is a potential softening mechanism, through grain-size sensitive (GSS) creep (Dijkstra *et al.*, 2002), during syn-magmatic extensional shearing (Kaczmarek and Müntener, 2008). The Pyrenean peridotites appear to be in a different situation. They are spinel lherzolites formed by asthenospheric melt-related refertilization of previously depleted harzburgites of an Archean (>2 Ga) mantle (Reisberg and Lorand, 1995; Roux *et al.*, 2007). The refertilization event is suggested to reflect the Late Variscan magmatic event (Fig. 7), contemporaneous with the emplacement of lower crustal granulite and occurred in spinel stability field at about 50 km. After thermal re-equilibration, the late amphibole-pyroxenite dykes show no evidence for widespread refertilization and rapid cooling at 104 Ma, contemporaneous with alkali basaltic lavas emplaced during the Cretaceous rifting (Fabries *et al.*, 1991; Henry *et al.*, 1998). Refertilization at the base of a 1.3–1.4 Ga subcontinental mantle (Reisberg *et al.*, 1989; Pearson and Nowell, 2004),

possibly as old as 1.6–1.8 Ga (Sánchez-Rodríguez and Gebauer, 2000; Marchesi *et al.*, 2010), by melt-rock reactions is also identified in Ronda lherzolites (Garrido and Bodinier, 1999) and the pyroxenites of Beni Bousera (Varas-Reus *et al.*, 2017) (Fig. 7). They have preserved the imprint of successive stages of exhumation from depths > 140 to 85 km by decompression and cooling from diamond field to graphite-garnet lherzolite facies (Garrido *et al.*, 2011). This occurred during the Jurassic (Wal and Vissers, 1993) as indicated by Early Jurassic to Late Jurassic-Early Cretaceous U-Pb zircon ages in garnet pyroxenites and eclogite (Sánchez-Rodríguez and Gebauer, 2000). This initial event was followed by cooling and exhumation, leading to garnet-spinel mylonite, high heat flow and partial melting at 21–22 Ma (Garrido *et al.*, 2011) (Figs. 7 and 8), likely linked to delamination of the Alboran slab seen in Figure 3, and responsible for the observed anomalous topography (Fig. 4) and thin lithosphere (Fig. 2). Despite recent melting, Re-Os dates on sulfides document preservation of melting events of the European-North African mantle at 1.6–1.8, 1.2–1.4 and 0.7–0.8 Ga (Marchesi *et al.*, 2010). Some similar Re-depletion ages from peridotite xenoliths of the Calatrava volcanic field (2 Ma) (González-Jiménez *et al.*, 2013) report the oldest mantle-crust magmatic events at ca. 1.6–2.0 Ga. Those ages are consistent with the original Paleoproterozoic mantle below W-Europe and N-Africa, related to Columbia supercontinent assembly. The crust and mantle were then remobilized at 600 Ma during the Cadomian orogeny and at 300 Ma during a melting event following the Hercynian orogeny. This pattern of Re-Os ages is shared by most Cenozoic magmatic provinces throughout Europe and northern Africa (*e.g.*, Massif Central, Rhenish Massif, Bohemian Massif, Pyrenees, Azrou) (González-Jiménez *et al.*, 2013). The eastern Betics and Beni Boussera Massif, Sicily and Adria, in contrast, appear to preserve an older Archean (2.2–2.6 Ga) lithospheric mantle.

3.2.4 Variscan to post-Variscan magmatic evolution on the northern margin of WAC

The Moroccan Variscan Belt driven by moderate convergence resulted from the inversion of the NW Gondwana margin. It was then displaced relative to its Iberian counterpart by large transcurrent movement during the Late Carboniferous (Mattauer *et al.*, 1972; Houari and Hoepffner, 2003) and Permian (Hoepffner *et al.*, 2006; Michard *et al.*, 2010) (Fig. 6), which significance and age are greatly debated for Pangea reconstruction (Domeier *et al.*, 2020). The Pan-African crust of Anti-Atlas was weakly overprinted by Late Variscan shortening (Helg *et al.*, 2004; Séverine *et al.*, 2004; Burkhard *et al.*, 2006). Pan-African granitoids (625–552 Ma) involved in the Variscan Belt (Moroccan Meseta) (Fig. 7) originally formed at the end of the Cadomian-Pan African orogeny. In the Central Meseta, Nd model ages of 0.8–1 Ga of Early Paleozoic gabbro, dolerites and rhyolites dated to Cambrian-Early Ordovician (519–479 Ma) reveal they have a relatively primitive signature (Ouabid *et al.*, 2020). This part of the Moroccan Meseta basement together with the Anti-Atlas formed the NW Gondwana rifted margin. In the Western Meseta, depleted Nd model ages from syntectonic Variscan ultramafic-granitoid magmatism, and calc-alkaline granitoids of the Jebilet Massif (330–300 Ma) reveal contribution from Proterozoic (1.7–0.8 Ga) and Eburnean crust (1.9 Ga), in addition to a juvenile mantle component (younger Nd model ages of 1.3–1.5 Ga). This evolution marks the progressive cessation of subduction and lithosphere delamination (Fig. 7).

Magmatism that occurred during Late Variscan transpressional stage produced increasing heat flux that caused partial-melting of the Proterozoic metasediments (Essaifi *et al.*, 2014). Carboniferous-Early Permian zircon U-Pb ages recovered from crustal xenoliths sampled in mafic Triassic (~ 235 Ma) lamprophyre dykes indicate that HT metamorphism may have been responsible for granite emplacement (Dostal *et al.*, 2005). Old zircons dated at ~ 2 Ga point to the presence of the Eburnean basement below the Jebilet Massif, indicating this domain was part of the NW Gondwana margin. Nd isotopic data from the same Triassic dykes yielded model ages of 0.6–0.8 Ga consistent with Pan-African/Cadomian magmatism. This Triassic magmatism correlates with other Late Permian (264–255 Ma) lamprophyres dykes, dolerites, and gabbros documented in the Tafilalt Basin of the Anti-Atlas sourced from a deep metasomatized mantle that heralds the CAMP event (Najih *et al.*, 2019).

The northern margin of the Anti-Atlas was reactivated during the Atlantic and Tethys rifting, as recorded in the High and Middle Atlas Rift systems in the Late Permian-Early Triassic to the Early Jurassic (Frizon de Lamotte *et al.*, 2008). Rifting was accompanied by widespread lava flows, sills and dykes of the CAMP (201 Ma), encompassing the Anti-Atlas, Central and High Atlas, and Western and Eastern Meseta (Marzoli *et al.*, 2019) (Fig. 8). Partial melting associated with Moroccan CAMP lavas occurred in the asthenospheric mantle between 110 and 55 km (Fig. 7), which is the range of lithosphere thickness inferred from geophysics (Fig. 2). It is characterized by relatively higher potential temperature (1430 °C) possibly triggered by a plume (Tegner *et al.*, 2019b). The combined effects of tectono-magmatic events are responsible for the sharp thickness difference observed on the northern margin of the African craton. This geometry in turn triggered small-scale edge-driven convection at the origin of episodic Cenozoic alkaline magmatism and high topography (Missenard and Cadoux, 2012; Kaislaniemi and van Hunen, 2014) (Fig. 7).

Younger Upper Jurassic to Lower Cretaceous and Cenozoic magmatic events are recognized in the High Atlas (Fig. 7). They are interpreted to reflect melting of the lithospheric mantle in areas previously affected by rifting and CAMP magmatism (Bensalah *et al.*, 2013). The region is marked by anorogenic Miocene to Quaternary alkaline volcanism that developed in a narrow SW-NE-trending corridor of thinned lithosphere and high heat flux dubbed the "Moroccan Hot Line" (Missenard *et al.*, 2006; Frizon de Lamotte *et al.*, 2009) (Figs. 6b, 7 and 8). Mantle xenoliths from Middle Atlas lavas show evidence for a metasomatized mantle (Wittig *et al.*, 2010a, 2010b; Malarkey *et al.*, 2011), indicating lavas derive from a 1.7 Ga residual mantle (Wittig *et al.*, 2010a). This age is consistent with Nd isotopic data from lherzolite and wehrlite xenoliths that reveal a Neo- to Paleo-Proterozoic depletion event (Raffone *et al.*, 2009). Detailed isotopic and trace elements analyses confirm these lavas formed by partial melting of a metasomatized mantle near the lithosphere-asthenosphere boundary at 65 km (Bosch *et al.*, 2014), a depth similar to the current lithosphere thickness. Refertilization of the lithosphere by alkaline melts is interpreted to indicate a flux of hot asthenospheric mantle,

induced by edge-driven convection in combination with enriched plume materials. This mechanism was probably effective since the Late Cretaceous and was enhanced during the Cenozoic by the retreat of the Alboran slab.

3.2.5 Summary: plume-related, subduction and rifting events in peri-Gondwana terranes

The succession of metasomatic and tectonic events in northern Gondwana, during the Neo-Proterozoic convergence (Cadomian arc), Ordovician rifting (back-arc extension), Late Paleozoic subduction and orogeny (Variscan collision) and Permian extension (Pangea breakup/Tethys opening) caused a marked thermo-chemical thinning of the SCLM, and the formation of a juvenile arc crust (Fig. 7). One can distinguish two main tectono-magmatic events that have profoundly thinned the SCLM. The first one is the Cadomian subduction and backarc rifting at 500–600 Ma, the second one is Pangea assembly and breakup in the Permian at about 270 Ma, which is the last main magmatic event and therefore should be considered as the tectono-thermal age of the lithosphere in Central Europe (Fig. 8). Chemical thinning has additionally been enhanced by mechanical removal of the SCLM during delamination (Fig. 7). In addition to these events, it has been proposed that the thermal insulation below Pangea supercontinent produced an increase of the potential temperature (up to 100 °C) of the convective mantle responsible for the CAMP event on the Atlantic margins and initial Pangea breakup (Wilson, 1997; Marzoli *et al.*, 1999a, 199b, 2004) at 200 Ma (McHone, 2000; Coltice *et al.*, 2007, 2009; Ganne *et al.*, 2016; Peace *et al.*, 2019), leading to final Central Atlantic breakup at ca. 185 Ma. The contribution of the Late Cenozoic subduction and delamination in the Mediterranean region to the current SCLM thickness cannot be ignored but is yet to be estimated.

3.3 Implications for lithosphere-asthenosphere and crust-mantle coupling

3.3.1 Strong plate-mantle and crust-mantle coupling of cratonized lithosphere

The structure of Baltica conforms well with the typical structure of a craton (Fig. 7). Based on Griffin and O'Reilly (2007), we follow Afonso *et al.* (2008) to suggest that Baltica is composed of two layers: 1) one shallow depleted Archean mantle layer (dunite/harzburgite) topped by spinel lherzolite (not represented in Fig. 7), and 2) a deeper Proterozoic refertilized layer, composed of depleted lherzolites in the garnet field, possibly overlying a melt-metasomatised layer in contact with the asthenosphere. Such depleted mantle is expected to be stable due to its buoyancy and high viscosities (10^{23}–10^{24} Pa.s) relative to the asthenosphere (Ghosh *et al.*, 2013; Wang *et al.*, 2015). Such high viscosities should result in larger plate-mantle coupling that, in addition to lower viscosities of Phanerozoic lithosphere, is required to explain plate motions and lithospheric stresses (Ghosh *et al.*, 2013). Such cratonic lithospheres are also cold (900° C on average, Vs = 4.7; see also Fig. 2c) and thick (250 km or more; see Fig. 2b) according to global average (Poudjom Djomani *et al.*, 2001; Lee *et al.*, 2001; Carlson *et al.*, 2005).

In Figure 9, we show the compositional layering of the lithosphere of Europe inferred from data presented previously for both a stable Archean lithosphere of 3 Ga and a Phanerozoic lithosphere of 300 Ma (right panels in Figs. 9A and 9B). The depth-dependent rheology (viscosity) and temperature profiles calculated for these two lithospheres are also presented (left panels in Figs. 9A and 9B) (see Mouthereau *et al.*, 2013 and Supplementary File S1 for calculation of the temperature profiles). Based on the continental geotherm calculated, we derive the corresponding yield stress profiles. A homogeneous brittle property of rocks is assumed for the upper part of the lithosphere (Byerlee's law of rock failure) and the ductile-viscous term is represented by non-linear power law with three sets of material parameters that correspond to the properties of four lithological layers: upper crust (wet quartzite), lower crust (diabase), mantle and asthenosphere (olivine) (see Supplementary File S1 for the governing equations and rheological parameters material properties). The yield stress profile is then converted to an effective viscous profile to compare with viscosity values inferred from global models that include convection (*e.g.*, Ghosh *et al.*, 2013) using the relation $\eta_{\mathrm{eff}} = \frac{\Delta\sigma}{\dot{\epsilon}}$ where $\Delta\sigma$ is the deviatoric stress and $\dot{\epsilon}$ the background strain rates fixed to $10^{-15}\,\mathrm{s}^{-1}$.

The continental geotherm for the Archean lithosphere assumes a lithosphere thickness of 250 km. Note that thermal models of the continental lithosphere suggest that 400–700 Myrs are required for the thermal structure to become stationary (*e.g.*, Burov and Diament, 1995; using conductive cooling for an equilibrium thermal thickness of 250 km). So we must consider the Archean cratonic lithosphere as thermally equilibrated. We predict a Moho temperature of ~400 °C at 30 km (Fig. 9A) consistent with T_{Moho} of 350–500 °C estimated based on modelling of heat flow in the East European Craton (Čermák and Bodri, 1986). The calculated mantle heat flow is 13 mW/m^2 in the range of values derived from xenoliths (Kukkonen and Peltonen, 1999) for Fennoscandia, and more generally in agreement with heat flow studies showing that the mantle heat flux is 15 mW/m^2 or lower for Archean cratons (Jaupart *et al.*, 2015). The large viscosity of 10^{24} Pa.s estimated at 100–110 km (Figs. 9A and 9C) is consistent with geophysical constraints for the Archean-Proterozoic lithosphere of Baltica that is defined by a stiff lithosphere with high effective thickness larger than 80 km (Fig. 2) (Pérez-Gussinyé *et al.*, 2004).

Baltica has been thinned on its margin by thermal erosion and addition of alkaline plume-related magmas at ca. 615 Ma. This event triggered rifting between Laurentia and Baltica, leading to the opening of the Iapetus (Tegner *et al.*, 2019a) and Tornquist Sea. These refertilization events increase the density and weaken the cratonic lithospheric mantle by addition of water or other volatile elements and melts. The newly formed lithosphere on the edge of Baltica became prone to strain localization during subsequent tectonic stages. Plume-related magmatism provided the necessary conditions for subduction initiation and building of the Caledonian orogen. Together with Baltica margin, Avalonia is represented by a thinner and younger lithospheric mantle (Fig. 7). We infer it is formed by less depleted Proterozoic mantle represented by garnet-bearing lherzolite topped by spinel-bearing lherzolite. The thinner

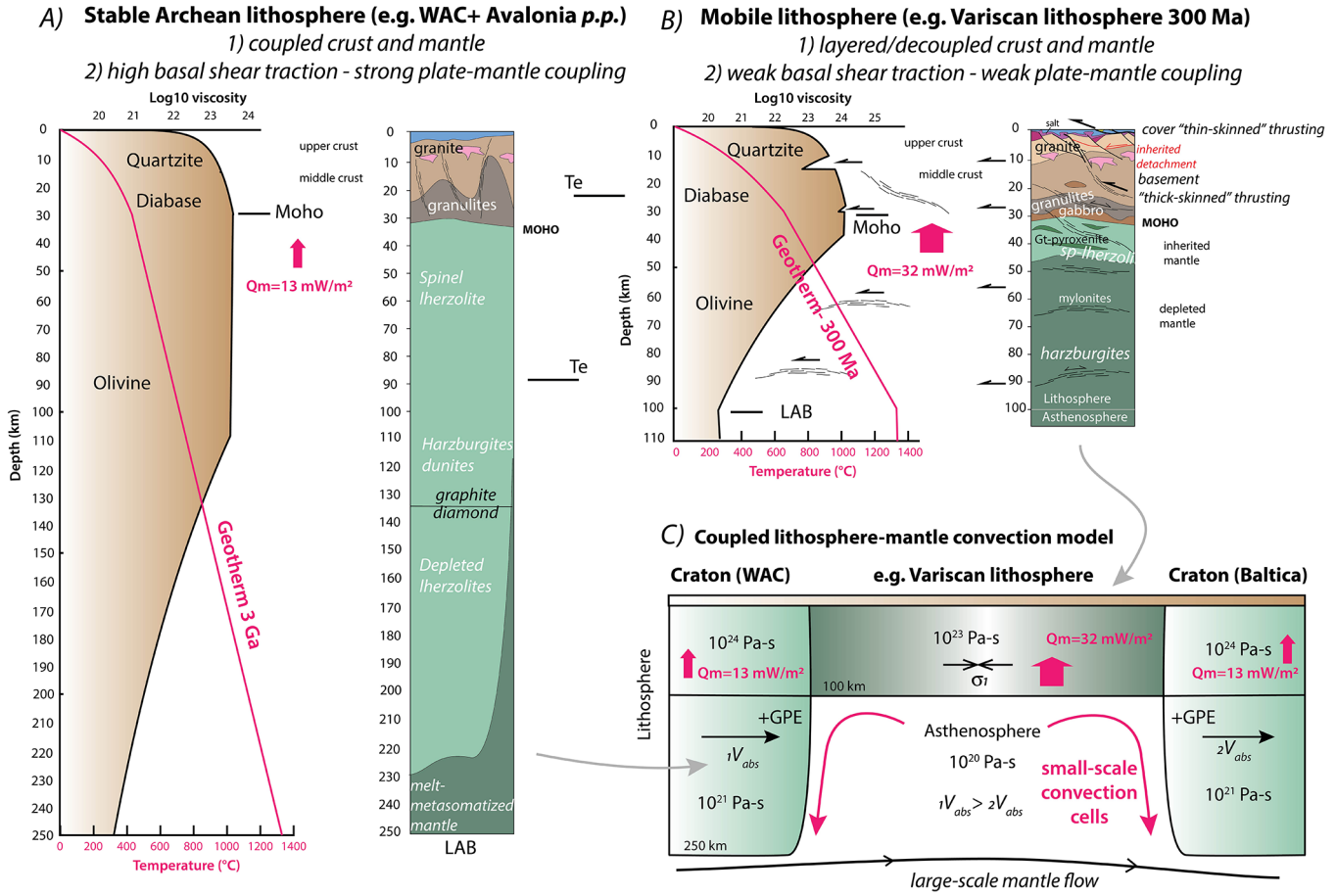

Fig. 9. Age-dependent rheology profiles (viscosity) for (A) Archean Baltica/Reguibat shield (Paleo-Proterozoic margins) and (B) Phanerozoic lithosphere involved in Africa-Europe convergence. Thickness, temperature and composition determine the depths and numbers of mechanical decoupling levels in crust and mantle. These two contrasting rheological profiled ultimately define lateral viscosity profiles that reproduce well the first order pattern of current stresses and basal traction exerted by mantle flow at the base of the continents (C). The mantle heat flux Qm is larger for the Phanerozoic lithosphere to explain the lack of thermal relaxation.

lithospheric mantle is assumed less viscous at its base, implying a weaker plate-mantle coupling for Avalonia compared to Baltica. The lack of crustal deformation however suggests that crust and mantle remained coupled during the Mesozoic and the Cenozoic, which is arguably related to low Moho temperatures of 400–500 °C (Fig. 9A).

3.3.2 Variscan and post-Variscan lithosphere: weak plate-mantle coupling and crust-mantle coupling

It is expected that the cumulative effect of tectonics, metamorphism and magmatism from 1–2 Ga to ca. 300 Ma and locally as young as 21–22 Ma resulted in considerable mechanical weakening of the lithosphere of Central Europe (Fig. 9B). The addition of volatiles during subduction, the incorporation of weak and hydrous minerals (*e.g.*, plagioclase or serpentines) during Paleozoic and the Mesozoic rifting combined with the transient inputs of heat from the mantle together contributed to reduce the strength of the lithosphere. These successive events left a lithologically anisotropic crust and mantle with a thin layer of old and refractory mantle preserved in the uppermost mantle (Figs. 7 and 9B). Thermomagmatic thinning during the Early Jurassic CAMP magmatic event (Fig. 8), then from Late Cretaceous to Quaternary associated with alkaline volcanism from Europe to High Atlas, suggest a continuous rising of sub-alkaline melts in the hot asthenosphere. These heating events acted collectively to increase the mantle heat flux. We therefore anticipate the European lithosphere was not appreciably thermally relaxed after the Variscan orogeny (300 Ma) and remained weak until present, as shown by the low elastic thickness of about 20 km (Fig. 2d).

To provide a first-order picture of the 300 Ma-lithosphere rheology, we adopt in Figure 9B the same approach as for cratons to obtain the geotherm and the viscosity profile but for a lithosphere thickness of 100 km (Supplementary File S1), which corresponds to the average LAB depth deduced from geophysical constraints (Fig. 2b). This implies that the lithosphere did not change thickness over the past 300 Ma at the regional scale. Because this also means the lithosphere did not cool, the mantle heat flow must increase to adjust to the new boundary conditions. A greater output from the mantle is indeed expected due to the relatively recent tectonic and magmatic activity. We predict a present-day T_{Moho} of about 650 °C, and mantle heat flow of 32 mW/m^2. Such high temperatures agree with Moho temperature of ~550–650 °C

(Müntener *et al.*, 2000) estimated in the Variscan basement during the Jurassic. There is also an abundant literature on mantle mylonites formed at 800–900 °C in the spinel and plagioclase field (30–80 km), including those found at Lherz, Ronda and Lanzo (Precigout *et al.*, 2007). These results indicate a mobile mantle and a higher temperature gradients relative to Archean cratonic mantle. Our predicted temperatures in the uppermost mantle (30–80 km) vary between 650 and 1100 °C. They are in the range of temperatures defined in mantle mylonites that are thought to have developed during the Jurassic-Cretaceous rifting or earlier during the Permian. These data collectively lend support to the stationary thermal structure of the European lithosphere over the past 300 Myr.

One main implication of our modelling is the requirement of long-lived contrasting mantle heat flux between the Phanerozoic lithosphere of Europe and the adjacent cratons. In our view this reflects the contributions of 1) small-scale convection cells triggered by lateral temperature/buoyancy contrasts on craton margins similar to edge-driven convection (*e.g.*, King and Anderson, 1998), 2) asthenospheric flow triggered by rift propagation (*e.g.*, Mondy *et al.*, 2017) during the Mesozoic (Atlantic, Tethys) combined with thermal insulation below Pangea at the origin of plume-related inputs (*e.g.*, CAMP), and 3) slab-induced mantle flow for the most recent tectonic evolution of the region (*e.g.*, Faccenna and Becker, 2010). In addition, the positive feedbacks between short scale convection cells and the whole mantle convection could have also contributed to produce the higher heat flow below Central Europe.

Based on inferences from global models of lithosphere-mantle coupling (Ghosh *et al.*, 2013; Wang *et al.*, 2019) and in accordance with our viscosity profiles (Fig. 9) this type of relatively young lithosphere appears low viscous (*e.g.*, 10^{23} Pa.s) relative to cratons (10^{24} Pa.s) and weakly coupled to the low viscosity asthenospheric channel (10^{20} Pa.s). We infer that both buoyant cratonic lithospheres (WAC and cratonic core of Baltica, Karelia) are acting as lithospheric buttresses and strongly coupled to the asthenosphere. They build-up stresses and localize strain in regions formed by the lithosphere of peri-Gondwanan terranes that is hotter and weaker (Fig. 9C).

These results strengthen the view that the margins of cratons are long-lived zones of weakness that localize deformation during the Wilson cycle (Audet and Bürgmann, 2011). Here we further demonstrate that such weak lithospheres are made of a tectonically sheared, ductile and compositionally heterogenous mantle (Fig. 9B). Because of the weak coupling between crust and mantle, and their weak mantle roots, the Phanerozoic lithospheres preferably deform during compression by thick-skinned tectonics (Mouthereau *et al.*, 2013). This explains the widespread occurrences of Variscan basement involvement in the external domains of mountain belts like in the Alps or the Pyrenees (Lacombe and Mouthereau, 2002; Mouthereau *et al.*, 2013, 2014; Bellahsen *et al.*, 2014; Jourdon *et al.*, 2019).

3.4 lithospheric cross-section of Europe accounting for mantle composition and architecture

To provide a precise structural framework for crust and mantle evolution and architecture summarized in Figures 7 and 9, a lithosphere-scale geological section has been established (Figs. 10 and 11). This novel 4000 km-long structural cross-section stretches across Europe and North Africa. We have adopted interpretations from seismic reflection programs that imaged the crustal structure of Europe such as the IBERSEIS in Spain (Simancas *et al.*, 2003; Carbonell *et al.*, 2004), ECORS in France (Bois and Party, 1990), DEKORP in Germany (Heinrichs *et al.*, 1994; Dekorp Basin Research Group, 1999), and international initiative like EUROPROBE and BABEL experiments in different countries across the Trans-European Suture Zone (TESZ) and the Baltic Sea (Babel Working Group, 1993). This was accompanied with more local seismic campaigns and geophysical acquisition that were integrated in geological interpretations labeled “a” to “m” in Figure 10. Moho depths and LAB depths are inferred from data presented in Figure 2. These regional sections were then projected onto our transect to form a composite lithospheric section at the scale of Europe. For instance, we have projected the ECORS seismic sections obtained across the Armorican Massif “i” and “j” and merged it with section “k” and “l” of the Rhenish Massif to connect with DEKORP section from the Harz Mountains and German Basin to the TESZ and Baltic Sea. Where offsets still persist after merging, our section was completed based on our own interpretations. By the addition of constraints on the laterally variable mantle depletion ages, crustal and lithosphere thicknesses, our section does not overlap, and rather complement, with earlier lithosphere scale sections published across the Mediterranean region in the TRANSMED Atlas (Cavazza *et al.*, 2004).

Figure 10 first depicts lithosphere thinning below peri-Gondwanan (Cadomia) terranes documented by geophysical constraints (Fig. 2) and our synthesis of the tectonic and magmatic evolution (Fig. 7). Mantle thinning correlates with the depletion ages younger than 1 Ga, locally falling below 0.3 Ga, reflecting the significant thermal erosion and chemical overprint during the successive Cadomian subduction, Variscan subduction and Late Variscan-Permian post-Pangean heating event (see also Fig. 9). It should also be noted that the lithosphere thinning most affects lithospheres that were involved in the Variscan orogeny. Avalonia, in contrast, preserves an older and variably thicker mantle, about 100 km close to Armorica but is nearly 200 km when approaching the TESZ. Northern Africa depicts strong lithospheric attenuation across the transition from Anti-Atlas to High-Atlas. This limit seems to overlap with the position of CAMP and more recent Cenozoic magmatism. This is responsible for drastic mantle thinning from 250 km below the Reguibat Shield to less than 100 km below the High Atlas (Fig. 2b). These observations suggest an age- and depth-dependence on mantle thinning controlled by melt-enhanced weakening during successive subduction, extension and delamination. The Late Variscan dextral strike-slip faulting (Fig. 6) appears to have been preferentially localized in these weak domains leading to the segmentation of peri-Gondwanan terranes in the Atlas, Rif and the Betics, in Iberia (Iberian Range, Pyrenees) and further north along the northern Variscan front near the TESZ. The addition of plume-related volatile-enriched magma (CAMP) in the Early Jurassic enhanced or maintained this process of lithosphere thinning initiated in the Late Variscan. Magmatism was active until recently as indicated by Cenozoic magmatic from Morocco (“Moroccan Hot Line”) in the south, through Spain (Calatrava, Olot), Massif Central, up North associated

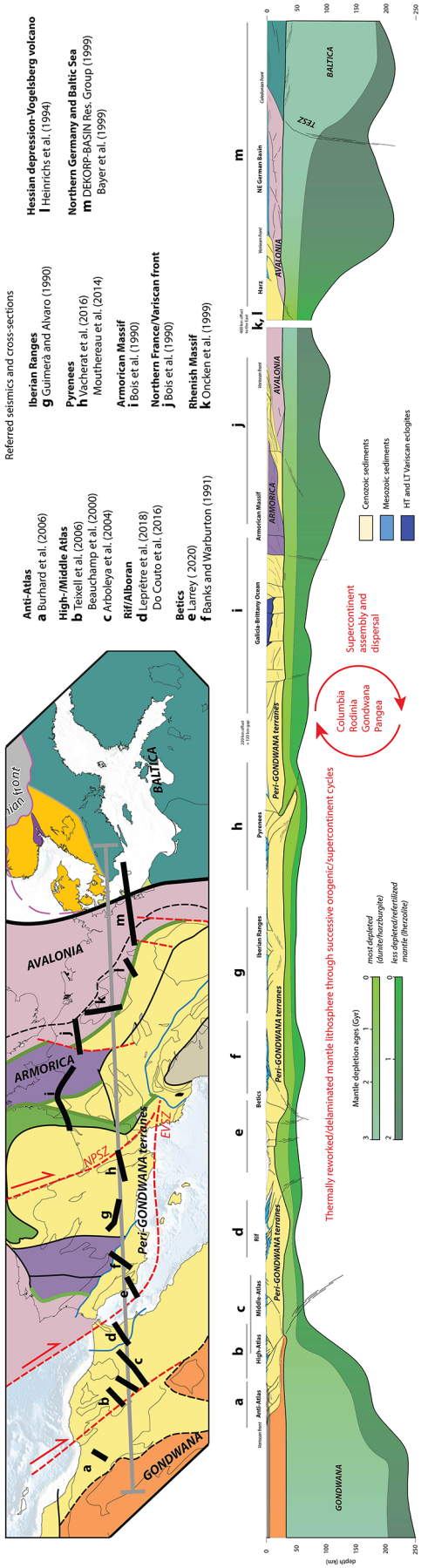

Fig. 10. Geological section of Western Europe showing the affinity of continental crust to Gondwana, Avalonia, Armorica (same color-coded crust as Fig. 6) as well as information on mantle depletion ages with color code identical to that of Figure 7. Referred seismics and cross-sections are after (Bois and Party, 1990; Guimera and Alvaro, 1990; Banks and Warburton, 1991; Heinrichs *et al.*, 1994; Bayer *et al.*, 1999; Beauchamp *et al.*, 1999; Oncken *et al.*, 1999; Dekorp Basin Research Group, 1999; Teixell *et al.*, 2003; Arboleya *et al.*, 2004; Burkhard *et al.*, 2006; Mouthereau *et al.*, 2014; Do Couto *et al.*, 2016; Vacherat *et al.*, 2016; Leprêtre *et al.*, 2018; Larrey, 2020).

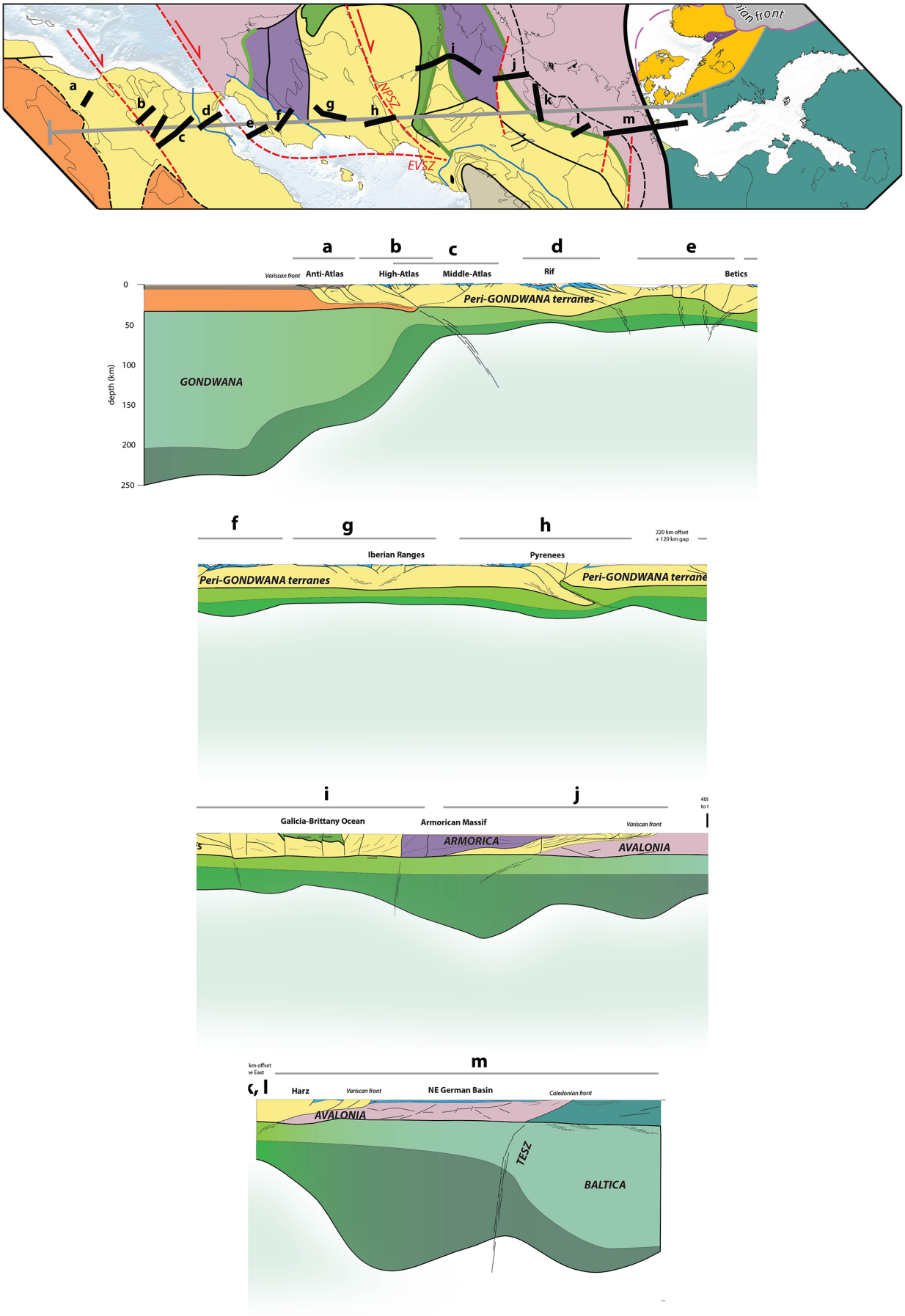

Fig. 11. Details of cross-section presented in Figure 10.

with the Cenozoic volcanic province in the Germany (Vogelsberg, Eger Massif) and Bohemian Massif.

From a tectonic perspective, Figure 11 reveals that lithosphere deformation involves decoupling levels in the crustal basement and mantle. This is indicated by crustal thrust ramps rooting into the middle and lower crust and below in mantle ductile shear zones. The observation of vertically distributed strain between crust and mantle is expected for Phanerozoic lithosphere (Mouthereau *et al.*, 2013) and is consistent with the weak crust-mantle coupling triggered by the thin and hot mantle lithosphere of Central Europe (Fig. 9).

Despite peri-Gondwanan terranes may be considered to first-order rheologically similar, orogenic deformation does not appear to be accommodated by a continuous mid- or lower crustal detachment. Instead the orogenic systems are discontinuous, reflecting additional weakening processes and strain localization in Mesozoic Rift domains (Atlas, Rif-Betics, Iberian Ranges, Pyrenees) possibly triggered by Late Variscan strike-slip faulting that accompanied the earliest stages of opening of the Tethys at the initiation of the Alpine cycle (*e.g.*, Angrand *et al.*, 2020). Crustal thinning and mantle exhumation during Alpine Tethys and Atlantic Rift evolution were also determinant. Among the important weakening processes is the transformation of the exhumed mantle in the plagioclase facies by melt-rock interactions (Chenin *et al.*, 2018).

4 Spatial and temporal constraints on orogenic evolution in Europe: inferences from low-temperature thermochronology

We have established in Sections 2 and 3 the relationships that exist between the structure of the lithosphere and its tectonic and magmatic evolution (*e.g.*, Figs. 2 and 7). In addition, the present-day topography of Europe has been suggested to reflect the long-term evolution of the continental lithosphere. Indeed, low-elevation and low-relief regions (Fig. 4) correspond to the stable Archean craton characterized by low mantle heat flux and strong coupling between and crust and mantle (Fig. 9). On the opposite, the Phanerozoic lithosphere, involved in the Variscan and Alpine orogenic cycles, is defined by high heat flow and weak crust-mantle coupling (Fig. 9) and shows the highest elevations and reliefs (Fig. 4). In this section, our main objective is to decipher the topographic evolution of Europe during the Cenozoic in order to further discuss the relationships with the lithosphere architecture.

4.1 Strategy

Low-temperature thermochronology resolves cooling histories of upper crustal rocks from which exhumation in orogenic systems can be inferred. Although exhumation does not equal surface uplift, the rates at which exhumation/cooling occur may be used as a proxy for the timing of uplift in orogens. Here, we use the onset of acceleration of cooling rates to define the periods of topographic uplift. The apatite fission-track (AFT) thermochronometer that has closure temperature of 80–120 °C is less sensitive to deep tectonic processes and hence appears suitable to resolve cooling/erosion of rocks in the upper 3–4 km (assuming thermal gradients of 25–30 °C/km) and therefore uplift.

It must be reminded that cooling in orogens may be complex due to the architecture and the thermal regime inherited from the rifted margin thermal evolution, especially during the first stages of collision. In their coupled thermo-mechanical and thermochronological models of inverted rifted margin, Ternois *et al.* (2021) have distinguished two periods of cooling (Fig. 12). The first period corresponds to the onset of the tectonic inversion on the hyper-extended distal margin that is controlled by processes other than erosion, including post-rift thermal relaxation accentuated by the inversion-induced downward deflection of the isotherm. In their study, Mesalles *et al.* (2014) indeed demonstrated cooling of mid-crustal rocks in incipient submarine accretionary prism. In case post-rift cooling is compensated by heating caused by sediment burial, as recorded in the Pyrenees, the initial cooling is not observed. An isothermal cooling stage is recorded instead (Vacherat *et al.*, 2014). Note that erosion caused by submarine current is documented in young emergent orogens like Taiwan and are associated with dynamic reorganization of the drainage system (Giletycz *et al.*, 2015; Das *et al.*, 2021) but these processes do not result in recordable exhumation by low-temperature data. In practice, we have searched to isolate the period of orogenic growth when topography is compensated by a crustal root and its evolution coupled with surface erosion, by determining the timing of first acceleration of cooling after plate convergence onset (*i.e.*, 84 Ma). We selected sampling sites along our 4000 km-long transect so as to make a homogeneous dataset based on sites sharing a common thermochronometer, that is AFT (some sites also contains zircon fission-track and U-Th/He data), which T-t paths are computed using the same numerical models QTQt or HeFTy (Ketcham, 2005; Gallagher *et al.*, 2009; Gallagher, 2012). Timing of first major cooling events and cooling rates were then calculated for each path (Fig. 13). Strong variations may be observed along a single orogenic segment due to model resolution and specific factor related to the sequence of thrusting. To account for these variations while keeping the main picture of the time-integrated orogenic evolution, we plot our results as boxplot graphs by calculating minimum, quartiles Q1 (25%) and Q3(75%), median and maximum ages of maximum cooling rates (Fig. 13; see also Supplementary Material Figure S2). In practice, we have focused our study in regions of Variscan basement that present AFT ages younger than 80 Ma. We have excluded time-temperature histories that were obtained for regions too far from our transect, like the Alps, the Apennines and the Dinarides. Independent information on regional and local tectonics and sedimentary record have allowed to further identify and discuss the potential modulation of the cooling record by climate, fluid circulation and non-isostatic component on crustal cooling and exhumation. We first review the AFT ages record in each tectonic provinces of Europe (Figs. 14 and 15). Published time-temperature paths are then analysed to obtain the timing of increased erosion from which a topographic evolution can be defined.

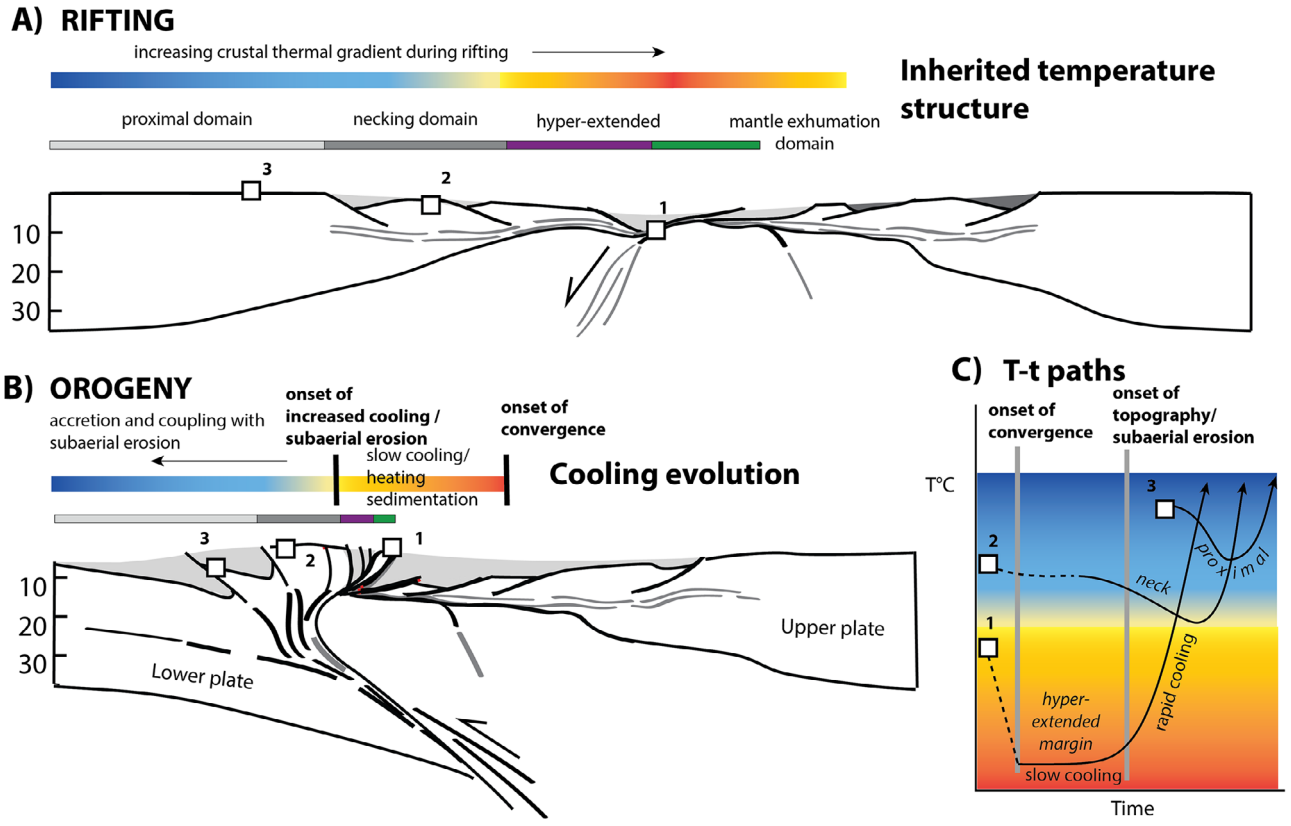

Fig. 12. Cooling evolution that results from the inversion of rifted margin (A), leading to the formation of a doubly-vergent orogen (B) (modified after Ternois *et al.*, 2021). Cooling paths are shown for particles labelled 1, 2 and 3 located on the lower plate during building of the orogenic wedge. Time-temperature paths shown in (C) have been constrained based on thermo-mechanical modelling of rift inversion (Jourdon *et al.*, 2019). Cooling evolution reflects transition from initial accretion of the hot distal margin to accretion of cooler proximal/neck zone and increased coupling with erosion.

4.2 Apatite fission-track data across Europe and North Africa

To examine the spatial and temporal topographic evolution of the European lithosphere, we have compiled 5440 apatite-fission track (AFT) ages from magmatic rocks or reset sedimentary rocks from Western Europe and Northern Africa (Fig. 14a and Supplementary File S2). The thermochronogical dataset builds on a previous global compilation (Herman *et al.*, 2014), complemented by recent studies and a novel compilation made for the OROGEN project.

AFT ages range between 16 Ma (Q1 = 25%, first lower quartile) and 160 Ma (Q3 = 75%, third upper quartile), with the lowest value of 1.7 Ma recovered from gneiss of the Aar-Gotthard Massifs (Michalski and Soom, 1990) and upper bounds at 1027 Ma are found in gabbro of Fennoscandia shield from southern Finland (Kohn *et al.*, 2009). To limit our discussion to the lithosphere tectono-thermal events we have interpolated AFT data within a 1000 km search radius (Fig. 14b) and contoured data according to geologically meaningful ages of 250, 150, 80 and 30 Ma.

Rocks carrying AFT ages older than or close to 250 Ma indicate they preserve Paleozoic and even earlier Precambrian cooling events. These old AFT ages are documented close to or within the cratonic areas of the WAC in eastern Reguibat Shield (Leprêtre *et al.*, 2017) and the Baltic shield, in southern Sweden (Cederbom *et al.*, 2000) or southern Finland (Kohn *et al.*, 2009) (Figs. 14 and 15). They are also recognized in northern Scotland and northern Ireland (Green, 1989; McCulloch, 1993; Allen *et al.*, 2002) of the Laurentian and Caledonian domains. Those ages are therefore found preferentially in regions of Europe defined by thick lithosphere and low thermal flux (see Figs. 2 and 9).

They reveal very slow cooling in continental domains that remained poorly affected by exhumation (below 3 km) or magmatism during to Mesozoic rifting and Cenozoic collision phases, but with some possible imprints by the Late Carboniferous-Permian magmatism (Fig. 8).

AFT dataset ranging between 250 Ma and 80 Ma indicates cooling histories related to periods of Mesozoic rifting in Western Europe (Figs. 14 and 15). We have recast our data relative to 150 Ma to allow distinction between the thermal evolution associated with Central Atlantic/Alpine Tethys rifting and the younger events related to the southern North Atlantic opening and Pyrenean rifting.

Rocks with ages between 250 Ma and 150 Ma are widespread in Europe. They are present from UK, Ireland, Southern Norway and Sweden to western France (*e.g.*, Armorica Massif, Massif Central, Ardennes), Spain (Galicia, Central system) and in the domain extending between

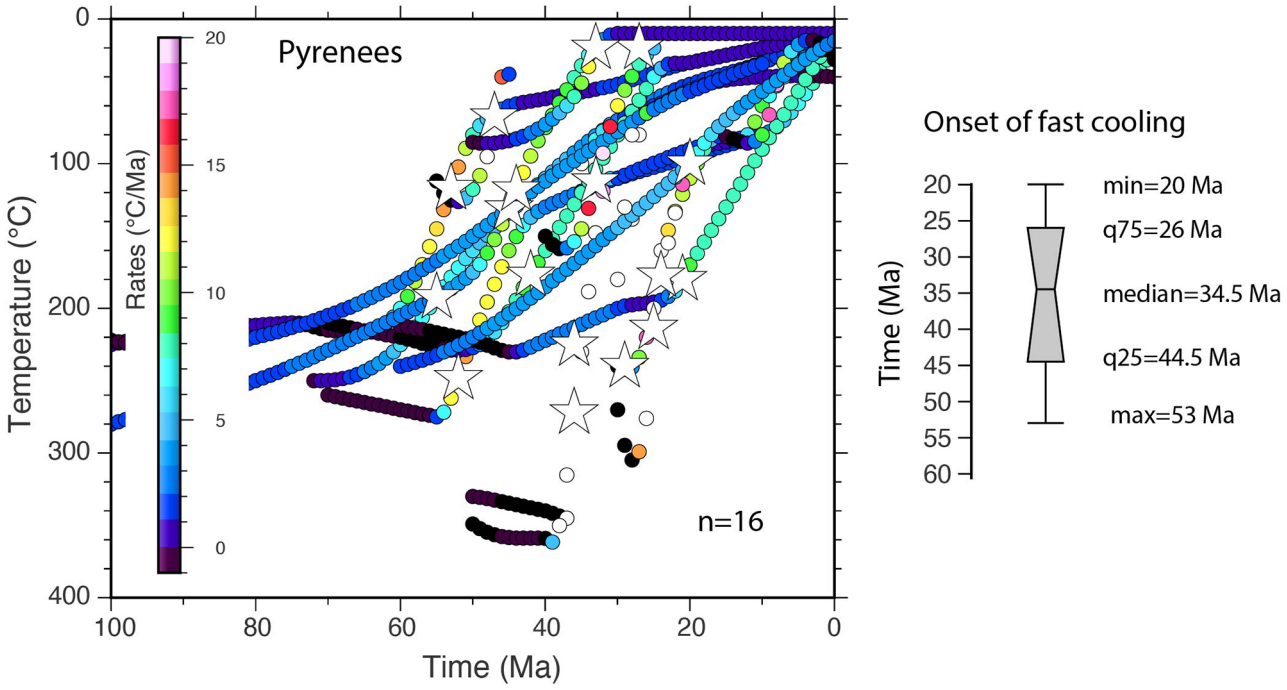

Fig. 13. Principle of the analysis of published cooling paths (n = 16) with example taken from the Pyrenees. Left: Cooling paths are colored as a function of cooling rates. Stars depict the time of maximum cooling that is assumed to reflect the period of orogenic growth and exhumation. Right: box-plot showing temporal distribution of exhumation maximum. From this we infer that exhumation reached a climax between 44.5 and 26 Ma, which correspond to the time at which orogenic topography and crustal root developed. In this example model cooling histories are after (Gunnell *et al.*, 2009; Bosch *et al.*, 2016; Vacherat *et al.*, 2016; Fillon *et al.*, 2021; Waldner *et al.*, 2021).

WAC and the High Atlas (Fig. 14). These ages reflect tectono-thermal events that temporally overlap with the timing of initial rifting in the north-central Atlantic and in the Alpine Tethys (Ligurian Tethys) (Fig. 15). The attribution of AFT ages to either of these two rift phases is challenging. In Morocco, for instance, the distinction between the different tectonic events may be particularly difficult as the Moroccan Atlas and Rif also recorded CAMP (201 Ma) magmatic event that overlaps with Late Permian-Early Triassic and the Early Jurassic rifting (Frizon de Lamotte *et al.*, 2008; Marzoli *et al.*, 2019), thus leading to controversial interpretations (Gimeno-Vives *et al.*, 2019, 2020; Michard *et al.*, 2020). This problem has also been raised in the Iberia peninsula based on zircon fission-track thermochronology (Rat *et al.*, 2019).

Besides, the thermal imprint of the Alpine collision (Alps, Apennines, Dinarides) is so large that the pre-collisional cooling ages from the Tethyan paleomargin are generally not preserved. Some studies, however, have reported AFT ages consistent with the Alpine Tethys evolution, such as in Sardinia (Malusà *et al.*, 2016) or Catalan Coastal Range (Juez-Larré and Andriessen, 2006). In summary, the distribution of AFT ages in the 250–150 Ma range shows affinity with regions surrounding Avalonia and peri-Gondwana terranes (Cadomia-Iberia, Armorica), and in particular with the Variscan Belt in France and Spain (Fig. 14). They are therefore correlated with thin lithospheric domains characterized by LAB shallower 150–100 km, higher mantle heat flow and a metasomatism mantle (Figs. 2, 7 and 9).

The domain comprising AFT ages between 150 and 80 Ma includes rocks that recorded cooling during a transitional period between the Early Cretaceous rifting and the onset of convergence between Africa and Europe (Figs. 14 and 15). They are found associated with: 1) the major Alpine orogenic systems in North Africa, western Iberia and Pyrenees; 2) the Massif Central (Peyaud *et al.*, 2005; Barbarand *et al.*, 2020), the Rhine graben (Timar-Geng *et al.*, 2005; Dresmann *et al.*, 2008), and are found spatially correlated with the mid-Cretaceous Vocontian and south Provence Basins (Graciansky and Lemoine, 1988) and the Helvetic Alps (Cardello and Mancktelow, 2014; Tavani *et al.*, 2018); 3) Ireland and Central West Britain where these ages reveal cooling associated with the emplacement of the Icelandic plume and magmatism (Cogné *et al.*, 2016).

AFT ages between 80 and 30 Ma are distributed in regions that recorded syn-orogenic exhumation during the AF/EU plate convergence. They are found in the High Atlas, Iberian Range, Pyrenees and Provence, and Corsica-Sardinia and the Alps (Fig. 14). Variscan Massifs preserve Late Cretaceous to Early Cenozoic AFT ages like the Black Forest and Vosges (Timar-Geng *et al.*, 2005), Harz Mountains (Eynatten *et al.*, 2019), Holy-Cross Mountains (Botor *et al.*, 2018), Sudetes/Bohemian Massif (Botor *et al.*, 2019), south Carpathians (Fügenschuh and Schmid, 2005) and eastern Carpathians (Gröger *et al.*, 2008).

We have also distinguished orogenic domains with AFT ages younger than 30 Ma. This is a period of major tectonic

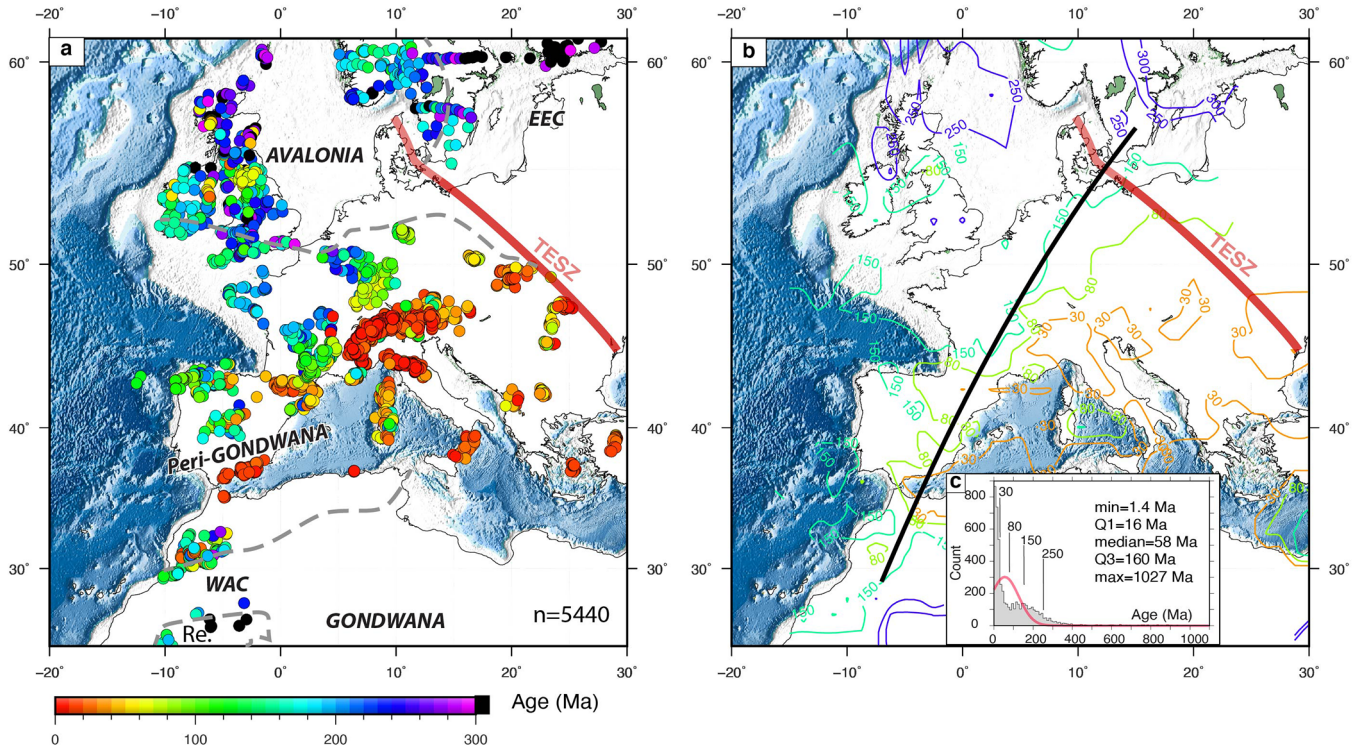

Fig. 14. Distribution of apatite fission-track (AFT) cooling ages in Western Europe and northern Africa (a) based on a compilation of 5440 analyses (see Repository). Colored contour lines of AFT ages from the interpolation of individual dates in (a) based on 1000 km search radius. (c) Histogram with 10 Ma bins and Gaussian distribution (red) centered on the median with L1 scale of AFT age. (c) Minimum, quartiles Q1(25%) and Q3(75%), median and maximum of AFT data. Lines labeled 1 and 2 correspond to sections in Figure 15. TESZ: Trans-European Suture Zone.

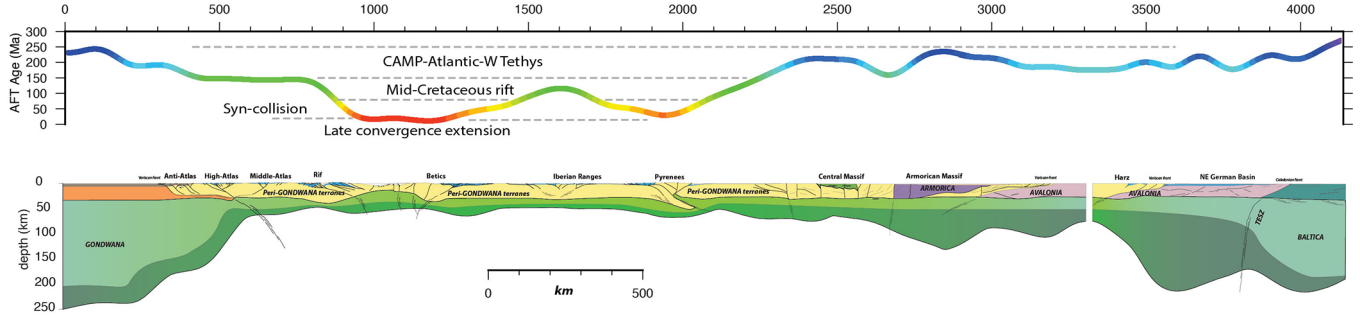

Fig. 15. Distribution of apatite fission-track (AFT) age after data gridding extracted along profile 1 (see location in Fig. 12), same color coded as Figure 12. Below is the structural section of reference presented in Figures 10 and 11.

reorganisation in western Mediterranean region that resulted in the formation of the Mediterranean arcs, including the Apennines, Betic-Rif, Maghrebides, Carpathians, southern Dinarides and external Hellenides controlled by the dynamics of retreating slabs (Royden and Faccenna, 2018). AFT younger than 30 Ma are found also in older collisional orogens like the Pyrenees, the High Atlas, the Alps and sporadically in the Cantabrians, the Iberian Central System. Northern Europe is not affected by this late cooling.

The distribution of syn-collision (80–30 Ma) to late-post-orogenic (< 30 Ma) AFT ages and to a lesser extent the ones in the 150–80 Ma range depict along our transect (Fig. 15) a good match with the thinnest, youngest and less depleted lithosphere (Figs. 1 and 2), stretching between the southern Massif Central and the Rif-Betic region. Outside of that domain (see also Figs. 6 and 14), the lithosphere of Avalonia north of the Variscan front (Fig. 15) shows a majority of old, pre-Alpine AFT ages. Below we focus on cooling and exhumation events in the region containing the syn-collision AFT ages that predominantly correlates with the peri-Gondwanan lithosphere.

4.2.1 Late Cretaceous-Paleogene cooling and exhumation in Harz Mountains, Sudetes and Vosges-Black Forest

Late and post-Variscan basement (Carboniferous, Permian) exposed in the Bohemian Massif and Harz Mountains are

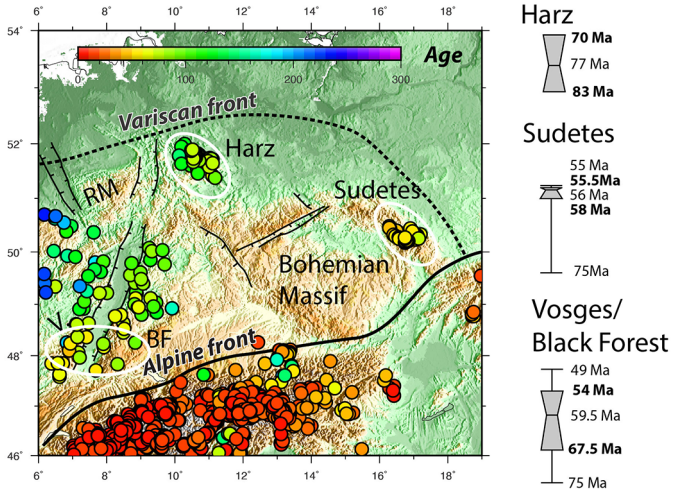

Fig. 16. AFT ages in Western-Central Europe and distribution of the timing of maximum post-mid-Late Mesozoic cooling/exhumation in Harz Mountains, Sudetes and Vosges-Black Forest. This timing inferred from modeled cooling histories is considered to reflect the period of main Cenozoic topographic growth. Cooling histories used in our study are (Timar-Geng *et al.*, 2005; Eynatten *et al.*, 2019; Sobczyk *et al.*, 2020).

covered by thin and discontinuous Jurassic and Early Cretaceous rocks. After a period of erosion and weathering, subsidence resumed during the Late Cretaceous forming the Subhercynian Cretaceous Basin (Voigt *et al.*, 2006) in Germany and the Bohemian Cretaceous Basin. In the Sudetes, low-temperature thermochronological data indicate that the Late Carboniferous-Permian basement underwent a burial of ca. 6.5 km during the Late Cretaceous followed by exhumation at 85–70 Ma (Danišík *et al.*, 2012). This exhumation is associated with the Late Cretaceous-Paleogene far-field compression and intraplate tectonic inversion of Mesozoic Rift Basins recognized in central Europe (Mazur *et al.*, 2005; Kley and Voigt, 2008). To precise the timing of cooling we have compiled time-temperature paths published from the Harz Mountains, Sudetes and Vosges Massif (Fig. 16).

Time-temperature paths in the Harz Mountains show cooling from 85–86 Ma contemporaneous with the deposition of syn-tectonic Coniacian-Santonian strata in the footwall of the inverted Harz Mountains (Voigt *et al.*, 2006). The maximum cooling is recorded between 83 and 70 Ma at rates of 4–12 °C/Ma (Eynatten *et al.*, 2019) equivalent to exhumation of 0.1–0.4 km/Ma (assuming thermal gradient of 30 °C/km).

Carboniferous gneiss dome from NE Bohemian Massif in the Sudetes recorded mid-Triassic to mid-Cretaceous erosion and burial in the Late Cretaceous that formed the Bohemian Basin and the intra-Sudetic Basin. Time-temperature paths indicate maximum cooling occurred between 58 and 55.5 Ma (1–6 °C/Myr or 0.03–0.2 km/Myrs) although exhumation started as early as 75 Ma (Sobczyk *et al.*, 2020). Thermal modelling of AFT data from the intra-Sudetic Basin also documents initial cooling in the Late Cretaceous at 89–72 Ma (Botor *et al.*, 2019) with maximum cooling between 60 and 50 Ma with 3–4 km of cumulated erosion since the Cenomanian. An earlier stage of exhumation at 85–75 Ma is indicated by a phase of rapid cooling from 120 °C in the northern Saxo-Bohemian Massif (Mid-German Crystalline rise) (Thomson and Zeh, 2000). The Lusatian block located north of the ENE-WSW-directed Eger graben also reveals an acceleration of exhumation between 95 and 70 Ma (Ventura *et al.*, 2009). This Upper Cretaceous event slightly predates an early magmatic pulse at 68–59 Ma centered in the Eger graben (Ulrych *et al.*, 2008), which is part of the Late Cretaceous to Cenozoic Central European Volcanic Province. The region then recorded the Eocene extensional phase and magmatism of the West-European Rift from ca. 42 Ma to 16 Ma (Dèzes *et al.*, 2004; Ulrych *et al.*, 2011). Volcanic activity has continued until the Quaternary in the Eifel volcanic field of the Rhenish Massif (Goes *et al.*, 2000; Schmincke, 2007; Meier *et al.*, 2016).

Cooling history of the Variscan basement in the Vosges and Black Forest was impacted by high geothermal gradients (Timar-Geng *et al.*, 2005). During Late Jurassic, the temperature evolution of the Vosges and Black Forest Massif is interpreted to reflect hydrothermalism, uplift and tectonic inversion of Variscan structures (Dresmann *et al.*, 2008). Two more phases of cooling dated to the Late Cretaceous-Paleogene and the Bartonian-Priabonian are also reported (Timar-Geng *et al.*, 2005). The latter Late Eocene phase of cooling is interpreted to result from denudation associated with rift flank uplift during the formation of the Upper Rhine Rift (Danišík *et al.*, 2010). An earlier episode of heating related to magmatism and initial subsidence is also reported during the Lutetian. Ages of maximum cooling from the first Late Cretaceous-Paleogene event are constrained to range between 67 and 54 Ma (Fig. 16). These ages are comparable with the earliest magmatic event dated to 60 Ma (Keller *et al.*, 2002), that is attributed to rifting (Hinsken *et al.*, 2007). Time-temperature paths show onset of cooling as early as 80–70 Ma, with some cooling paths indicating acceleration at 75 Ma (Fig. 16). Low-temperature constraints from the Ardennes Massif (Barbarand *et al.*, 2018) document a Late Jurassic-Early Cretaceous exhumation event but Cenozoic exhumation remained very limited.

In our view, there is no significant difference in the timing of initial fast cooling recorded in the Harz Mountains, the Bohemian Massif and the Vosges Massif. Exhumation started at 80–70 Ma then increased in the Paleogene at ca. 55–50 Ma. The topographic fingerprint of the AF/EU convergence in Western-Central Europe likely reached a climax in the Paleocene-Eocene, that is slightly before, or synchronous with, the onset of extension and magmatism associated with the Central European Volcanic Province. A terminal Miocene (post-Burdigalian) topographic uplift in the Vosges-Black Forest is indicated by the occurrence of Burdigalian shallow-marine sediments of the Upper Marine Molasse (Giamboni *et al.*, 2004; Hinsken *et al.*, 2007). It temporally correlates with the establishment of the Kaiserstuhl volcanic complex at 18–16 Ma. At a larger scale it coincides with the Miocene plume-related volcanic event documented in Western Europe that is closely related to the previous Eocene Rift system.

4.2.2 Cooling histories in Massif Central, Pyrenees, Cameros, Sardinia

The Massif Central is characterized by contrasting crustal cooling histories that have been synthesized in a number of

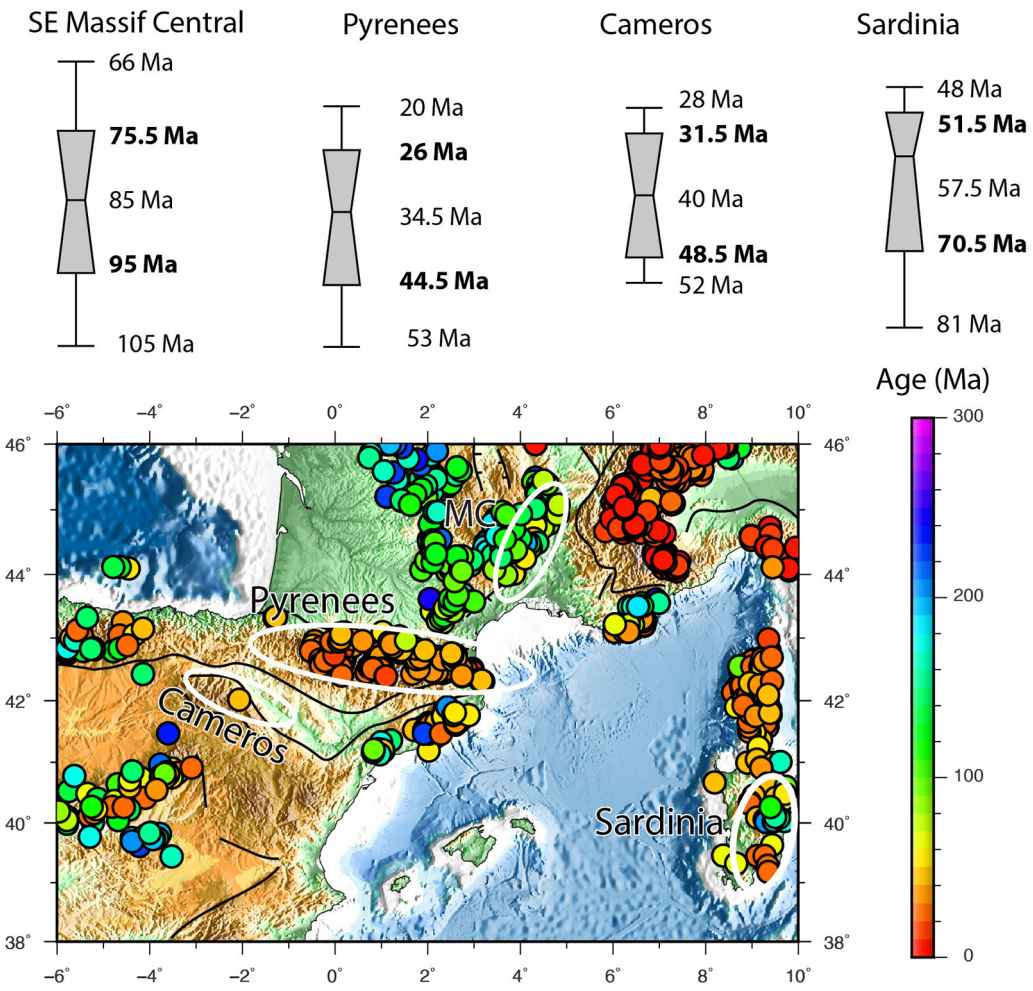

Fig. 17. AFT ages in Western Europe and distribution of the timing of maximum post-mid-Late Mesozoic cooling/exhumation in SE Massif Central, Pyrenees, Cameros and Sardinia. This timing inferred from modeled cooling histories is considered to reflect the period of main Cenozoic topographic growth. Cooling histories are after (Gunnell *et al.*, 2009; Río *et al.*, 2009; Bosch *et al.*, 2016; Malusà *et al.*, 2016; Vacherat *et al.*, 2016; Rat *et al.*, 2019; Olivetti *et al.*, 2020; Fillon *et al.*, 2021; Waldner *et al.*, 2021).

recent papers (Barbarand *et al.*, 2001, 2013, 2020; François *et al.*, 2020; Olivetti *et al.*, 2020). These studies shows that while the western Massif Central (Limousin, Vendée, Rouerge) depicts AFT ages generally much older than 100 Ma, its eastern and southern margins (Morvan, Cévennes, Montagne Noire) are defined by ages younger than 100 Ma, often Late Cretaceous (Olivetti *et al.*, 2020).

AFT data analyses from the Variscan basement exposed in the Morvan Massif, south of Paris Basin, reveal a Late Cretaceous-Paleocene exhumation event (65–50 Ma) (Barbarand *et al.*, 2013). Time-temperature constraints from the eastern Massif Central (Olivetti *et al.*, 2020) reflect an interval of maximum cooling ranging between 95 to 75 Ma at rates 3–5 °C/Myrs (0.1–0.15 km/Myrs), which is transitional between the mid-Cretaceous rifting and the onset of tectonic inversion of the margin during the Pyrenean-Provençal orogenic event (Fig. 17). Despite the Late Cretaceous exhumation event, topographic reconstruction on the southern margin of the Massif Central (Cévennes) argued for a post-34 Ma uplift based on preservation of marine sediments until Late Eocene (Lettéron *et al.*, 2018; Olivetti *et al.*, 2020) or Early Oligocene in the Velay region (Turland *et al.*, 1994), which is not well resolved by AFT data (Barbarand *et al.*, 2001). As for the Vosges-Black Forest Massif and other regions of the Central Europe Magmatic Province, magmatism and extension-related topography affected the Massif Central. Pre-extension magmatism occurred as early as 62–57 Ma, then increased during the Late Eocene-Lower Miocene rifting episode that formed the Limagne graben (37–22 Ma) and renewed mostly between 9–6 Ma and 3.5–0.5 Ma with the emplacement of the Chaîne des Puys (Michon and Merle, 2001). Plume-like volcanism has been suggested to result from shallow mantle upwelling triggered by decompressional melting pockets ahead and around Ionian retreating slab (Faccenna *et al.*, 2010). Post-Miocene (post 13–11 Ma) surface uplift and erosion are documented in the Massif Central (Olivetti *et al.*, 2016; Fauquette *et al.*, 2020) likely associated with late-stage volcanism and ongoing plate convergence.

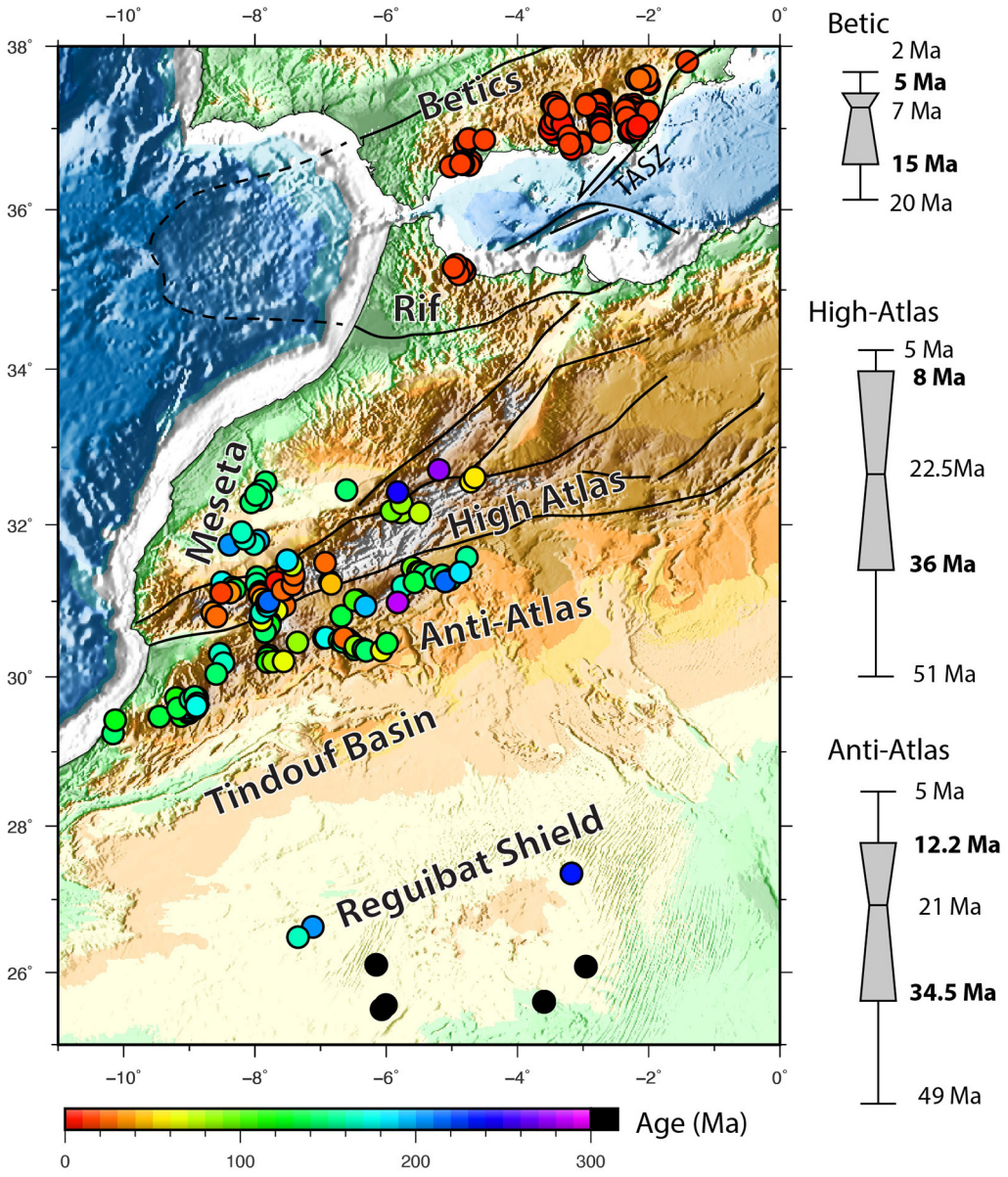

Fig. 18. AFT ages in Western Europe and distribution of the timing of maximum post-mid-Late Mesozoic cooling/exhumation in SE Massif Central, Pyrenees, Cameros and Sardinia. This timing inferred from modeled cooling histories is considered to reflect the period of main Cenozoic topographic growth. Data for Anti-Atlas are from (Malusà *et al.*, 2007; Ruiz *et al.*, 2011; Oukassou *et al.*, 2013; Sehrt *et al.*, 2017), for High Atlas after (Barbero *et al.*, 2007; Balestrieri *et al.*, 2009; Leprêtre *et al.*, 2018), Betics (Vázquez *et al.*, 2011; Janowski *et al.*, 2017; Daudet *et al.*, 2020).

Along the transect, the Pyrenean Belt has been the target of numerous low-temperature thermochronology studies with only a few of them providing AFT-based time-temperatures paths in Variscan basement modeled with QTQt or HeFty (Bosch *et al.*, 2016; Vacherat *et al.*, 2016; Fillon *et al.*, 2021). Cooling histories from the Axial Zone reveal a period of maximum exhumation between 44 and 26 Ma at rates of 10–30 °C/Myr (0.5–1 km/Myr), punctually reaching 100 °C/Myr (3 km/Myr), one of the fastest erosion rates measured along our transect (Fig. 17).

Different paleoaltitude estimates confirm that the topography of the Pyrenees formed in the Bartonian-Priabonian 41–34 Ma (Huyghe *et al.*, 2012; Curry *et al.*, 2019). The growth of orogenic topography therefore postdates a long-lasting phase of progressive accretion initiated at 70–75 Ma in Central Pyrenees (Mouthereau *et al.*, 2014). Modelling of the inversion of a salt-rich hyper-extended margins reproduces well such long delays between the onset of collision and the rise of orogenic topography (Mouthereau *et al.*, 2014; Jourdon *et al.*, 2020a). Alternatively, the time delay could mirror the duration of the deformation event in the most distal part of the margin until the inversion of the necking and proximal domains occurs (*e.g.*, Mouthereau *et al.*, 2014; Mesalles *et al.*, 2014; Vacherat *et al.*, 2014; Ternois *et al.*, 2021). A late post-orogenic uplift is well identified in the last 10 Myr synchronous with an uplift of 500 m detected in the eastern Pyrenees (Suc and Fauquette,

2012; Huyghe *et al.*, 2020), and the late post-orogenic exhumation of about 1 km linked to reactivation of Mesozoic rift-related crustal architecture in the West (Fillon *et al.*, 2021). But this post-10 Ma uplift seems to have been large-scale as inferred by post-tectonic piedmont erosion of nearly 2 km in the southern Pyrenees in the last 9 Ma (Fillon and Beek, 2012; Fillon *et al.*, 2013) and based on ca. 600 m of fluvial incision of the Ebro Basin (Garcia-Castellanos and Larrasoaña, 2015). The drivers of this large-scale uplift are debated as they may include different ingredients such as asthenospheric temperature anomaly below Iberia (Conway-Jones *et al.*, 2019), long-term dynamic support in eastern Pyrenees caused by lithosphere thinning and magmatism trapped in the lithosphere during the opening of Gulf of Lion (Huyghe *et al.*, 2020). Another mechanism not specific to the Pyrenees may alternatively explain a dynamic support such as the subduction-related plume-like magmatism during Ionian slab retreat (Faccenna *et al.*, 2010).

Time-temperature constraints in the Iberian Range are limited to the Cameros Basin because only the syn-rift Late Jurassic-Early Cretaceous sediments were sufficiently heated (up to 300 °C) for AFT data to record Cenozoic cooling (Río *et al.*, 2009; Rat *et al.*, 2019). Exhumation started at 60–50 Ma, and rates of exhumation reached a climax between 48.5 and 31.5 Ma (Fig. 17). These results are consistent with cooling history of the Pyrenees although maximum cooling rates of 2–12 °C/Ma (0.2–0.4 km/Myr) are noticeably lower. Movements along the Cameros main thrust may have lasted until the Tortonian. After ~ 9 Ma post-tectonic erosion occurred (Rat *et al.*, 2019). A larger-scale mantle contribution to uplift has been suggested for Iberia possibly explaining the post-30 Ma exhumation in mountain belt including the Iberian Ranges and the Pyrenees (Conway-Jones *et al.*, 2019). The long-lasting shortening inferred from geological data also argues that crustal orogenic processes are at play, perhaps combined with lithospheric and sublithospheric processes.

We have also included results from Sardinia. Based on published cooling histories we infer that acceleration of exhumation occurred between 70 and 51 Ma at rates between 4 and 8 °C/Ma (0.1–0.2 km/Ma) (Fig. 17). This is consistent with a Late Paleocene to Middle Eocene phase of contraction recognized in Sardinia and Corsica (Dieni *et al.*, 2008). These cooling ages further reveal that Sardinia preserves exhumation stages related to the onset of convergence and has not been affected by the rapid post-50 Ma exhumation documented in the Pyrenees. A counterclockwise rotation of Sardinia of 45° relative to Europe has been proposed between 50 and 30 Ma based on paleomagnetic data (Advokaat *et al.*, 2014) that could explain this difference. Alternatively, the preservation of Sardinia from Pyrenean crustal thickening and exhumation could be related to the southern paleoposition of Sardinia at distance from the mid-Cretaceous Pyrenean Rift (*e.g.*, Angrand and Mouthereau, 2021). Magmatism in Sardinia is dated from 38 to 12 Ma (Lustrino *et al.*, 2009) and was contemporaneous with early extension in the Mediterranean Sea and opening of the Gulf of Lion.

4.2.3 Cooling histories in the Betics, High-Atlas and Anti-Atlas

The Betic-Rif arc formed in response to Neogene tectonic reorganization along the margins of Africa and Iberia imposed by west-directed delaminated slab retreat, tearing and slab detachment. AFT ages are much younger than the surrounding domains of North Africa (Atlas) and northward in the Iberian Range (Fig. 18). Thermal modelling of low-temperature data from the Betic-Rif reveals increased exhumation of the Variscan basement from 20 Ma (Sierra de Gador; (Janowski *et al.*, 2017)), 15 Ma in the Rif (Romagny *et al.*, 2014) and 6 Ma (Sierra Nevada; (Vázquez *et al.*, 2011)) at rates up to 40–54 °C/km (equivalent to 1.3–1.8 km/Ma). This timing agrees with other geochronological constraints from higher temperature thermochronometers that reveal a high-temperature event ca. 20 Ma and rapid cooling of 200 °C/Ma (Platt *et al.*, 2003). The Miocene tectonic event has overprinted older, subduction-related Late Eocene-Early Oligocene events (Monié and Chopin, 1991; Bessière *et al.*, 2021). An older contractional event has been reported ca. 50 Ma based on thermal evolution of accreted Cretaceous flysch sediments (Daudet *et al.*, 2020). A Paleocene-Eocene cooling event is also in good agreement with the formation of a Paleogene Foreland Basin onto the Iberian margin, reflecting the development of an orogenic topography. A widespread pre-Oligocene erosional surface is recognized in many places of the Western Mediterranean, including the Balearic promontory, Valencia Basin, Sardinia and Corsica. This large-scale uplift event and erosion is arguably related to the growth of pre-Alboran topography when the region recorded increasing shortening (see Sect. 5 below). This proto-Betic orogenic stage ended before the Burdigalian ca. 20 Ma which marks the onset of widespread extension and HT metamorphism in the region.

Post-20 Ma exhumation of the Betics reported from thermochronology is independently inferred based on the occurrence of Late Tortonian marine platform, 7.2 Ma in age, now at an elevation of 1600 m in the eastern Betics (Braga *et al.*, 2003; Janowski *et al.*, 2017). This late uplift is contemporaneous with the onset of contraction both onshore (Weijermars *et al.*, 2007; Do Couto *et al.*, 2014; Giaconia *et al.*, 2014), and offshore in the Alboran domain (Martínez-García *et al.*, 2017). Quaternary erosion rates of 0.14–0.4 km/Myr inferred from river terraces (Geach *et al.*, 2015; Larrey *et al.*, 2020) reveal that uplift is still ongoing and likely associated with active strike-faulting along the Trans-Alboran Shear Zone (Fig. 18). The Tortonian uplift is synchronous with slab detachment under the Iberia margin that triggered anorogenic alkaline magmatism (11–7 Ma and up to 18.5 Ma) (Duggen *et al.*, 2004). This type of volcanism is well recorded in whole Western Europe and includes in Iberia the Valencia Trough (~ 24–0.01 Ma), Calatrava Volcanic Province (~ 9–2 Ma) and Olot–Garrotxa (~ 10–0.01 Ma) in Catalonia. Older 16–29 Ma carbonate-rich alkaline magmas are also reported for Calatrava (Villaseca *et al.*, 2018).

The High Atlas results from the inversion of a Late Permian-Early Triassic to Early Jurassic Rift. A first local contractional episode is documented in the Late Cretaceous (post-Turonian) (Guiraud *et al.*, 2005) but orogenic topographic did not develop before the Bartonian-Priabonian (41–35 Ma) (Froitzheim *et al.*, 1988; Frizon de Lamotte *et al.*, 2008, 2009). Ages of 51 Ma and 36 Ma argue for increasing cooling/exhumation (Fig. 18). In addition to initial Eocene cooling, young dates of 8–5 Ma resolved by both AFT and apatite (U-Th)/He data reveal a second stage of exhumation. This second episode of uplift is contemporaneous with

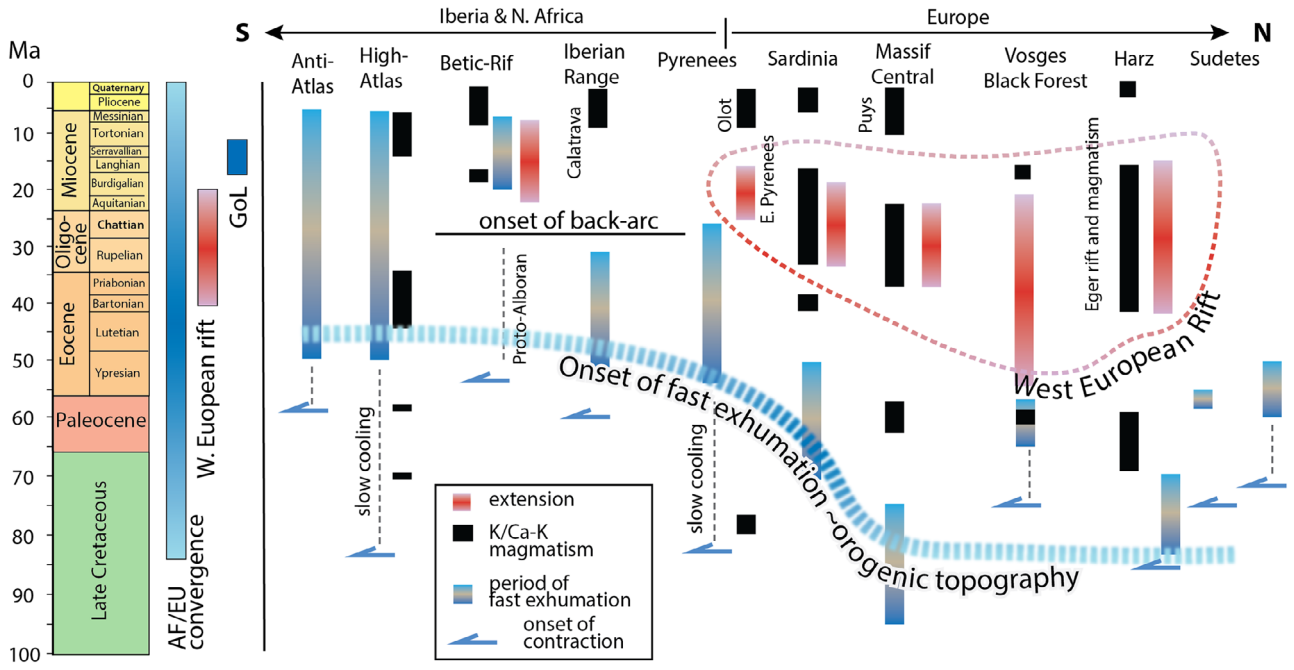

Fig. 19. Timing of contraction, period of orogenic growth as inferred from thermochronology and comparison with the main tectonic events that occurred in Central and Western Europe. Timing of AF/EU convergence, West European rifting, spreading in the Gulf of Lion are indicated.

mid-Miocene to Pliocene alkaline magmatism (15–6 Ma) (Harmand and Cantagrel, 1984) related to thermal erosion of the lithosphere (Missenard *et al.*, 2006). About the possible drivers, a combination of Canary plume-like magmatism and delaminated slab below Alboran has been proposed (Duggen *et al.*, 2003, 2009). We note that the magmatic influx in northern Morocco also occurred at 35 Ma at Azrou in Middle Atlas (Raffone *et al.*, 2009) and 44–33 Ma at Tamazert in High Atlas (Bouabdellah *et al.*, 2010), which is temporally synchronous with the early magmas emplaced during the formation of the Western European Rift. This suggests that part of the older exhumation signal might be related to this older magmatism. Cooling rates are on average close to 2–3 °C/Ma (< 0.1 km/Ma) but can reach up to 15–20 °C/Ma (about 0.5 km/Ma).

AFT ages in the Anti-Atlas are often older than in the High Atlas. Thermal evolution of the western Anti-Atlas and Tarfaya Basin indicates a component of heating and cooling during the Atlantic rifting (Ruiz *et al.*, 2011; Sehrt *et al.*, 2017, 2018). To the east, AFT analyses by Malusà *et al.* (2007) supplemented by apatite (U-Th)/He data from Ruiz *et al.* (2011) allow to resolve a recent Neogene-Pliocene cooling event at 12 and 5 Ma. Cooling paths further support an onset of Paleogene cooling 65–55 Ma (Sehrt *et al.*, 2017) but peaks in exhumation are not achieved before 49 Ma. Acceleration of exhumation occurred in Late Eocene-Early Oligocene contemporaneous with exhumation in the High Atlas. Cooling rates are 3–4 °C/Ma (about 0.1 km/Ma) throughout the Anti-Atlas indicating limited cumulated total exhumation of 1–3 km throughout the Late Cretaceous and the Cenozoic. The Reguibat Shield to the south shows Paleozoic to Jurassic and Cretaceous AFT ages. It has been suggested based on AHe data that this part of the WAC has experienced uplift and slow erosion related to Atlantic rifting and CAMP event (Leprêtre *et al.*, 2014; Leprêtre *et al.*, 2015).

4.2.4 Timeline of Cenozoic exhumation and tectonic events in peri-Gondwanan terranes

Figure 19 presents a synthesis of the exhumation events recognized in the young Phanerozoic lithosphere and their relationships with the Cenozoic tectonic and magmatic evolution of Western Europe and northern Africa. Geological data first confirm that contractional deformation spread rapidly after the onset of AF/EU plate convergence over Western and Central Europe and Northern Africa, between 80 and 60 Ma. One exception is the Massif Central, where the fastest exhumation occurred at 105–95 Ma. During mid-/Late Cretaceous the interactions of Europe with the east-moving Iberian blocks and northward drift of Adria may explain sporadic contraction and extension in the region (Angrand and Mouthereau, 2021).

One of the most striking results is depicted by the difference in the timing of fast exhumation between northern and southern Europe. We distinguish a north-eastern Europe domain, including Sardinia, defined by rapid exhumation synchronous with, or 10 Myrs after, onset of convergence and contraction. To the south-west, in a domain encompassing the Pyrenees (but excluding the eastern Pyrenees), Iberia and North Africa, fast exhumation is distinctively younger. In High Atlas and the Pyrenees, for instance, rapid exhumation starts from 50 Ma, which is ~ 30 Myrs after the onset of contraction. The acceleration of Africa/Eurasia convergence is arguably one main driver of this large-scale evolution. Alternatively, the onset of fast exhumation may reveal the inversion of buoyant and thicker proximal domains of rifted margin combined with subaerial erosion as for the Pyrenees (Fig. 12; Jourdon *et al.*, 2019; Ternois *et al.*, 2021). The shortening of thin and presumably hot crust of hyper-extended rift domains that did not lead to subaerial topography is not recorded by

low-temperature thermochronology data in the basement. This period has been resolved successfully by thermochronological analyses conducted on inverted Late Jurassic to Cretaceous Rift Basins (Whitchurch *et al.*, 2011; Mouthereau *et al.*, 2014; Vacherat *et al.*, 2014; Rat *et al.*, 2019; Daudet *et al.*, 2020). Western and eastern domains can be tectonically distinguished during the Eocene-Oligocene time (Fig. 19). The eastern domain is affected by extension and magmatism related to the opening the Western European Rift, whereas in the western domain the signature of extension is limited to sporadic magmatic pulses. The contrasting evolution appears to be geographically coincident with the transition between Alps (Adria) and Pyrenees (Iberia) which separation was effective after 35–30 Ma.

5 Plate kinematics of Africa-Eurasia convergence

We have shown in the previous sections that the architecture of the European lithosphere linked to the thermo-chemical evolution of its mantle exerts a first-order control on the topographic evolution of the collision between Africa and Europe (Figs. 14 and 15). In addition, exhumation patterns indicate this is the crustal architecture of the young, weak and mobile Phanerozoic lithosphere, inherited from episodes of rifting, that determine details of the topographic evolution during the earlier stages of convergence (Fig. 19). The latest stages of mountain building were however perturbed by the onset of the Western European Rift and the opening of the Mediterranean Sea. We have also demonstrated that plate-mantle coupling differs in Europe according to the thickness and the degree of depletion of the lithospheric mantle (Fig. 9). In this section, we explore the kinematic evolution of the AF/EU plate boundary from rifting to collision in order to discuss the respective roles of the lithosphere architecture and variations in plate-mantle coupling on the topographic evolution.

5.1 Current kinematics and stress patterns across Africa-Europe plate boundary: linking lithosphere evolution to plate-mantle coupling

The present-day absolute motions calculated in Western Europe from a No-Net-Rotation kinematic model, MORVEL56 (DeMets *et al.*, 2010; Argus *et al.*, 2011) show Africa (AF) or Nubia moving in the N40°E direction at a rate of 2.4–3 cm/yr and Eurasia (EU) in the N40-60°E direction at 2.1–2.3 cm/yr (Fig. 20). Using the same MORVEL model, inferred velocities of Africa relative to Europe illustrated in Figure 20a reveal the N-S convergence are the largest, up to 9.5 mm/yr, in the eastern Mediterranean, reducing to ~ 5 mm/yr in western Mediterranean. Along the Hellenic trench, where the Mesozoic Neo-Tethys Ocean is subducting, the fast Nubia plate subducting velocities of 4 cm/yr (Serpelloni *et al.*, 2013; Faccenna *et al.*, 2014) produces deep earthquakes down to 200 km. In the western Mediterranean, seismogenic deformation is concentrated on continental margins in the Maghreb and in Betic-Rif regions, south of Iberia, associated with NNW-directed AF/EU velocities that progressively align westwards parallel to the Gloria–Azores transform zone, in the Atlantic.

GPS velocities further reveal Anatolia-Aegea, Adria and Alboran, positioned along the Africa(Nubia)-Eurasia plate boundary, are moving independently from Africa (Fig. 20b). Surface movements of Adria and Anatolia-Aegea microplates in particular are well reproduced by a combination of plate convergence and uppermost mantle flow model, emphasizing the role of slab-induced flow in addition to long-wavelength mantle density anomalies (Faccenna and Becker, 2010). West-directed movements of Alboran Basin relative to Africa and Iberia indicate extrusion of an Alboran block (Koulali *et al.*, 2011; Nocquet, 2012; Palano *et al.*, 2015), along strike-slip shear domains in the Betics and the Trans-Alboran Shear Zone. Away from the plate boundary zone that accumulates strain and generates large earthquakes on tectonically-loaded faults, there is a much wider domain encompassing most of Europe, characterized by no significant GPS displacements (below 0.2 mm/yr) and devoid of earthquakes. This large domain defines a relatively stable Europe continental interior, where tectonic activity is not ruled by strain accumulation on faults and rapid stress increase (Calais *et al.*, 2016). Current crustal maximum horizontal stress (σ_{Hmax}) from the WSM2016 database shows a homogeneous compressional pattern oriented NNW-SSE to NW-SE (Fig. 20c), N145°E on average, parallel to shortening defined by stress inversion of focal mechanisms and GPS data (Heidbach *et al.*, 2018; Martínez-Garzón *et al.*, 2019). They are in good agreement with the relative plate AF/EU motion, and GPS data but at 90° to the APM (Fig. 20a). For comparison, stresses calculated from dynamic models combining plate convection and gravitational potential energy (GPE) calculated from lateral density variations and lithosphere thickness (Ghosh *et al.*, 2013) (see also Fig. 9) define a most compressional stress oriented parallel to σ_{Hmax} (Fig. 20c). It has been inferred that the European lithosphere can support statically significant deviatoric stresses over long geological intervals independent of transient stress loading/unloading at AF/EU plate boundary (Calais *et al.*, 2016). These results support the fact this is the coupling between age-dependent properties (composition and rheology) of the continental lithosphere (Fig. 9) and the vigor of convection that modulates stress and strain distribution in collision zones.

5.2 Kinematic reconstruction across the Africa-Europe plate boundary

5.2.1 new reconstruction accounting for Iberia plate fragmentation

The kinematic reconstruction of the Africa-Eurasia plate boundary in the Mesozoic-Cenozoic period is debated, especially regarding 1) the evolution of fragmented Adria and Iberia microcontinents, which moved independently from Africa, and 2) the nature, size and lateral extent of the Alpine Tethys between Africa, Iberia, Adria and Europe (Handy *et al.*, 2010, 2015; Le Breton *et al.*, 2017; van Hinsbergen *et al.*, 2019a, 2019b; Müller *et al.*, 2019; Angrand *et al.*, 2020; Romagny *et al.*, 2020). We present below the evolution of the Africa-Eurasia convergence based on the reconstructions of Angrand *et al.* (2020) and Angrand and Mouthereau (2021). This reconstruction has several specific features with respect to previous kinematic models: 1) the geometry of Iberia is revised

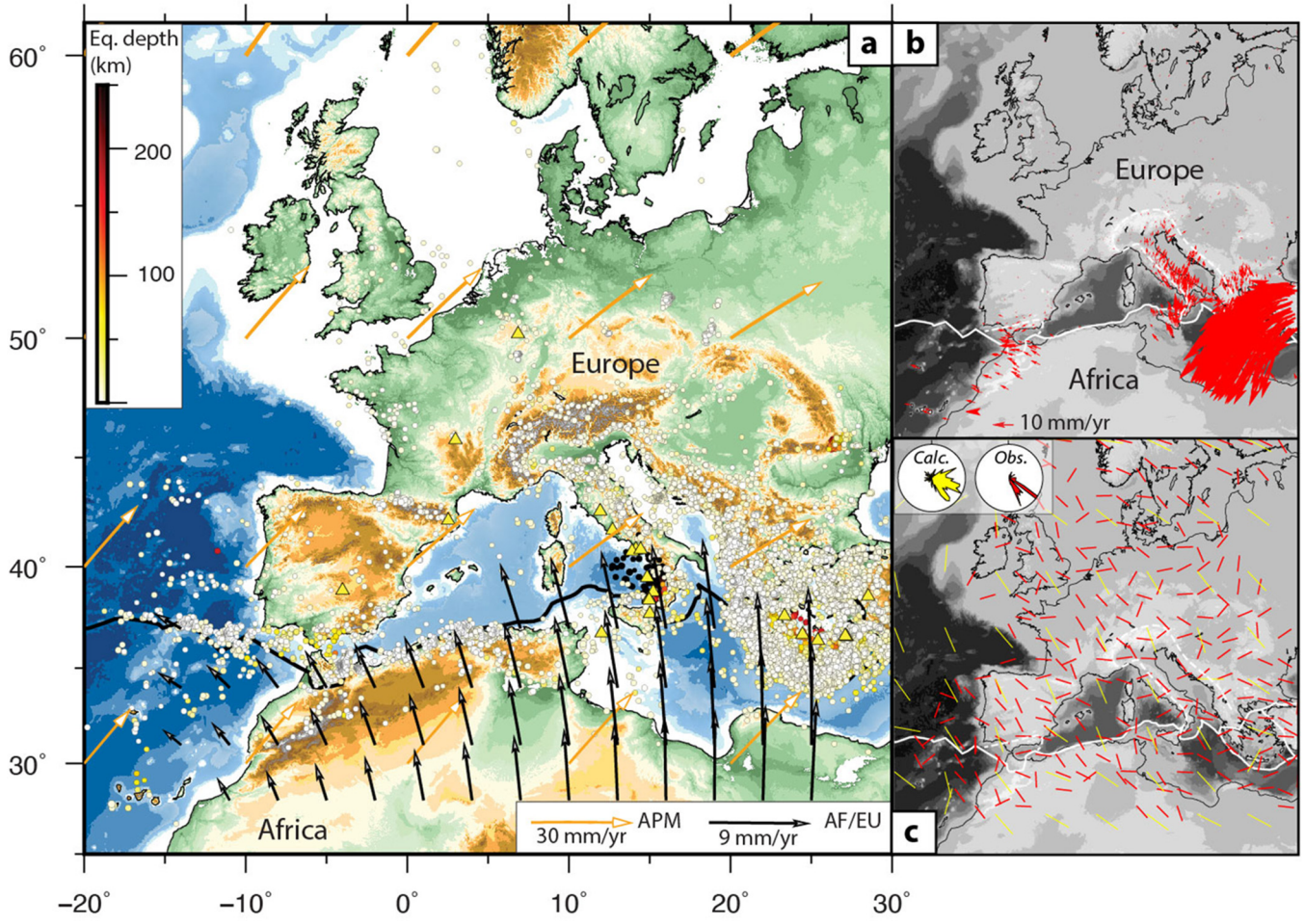

Fig. 20. (a) Present-day plate motions and earthquakes distribution across Europe and northern Africa plate boundary. Orange arrows refer to absolute plate motions calculated according to NNR-MORVEL56 model (Argus *et al.*, 2011). Black arrows are Africa velocities inferred from the same kinematic model but calculated in a Europe-fixed reference frame. Yellow triangle are plio-quaternary volcanoes. Earthquakes depths (0–250 km) and magnitudes (M > 3.5) are from the ISC (International Seismological Center) catalogue spanning the period 1990–2019. Black thick line is the plate boundary after MORVEL56 model (Argus *et al.*, 2011). (b) GPS results plotted relative to Europe fixed reference frame (Nocquet, 2012). (c) Smoothed representation of maximum horizontal compressional stress (SHmax; red bars) after the 2016 World Stress Map (Heidbach *et al.*, 2018) compare to maximum compressional deviatoric stress orientations (yellow bars) calculated from a global coupled lithosphere and mantle dynamic model (Ghosh *et al.*, 2013). Insets show rose diagrams of stress directions for both observed and model stress directions.

and now involves the Ebro, West Iberia and South Iberia blocks, moving separately between Europe and Africa since the Jurassic, 2) a reviewed chronology and kinematics, including the Paleogene "Pyrenean" collision onset in the Betics and the timing of intraplate deformation in the Iberian Ranges between South Iberia and Ebro blocks. The solution for Apulia and Africa is based on the model of Müller *et al.* (2019) that implements a reconstruction of Le Breton *et al.* (2017), and we adopted the solution of van Hinsbergen *et al.* (2019a, 2019b) for Eastern Europe. Along our transect the total AF/EU plate convergence to be accommodated is about 300 km. The reconstruction of Alboran (Internal Betics) accounts for maximum 150 km of shortening estimated from section balancing in the past 20 Ma across the Africa-Iberia plate boundary that overall agree with stratigraphic, structural and thermochronological constraints, indicating Alboran should be close to the Iberia possibly since the Paleogene (Daudet *et al.*, 2020; Pedrera *et al.*, 2020a, 2020b). Accordingly, we have restored Alboran 150 km to the south-south-east of its present position at 20 Ma, and about 240 km at 60 Ma (Angrand and Mouthereau, 2021), which amount falls in the limit permitted by convergence estimated between South Iberia and Africa (Macchiavelli *et al.*, 2017). We infer from these constraints that the westward movement of the Gibraltar Arc should be maximum 260 km since the Eocene. Larger displacement of 400 km has been inferred in another recent reconstruction based the reconstruction of the original thickness of the Betic orogenic wedge (Romagny *et al.*, 2020). In any case, the westward motion appears significantly smaller than the 600 km-long Alboran slab imaged beneath the Gibraltar arc

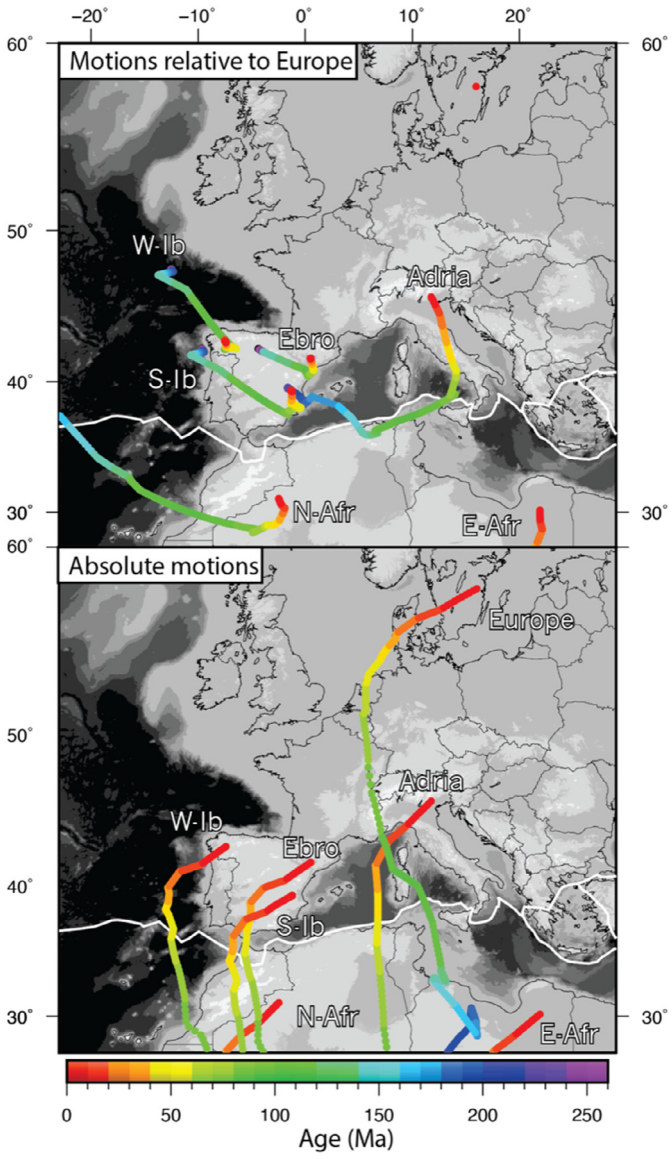

Fig. 21. Motions paths for Ebro, Adria, West Iberia, South Iberia, North Africa and East Africa microcontinents relative to fixed Europe and based on optimized mantle reference frame of Müller *et al.* (2019).

(Bezada *et al.*, 2013; Mancilla *et al.*, 2015b; Villasenor *et al.*, 2015; Palomeras *et al.*, 2017), which we suggest reflects backarc extension by retreating delamination from below Alboran terrane.

In this reconstruction Ebro forms with Sardinia-Corsica a continuous continental block tectonically distinct from Iberia and Europe, individualized along Early Carboniferous-Late Permian right-lateral shear zones. During the Late Jurassic-Early Cretaceous, the eastward drift of Iberia, Ebro-Corsica-Sardinia, and other smaller terranes (AlKaPeCa) is accommodated in a broad zone of left-lateral transtensional deformation. The fact that oblique extension is only slightly partitioned between strike-slip and pure extension explains our difficulty to identify unambiguously the strike-slip movement in the Pyrenees and Iberian Ranges. The presence of Triassic evaporites that decouple basement deformation from the sedimentary cover, further argues for the apparent lack of evidence of strike-slip faulting. When accounting for Adria motions, the opening of Alpine Tethys during the Lower Jurassic is seen to be characterized by oblique extension, between the Atlantic and the Neo-Tethys, and did not resulted in a large oceanic basin. Being segmented and floored only partially by oceanic crust, we interpret the Alpine Tethys as the result of the evolution of two rift segments. The western rift segment (Betic Ocean/West Ligurian Ocean) is positioned to the east of the Iberia paleomargin and extends between the Betics and the eastern Pyrenees. The eastern branch (East Ligurian Basin/eastern Maghrebian Basin) was the largest oceanized domain between Adria/Africa (Sicilia) later localizing retreating subduction zones on the western border of Adria.

From 35 Ma onward, the kinematics of the West Mediterranean is based on Romagny *et al.* (2020) with the noticeable exception for Alboran that we have placed farther west at 35 Ma. The Kabylides is interpreted to have moved southward with respect to Alboran in the Early Miocene. We infer that by the Late Eocene all Mesozoic oceanic domains and rifted margins were closed, resulting in an orogenic belt that will then be reworked during the opening of the West Mediterranean Sea. As convergence continued slab retreated toward the Ionian Basin, triggering the opening of the Ligurian-Provençal Basin and Gulf of Lion. In this model, the formation of the Alboran Sea is suggested to have occurred by subduction and retreating delamination.

5.3 Patterns of Africa/Eurasia kinematics and driving mechanisms

5.3.1 Pre-collision kinematic evolution

The main quantitative results of our kinematic model are summarized in Figures 21 and 22 for Africa, Adria, and peri-Iberian blocks in both fixed Europe reference frame and mantle reference frame. The direction of absolute plate motion when integrated over the Mesozoic-Cenozoic shows a primary N-S motion for both Europe and Africa (Fig. 21). The continental drift of Africa reveals control by upwelling of buoyant mantle from the African LLSVP (Large Low Shear Velocity Province) region associated with LIP eruptions (*e.g.*, Afar, CAMP, Etendeka, Karoo, Sierra Leone; see numbers labeled in Fig. 22d) and hot spots (Torsvik *et al.*, 2006; Burke *et al.*, 2008). The African LLSVP is also proven to be the main driver of the dynamic support of Africa (Moucha and Forte, 2011; Moore *et al.*, 2017). In association with mantle downwellings in subduction zones they form the convection conveyor belt driving the movement of Africa (Becker and Faccenna, 2011).

The opening of Central Atlantic resulted in SSE-to-E-directed motion of Africa, with respect to Europe, during the Early Jurassic (200–150 Ma). The migration of oceanic spreading into the southern North Atlantic during the Late Jurassic-Early Cretaceous (150–120 Ma) triggered the eastward drift of Iberia (Figs. 21 and 22). Between Africa and Europe, the movement of south Iberia occurred faster than, and oblique to, Adria after 140 Ma (Angrand *et al.*, 2020; Angrand and Mouthereau, 2021) which led to moderate contraction in the Alpine Tethys. The Bay of Biscay eventually opened in the

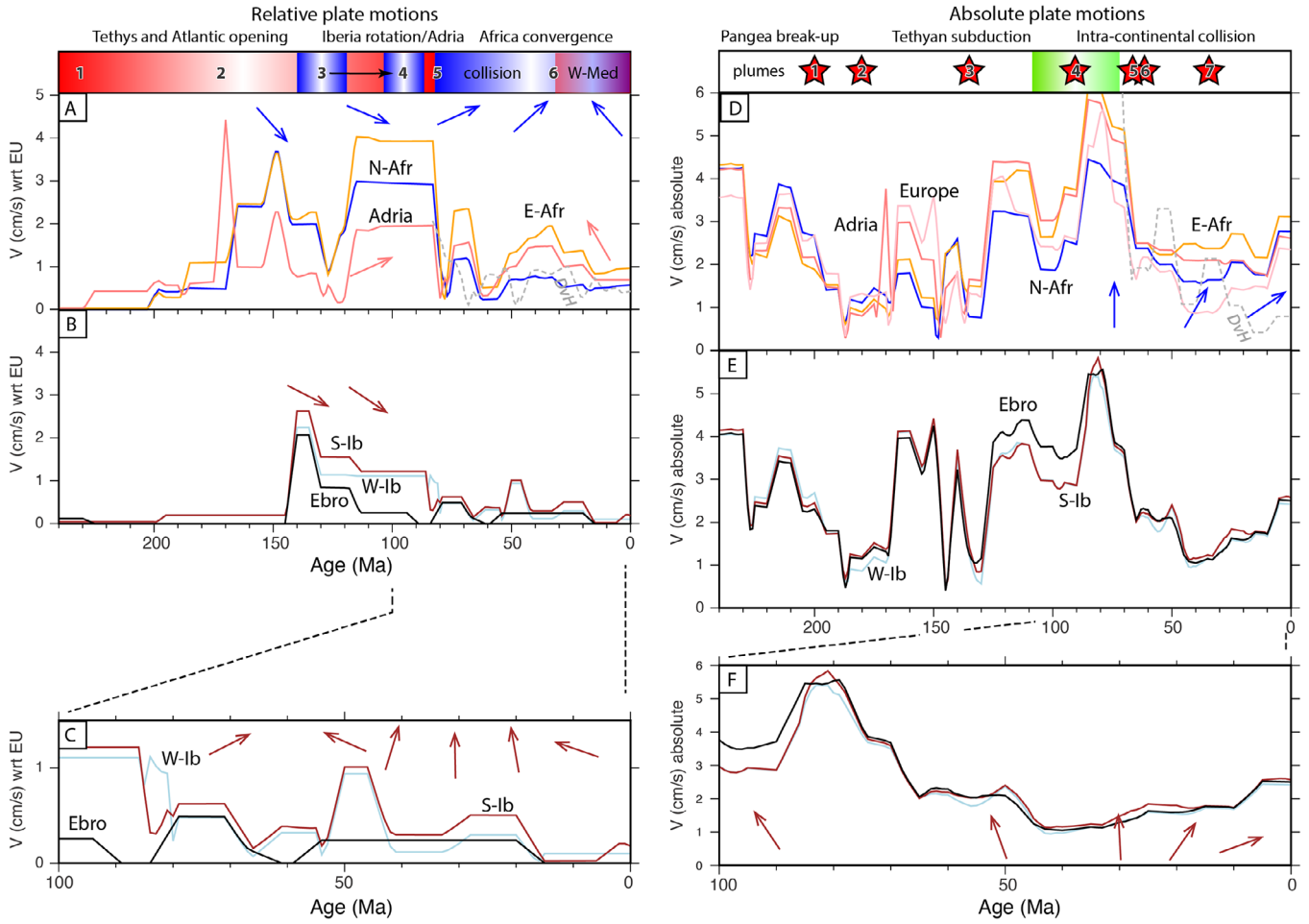

Fig. 22. Velocities (rates and direction) for Africa (N-Afr, E-Afr), Europe, Adria and Iberian terranes (W-Ib, S-Ib, Ebro) along paths defined in Figure 21. Graphs on the left panel (A, B, C) refer to relative plate motions, rates and direction (arrows), with respect to Europe and those on the right panel (D, E, F) are illustrating absolute plate motions (relative to mantle). (A) Relative motions for N-AFr (blue), E-Afr (yellow), Adria (pink). (B) Relative motions for W-Ib (grey), S-Ib (brown) and Ebro (black). (C) Zoom of (B) for the period younger than 100 Ma. (D) Absolute motions for N-AFr (blue), E-Afr (yellow), Adria (dark pink) and Europe (pink). (E) Absolute motions for W-Ib (grey), S-Ib (brown) and Ebro (black). (F) Zoom of (E) for the period younger than 100 Ma. Arrows depict the directions of motion (North up) with colors corresponding to each continental block. Motion for Europe and Africa are those of Müller *et al.* (2019). Grey dashed lines labelled DvH indicate Adria's motion according to model of van Hinsbergen *et al.* (2019a, 2019b). Contraction and extension in left panel are indicated in red and blue color gradients, respectively. Number in (A) refer to deformation regimes (red for extension, blue for contraction). Extension dominates in Western Europe as Neo-Tethys developed (1) followed by Atlantic (2). Rotation of Iberian terranes obliquely to Adria resulted in contractional episodes in southern Alpine Tethys (3). Early stages of clockwise rotation of Adria initiated subduction in the Alps (4). From Late Cretaceous, contraction spread rapidly over whole Europe (5). Kinematic reorganization occurred at 35–25 Ma as back-arc extension in the Western Mediterranean (6). Numbers and stars in (B) refer to plume-related magmatic events: CAMP LIP (1) at 200 Ma (Marzoli *et al.*, 1999a, 199b, 2019), Karoo LIP (2) at ~ 180 Ma (Jourdan *et al.*, 2005), Etendeka-Paranà plume (3) at 135–130 Ma (Marzoli *et al.*, 1999a, 199b; Beccaluva *et al.*, 2020), Morondava LIP (4) at 92–84 Ma, Réunion LIP (5) and Icelandic plume (6) at about the same time (62–65 Ma), Afar plume (7) at 45–30 Ma. Green color gradient indicates slowed Africa's motion during the Late Cretaceous-Paleogene.

Late Aptian (118 Ma), reactivating Jurassic Basins and fragmenting Iberia along inherited post-Variscan shear zones in the Pyrenees and Iberian Ranges. From 130–120 Ma, the absolute motion of Europe, Africa, Adria and other peri-Gondwanan terranes (Ebro, S-Iberia and W-Iberia) increased (Figs. 21 and 22). This is coincident with the acceleration of continental rifting in South Atlantic, after emplacement of the Etendeka igneous province (labeled 3 in Fig. 22d), a precursor event of oceanic spreading that weakened the southern Africa plate boundary (Brune *et al.*, 2016).

About this time, the Iberian blocks (Ebro and South Iberia) moved in the ESE direction (~ 120°E) at maximum rates of 1.5 cm/yr, while Adria positioned along the same Euler latitude but moving faster had a North-directed (N60°E) motion. This kinematics resulted in the closure of the eastern branch of the Alpine Tethys (Angrand and Mouthereau, 2021), and to the North of Adria, the subduction in the Alps (Eo-Alpine event) (Handy *et al.*, 2010; van Hinsbergen *et al.*, 2019a, 2019b). Differential movements between Iberia and Adria at the northern edge of Africa seems to have governed the complex

pattern of deformation in the Mediterranean, including episodic extension and contraction during the middle-Late Cretaceous. Velocities of Africa relative to Europe reached a maximum during the 120–80 Ma interval, in part due to a combination of mantle upwelling, active spreading in the southern Atlantic and slab pull along Tethyan subduction zones. Between 110 and 100 Ma absolute velocities of Africa and Adria appear to have slightly decreased (Fig. 22) consistent with the slowing of plate velocities globally (Müller *et al.*, 2019). Africa, Adria and Iberia then recorded in less than 20 Myr (100–80 Ma) an acceleration from ~3 cm/yr to above 6 cm/yr (North Africa) (Fig. 22).

5.3.2 Onset of collision: weak Western Europe caught in between two cratons

Both AF/EU convergence and absolute velocities decreased at 80–65 Ma as the direction of convergence changed to N-S orthogonal to plate boundary (Figs. 21 and 22). In Europe and northern Africa, the Late Cretaceous stage marks a transition from a tectonic regime moderately compressional around Adria to broadly contractional regime from East (Adria) to West (Iberia), and from Morocco in the south to northern Europe along the TESZ (Kley and Voigt, 2008). The reduction of Europe motion resulted in the increase of AF/EU convergence. Several mechanisms have been proposed to explain the Late Cretaceous (Santonian, 84 Ma) rapid slowing. The emplacement of Morondava LIP at 92–84 Ma (Torsvik *et al.*, 2000) between Madagascar and Seychelles would have induced the acceleration of the northward drift of Africa (labeled 4 in Fig. 22d) followed by collision with Europe and reduction of Africa motion. Such acceleration is also proposed to have induced Tethyan slab penetration into the denser lower mantle, in turn explaining the emplacement of several south Tethyan ophiolites between 100 and 75 Ma (Jolivet *et al.*, 2016). Alternatively, the emplacement of south Tethyan ophiolites could result from subduction initiation by pre-Deccan plume at about 100 Ma, hence unrelated to Neotethyan subduction dynamics to the north (Rodriguez *et al.*, 2021). In our view, the rapid spread of contraction over 4000 km is an indication of the first-order role played by the strong plate-mantle coupling below the viscous cratonic lithosphere of WAC and EEC (Fig. 23a). The arrival of the strong, buoyant and thick cratonic lithosphere of African/Gondwana against the strong Baltica craton, closed the Alpine Tethys and resulted in the built-up of resistive forces, thus limiting further indentation of Africa into the weak lithosphere of Europe (Fig. 23a).

5.3.3 Paleogene kinematic reorganisation: increasing role of North Atlantic

A general decrease of absolute velocities and clockwise rotation of 20–30° is recorded at 62–40 Ma for Europe, and at 57–35 Ma for North Africa (Fig. 22). This is combined with the onset of WNW-directed movement of Iberia over the 57–42 Ma time interval. The decrease of Eurasia velocity coupled to the less important reduction of Adria and North Africa velocities appear responsible for a second period of acceleration of AF/EU plate convergence at 55–50 Ma. This resulted in the Eocene phase of mountain building documented throughout Iberia all the way to the Atlas

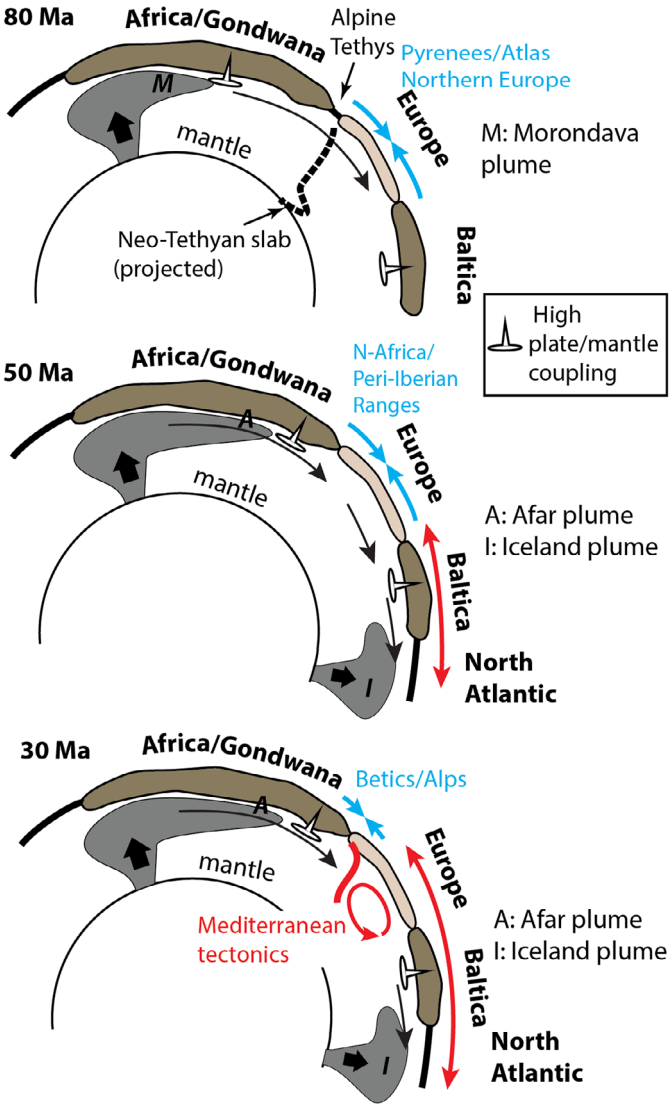

Fig. 23. Snapshots at 80, 50 and 30 Ma of the interactions between the deep drivers of plate motions, the buoyant cratonic lithospheres of Africa and Baltica and the weak Europe. The effect of peri-African plumes (Mondarava, Afar plumes) may have been counteracted by the Iceland plume after 50 Ma in Western Europe in connection with exhumation of Europe. Under AF/EU convergence, contraction (blue arrows) spreads in the whole of Europe during the Late Cretaceous but was progressively replaced by extension (red arrows) in association with the West Europe Rift and in the Northern Atlantic, and then in the Mediterranean region.

(Fig. 19). The slowing of Europe and Africa motions during the Paleocene-Eocene requires large-scale processes likely combining the effects of increasing gravitational potential in the Africa-Eurasia collision zone coupled to the development of 1) spreading ridges in the Labrador Sea at about 62 Ma (Abdelmalak *et al.*, 2019), North Atlantic at 54 Ma (Mosar *et al.*, 2002) and the rise of icelandic plume of the North Atlantic Igneous Province (Torsvik *et al.*, 2014) (Fig. 23), 2) slowing of convection cell below Africa at about 65 Ma linked to the emplacement of the Deccan LIP by Réunion plume (labeled 5 in Fig. 22d; van Hinsbergen *et al.*, 2011; Cande and Stegman,

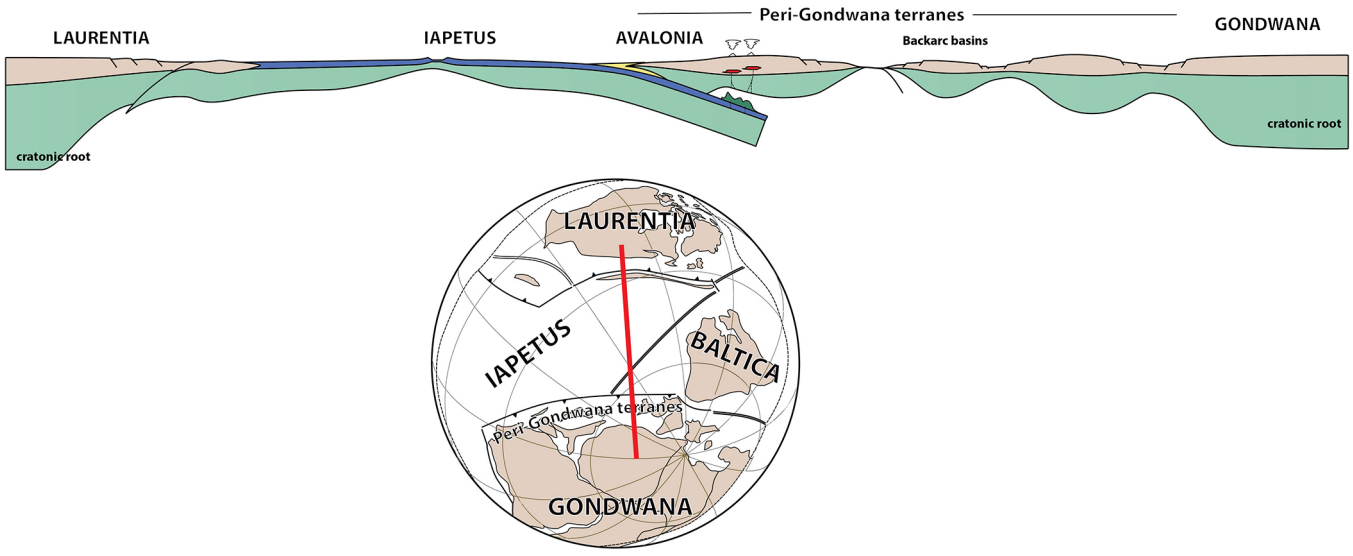

Fig. 24. Reconstruction of northern Gondwana, Iapetus and Laurentia at 600–500 Ma. Peri-Gondwana terranes that constitute the basement of Europe were thinned. Plate configuration is shown at 500 Ma after (Domeier, 2016).

2012), and 3) the penetration of Tethyan slabs in the lower mantle at 65–55 Ma (Faccenna *et al.*, 2013a).

This episode was followed by the increase of AF/EU convergence until 32 Ma in eastern Africa, 43 Ma in Adria and 50–40 Ma in northern Africa (Fig. 22a). For Iberia (South Iberia, Ebro blocks), in contrast, velocities relative to Eurasia dropped below 0.5 cm/yr after 40 Ma (Fig. 22b). Velocity reduction is connected to the progressive accretion of Iberian blocks to Europe after 40 Ma. After 35 Ma, the whole of AF/EU convergence dropped to 0.9–0.5 cm/yr and was maintained at this level or with a slight increase from 18–15 Ma to present (Fig. 22a). This period was coeval with back-arc extension in the Mediterranean region, corresponding to the *Mediterranean Tectonics* stage spanning from 35 to 8 Ma (Jolivet *et al.*, 2021), which also coincides with the counterclockwise rotation of Africa convergence. Remnant of Africa convergence to be accommodated in Iberia was transferred to the south in the Betics. We note that the model of Müller *et al.* (2019) adopted in our reconstruction and that of van Hinsbergen *et al.* (2019a, 2019b) shows relatively similar AF/EU velocities evolution in the past-30 Ma (Fig. 22a) but they noticeably differ in Africa absolute velocities (Fig. 22d). The slowing of Africa has been suggested to be synchronous with the initiation of continental rifting along the Red Sea at 25 Ma (McQuarrie *et al.*, 2003; Reilinger and McClusky, 2011) triggered by the arrival of Afar plume (Fig. 23) that emplaced from 45 to 30 Ma (Faccenna *et al.*, 2013b). The breakup of Arabia disconnected Africa from cold spots in the Tethyan subduction and led to progressive kinematic reorganisation of the region, including the opening of Gulf of Aden (Leroy *et al.*, 2004; ArRajehi *et al.*, 2010) and collision in the Zagros (Mouthereau *et al.*, 2012). The complex post-35 Ma kinematic evolution in the east was related in Europe to the reactivation of Late Cretaceous-Paleogene collision belts *e.g.*, in the Betics and the Alps caused by slab retreat and delamination in the Mediterranean (Fig. 23).

6 Discussion: imprints of long-term thermo-mechanical stability and inherited architecture on topographic evolution

6.1 Long-term thermal and rheological stability of the lithosphere and topography

The orogenic evolution of Western Europe cannot be understood without considering the profound and long-lived transformation of the continental lithosphere initiated at 750–500 Ma. During Rodinia assembly at 1.2 Ga, the protagonists of the Africa-Eurasia collision were part of resistant cratonic domains of Gondwana (West Africa Craton) and Baltica. Thermal erosion, thinning and refertilization by alkaline melts of the Archean SCLM during plume emplacement at about 600 Ma, Pan-African orogeny/Cadomian subduction and back-arc rifting at 570 Ma removed the Archean cratonic root from northern Gondwana (Fig. 24). The strength of the continental lithosphere of the newly formed peri-Gondwana terranes, comprising Avalonia and Armorica, was drastically reduced compared to remnants of Archean cratons. We suggest that Early Paleozoic Europe and northern Africa were in a thermal and mechanical configuration relatively similar to the one described at present (Fig. 9). This implies that the peri-Gondwanan lithosphere of Europe and North Africa have not been thermally relaxed for several hundred million years. Also required is the limited convergence, here estimated to 300 km along our transect of Western Europe, between the pre-Gondwana terranes and the adjacent cold and buoyant cratons in order to maintain these conditions. The nature of the subsequent tectono-magmatic events shows these assumptions are correct.

First, partial melting and magmatism during the Variscan orogeny argue for a combination of high mantle heat flux and high crustal heat flux related to the young radiogenic plutons

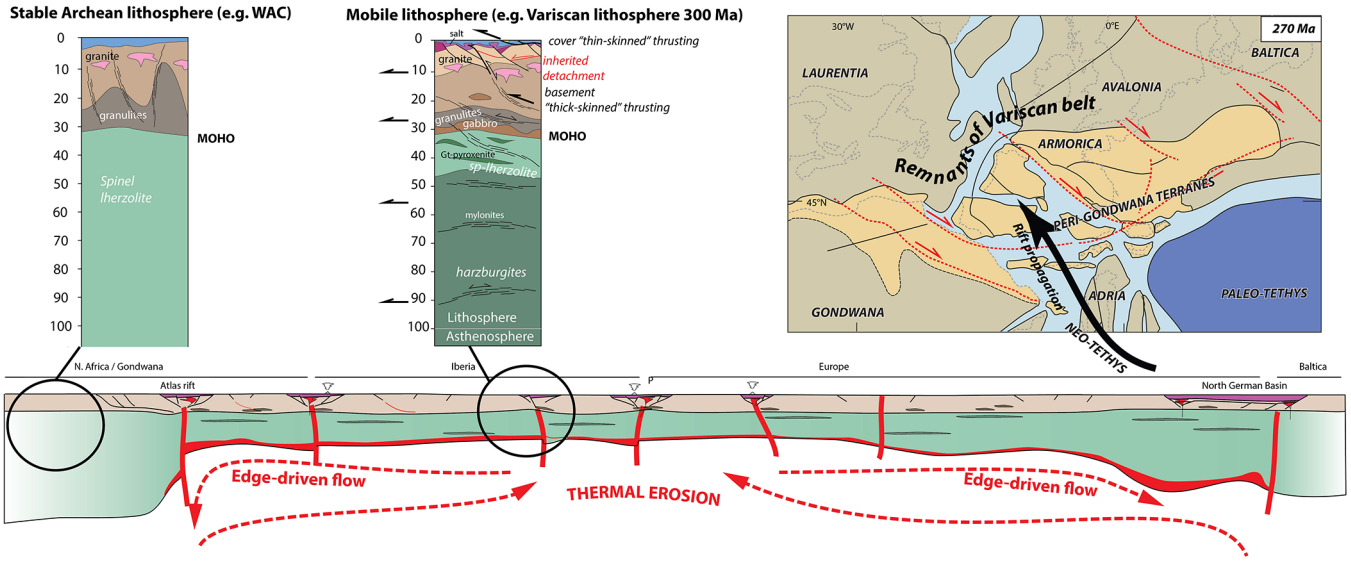

Fig. 25. Properties and architecture of the Europe lithosphere achieved during the Permian (270 Ma) leading to break-up of Pangea. Magmatism and distributed extension in Western Europe that has commenced in the Late Variscan period reflect lithosphere thinning and thermal erosion caused by a combination of small-scale convection cells on craton margins and the west-directed asthenospheric outflux related to the propagation of the Neo-Tethys south of the Paleo-Tethys. Reconstruction is after Angrand *et al.* (2020).

(*e.g.*, Vanderhaeghe *et al.*, 2020). There are also indications that the Variscan Belt did not form an orogenic Tibet-like plateau (Franke, 2014), which would require a mechanically strong cratonic lithosphere to maintain its high topography, as for the current India-Eurasia collision.

Late Carboniferous elevation of ~3 km estimated for the Variscan Belt (Massif Central) (Dusséaux *et al.*, 2021) and evidence of the lack of marked rain shadow that suggests moderate elevation of 2000 m during Late Carboniferous-Permian (Roscher and Schneider, 2006) supports this model. We have estimated that the mantle heat flow established during the Late Carboniferous-Permian (300–270 Ma) was maintained to high values of 32 mW/m^2 (Fig. 9). Thermal erosion and delamination are indicated at this time by calc-alkaline magmatism characterized by an increase of mantle source in the lava flows. This also reflects the transition towards increasing juvenile asthenospheric inputs related to the propagating Neo-Tethys ridge (Fig. 25) to the south of the closing Paleo-Tethys Ocean (*e.g.*, Angrand *et al.*, 2020). We have suggested that edge-driven convection induced by density contrasts with craton margins and the asthenospheric flow associated with rift propagation (Mondy *et al.*, 2017; Jourdon *et al.*, 2020b) are the principal mechanisms to explain a stable mantle heat flux. The lack of thermal relaxation and lithosphere thermal thickening following the Late Carboniferous-Permian event is also suggested by the lack of marine incursion until the Triassic (Bourquin *et al.*, 2011). The Early Jurassic CAMP event recognized in the northern margin of West African craton, Iberia and Brittany reveals high temperature in the asthenospheric mantle caused by deeply rooted plume, thermal insulation below Pangea or a combination of rifting and plume magmatism. Subsequent lithosphere thinning and inputs of heat from the mantle during the episodes of Jurassic-Early Cretaceous Atlantic and Alpine Tethys rifting contributed to keep the Europe lithosphere weak. The fact that these rifting events were essentially magma-poor is not an indication of a lower mantle heat flux. This reveals instead that rifting occurred in a depleted Permian mantle. There are also indications that the mid-Cretaceous, especially the Albian, was a period of topographic uplift, weathering and exhumation as revealed on the formation of paleosoils and karsts in Massif Central (*e.g.*, Marchand *et al.*, 2021), and possibly over most of the Variscan massif (Thiry *et al.*, 2006). The predominance of mature nearshore to continental sands deposited in Iberia (Rat, 1988; Rat *et al.*, 2019) and northern Africa (Lefranc and Guiraud, 1990) document the occurrence of large continental surfaces exposed to subaerial erosion during the mid-Cretaceous. In addition, the large majority of AFT ages over peri-Gondwanan domains are essentially younger than 300 Ma with 75% younger than 160 Ma. Those post-Variscan but pre-Alpine AFT ages suggest transient inputs of heat and burial caused by the kinematics of rifting during the Mesozoic. Taken together these data argue for a model in which the topography of Central Europe remained in part dynamically supported during most of the Mesozoic in line with the first-order long-term stability of thermal structure and strength of the lithosphere, at least over the past 300 Ma. This point is essential because this is the contrast in lithosphere strengths, between cratonic lithosphere and the weak Europe, and the degree of coupling with large-scale convection that explain far-field stresses and deformation in the collision zone.

6.2 Impact of rift maturity on topographic evolution and late collision evolution

Soon after the onset of Africa-Europe collision, in the Santonian, contraction spreads rapidly over the whole Western Europe and northern Africa margin (Fig. 26). We have

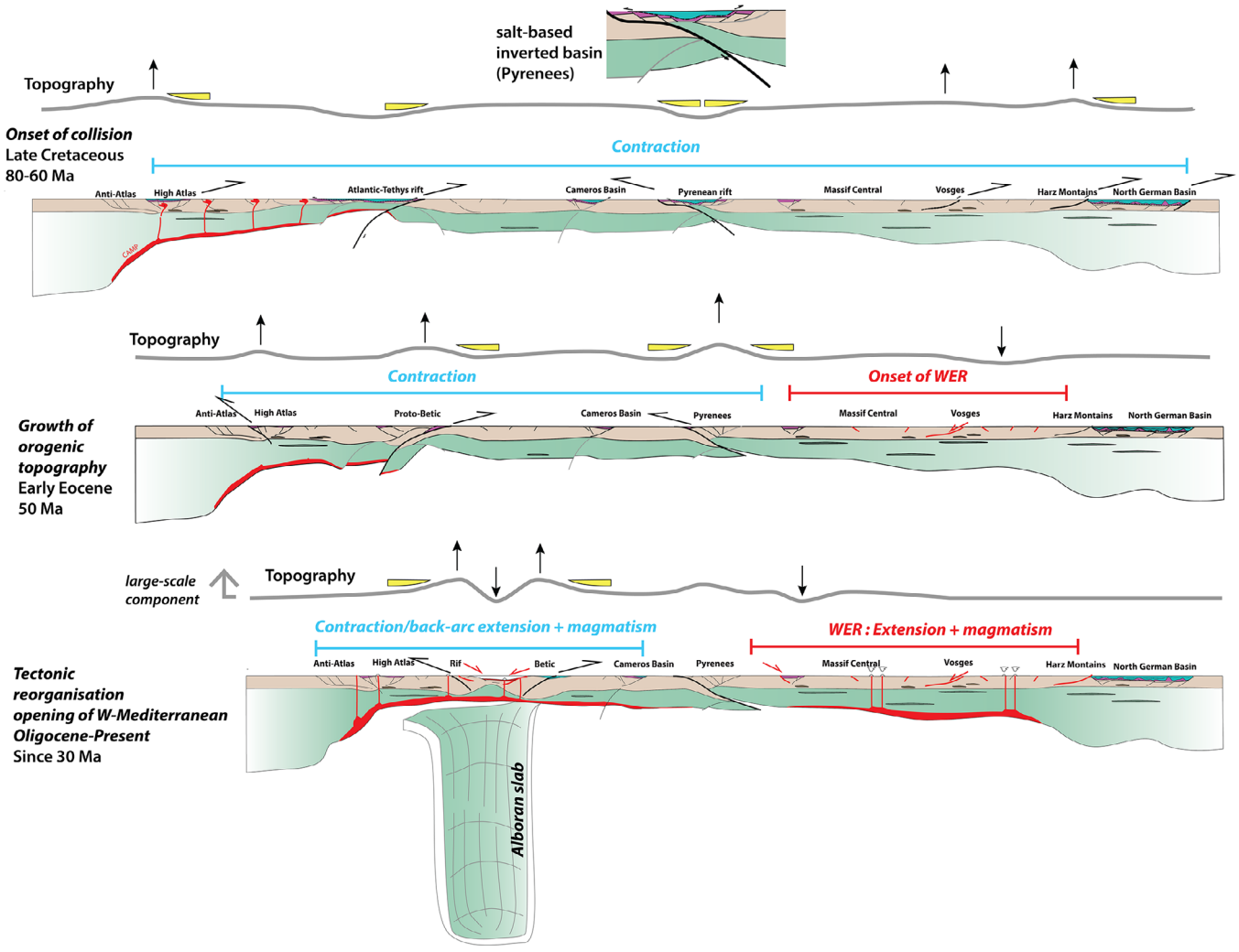

Fig. 26. Tectonic and topographic evolution of Western Europe during the Cenozoic convergence between the African and the European cratons. Lithospheric cross-sections at key time intervals depict the relationships between the thin European lithosphere inherited from the Late Variscan-Permian event, the architecture of variably thinned rift domains acquired during the Mesozoic and magmatism. The thick grey line depicts the evolution of the topography. Together with the arrows that symbolized rock uplift it is possible to qualitatively appreciate how the topography is changing in time and space. Yellow wedges corresponds to foreland basins or syn-contraction progressive unconformities.

suggested that this is the far-field stresses exerted by the convergence of buoyant, thick and strong cratonic lithospheres of Africa and Baltica that explain the strain distribution in the weak European lithosphere. Secondary effects related to the high strength of hyper-extended rift domains at the initiation of inversion in the Pyrenees (Dielforder *et al.*, 2019), the Betics and possibly in many other parts of the Mediterranean region further facilitated strain transfer throughout Europe. Crustal domains that were uplifted first (Atlas, Harz, Vosges, Sudetes) are also those with lower initial rift-related extension during the Mesozoic (Fig. 26). This transient Laramide-like stage of contraction in central Europe can therefore reflect the initial rift architecture. In contrast, extension associated with rifting along the Atlantic-Alpine Tethys segment led to much larger hyper-extended rift systems and oceanic basins in the Betic-Rif and in the Pyrenees. In these regions the rifted margins were also associated with thick pre-rift salt layer (Flinch *et al.*, 1996; Carola *et al.*, 2015; Flinch and Soto, 2017; Ducoux *et al.*, 2019; Daudet *et al.*, 2020; Izquierdo-Llavall *et al.*, 2020; Jourdon *et al.*, 2020a, 2020b; Pedrera *et al.*, 2020a, 2020b; Roca *et al.*, 2020). As expected, the onset of inversion in these domains did not result in subaerial topography as observed in Central Europe and were still largely submerged (Fig. 26). At 50 Ma, a major kinematic change occurred corresponding to accrued Africa/Eurasia convergence driven by plume activity in east Africa and below Iceland, and the opening of the North Atlantic. This led to closure of hyper-extended domains in the Pyrenees and the Betics that resulted in the onset of accretion of necking domains marked by rapid growth of orogenic topography. This is recorded by the increasing subaerial erosion and well-developed foreland basins. The change in the internal dynamics of orogenic systems appears synchronous with the opening of West European Rift (WER). From 40 Ma, our reconstruction indicates that Iberia and Ebro block were accreted to Europe and the proto-Betic domain was topographically mature in the south and coupled to mountain

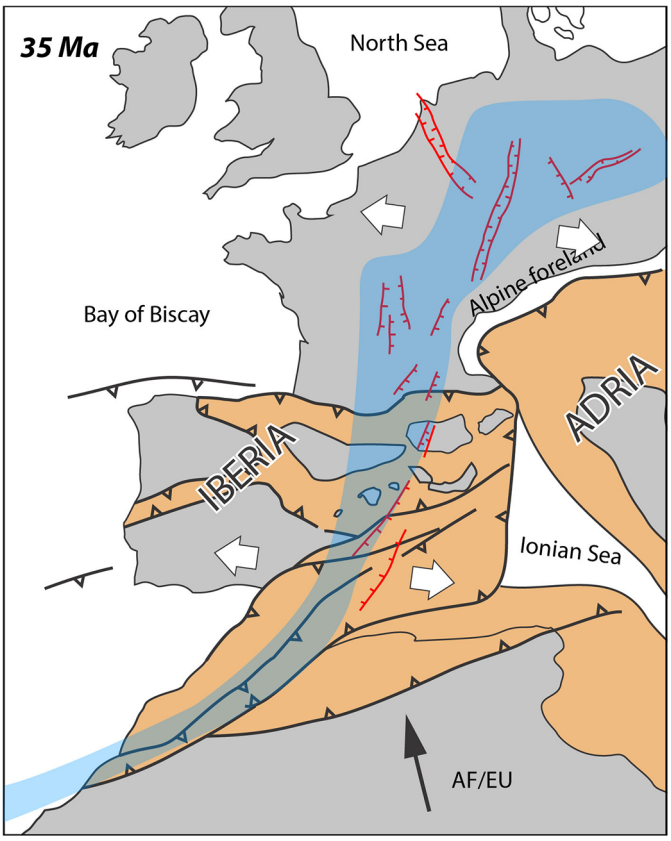

Fig. 27. Reconstruction at 35 Ma showing the EW-trending orogenic belts around Iberia and northern Africa, the orientation of normal faulting of the West European Rift, which is spatially coincident with the emplacement of the post-35 Ma magmatism (Villaseca *et al.*, 2018).

building in the Atlas (Fig. 26). By the Late-Eocene-Oligocene, the WER separates two distinct tectonic domains. In the West, the accretion of Iberia and Ebro blocks resulted in orogenic belts from the High Atlas to the Pyrenees. In the East, however, around Adria, the Ionian Basin and the European margin in the Alps are not yet closed (Fig. 27). From 35–30 Ma, the retreat of subduction front towards the East along the active plate boundary with the Ionian Basin opened the Western Mediterranean in the former mature "Pyrenean" orogenic domain (Fig. 27). However, considering the size of the Ionian Basin and the fact the Alpine Tethys region was lacking a large oceanic domain, it must be envisaged that the WER might have been the trigger of the West Mediterranean opening. In this reconstruction (Fig. 26) this is the size and the architecture of the rifted domains that dictate the timing and the vigor of exhumation in the collision zone. As rifted basins were progressively inverted to form mature orogenic belts, this is the motion of Iberia and Adria independently from Africa and large-scale lithospheric heterogeneities that controlled the post-collision evolution of in Europe.

7 Conclusions

In this paper our goal was to resolve how inherited properties of the continental lithosphere explain the patterns of mountain building in Europe. In this aim we have synthesized and analyzed constraints on the tectonic and thermal evolution of the Europe lithosphere, plate kinematics and temporal evolution of the orogenic topography. We show that the thermal and mechanical conditions necessary to form orogenic belts of Western Europe lie in the perennial contrast between a weak, thin and dense lithosphere of Central Europe made of a refertilized mantle and the strong, thick and buoyant cratonic depleted mantle of East European Craton and West African Craton. A pivotal trigger of mantle weakening is the thermal erosion and refertilization event of the continental lithosphere during the Neoproterozoic (750–500 Ma) when Western Europe lithosphere was positioned north of Gondwana and its evolution controlled by the subduction of Iapetus. The second key event was the Late Carboniferous and Permian (310–270 Ma) magmatic event as Pangea broke up and got heated at the end of the Variscan orogen. To maintain the contrasting rheologies between the Phanerozoic and Archean lithosphere of Europe, thermal relaxation beneath the Phanerozoic lithosphere must be compensated by an increase of mantle heat flux. We find that edge-driven convection on craton margins and the asthenospheric flow below Central Europe associated with Tethyan rifting are the main drivers. These events are suggested to have resulted in anomalous topography over Europe. Stress built-up and strain distribution during AF/EU collision are in turn explained by the different coupling with convection in the asthenosphere between the Phanerozoic and Archean cratonic lithospheres. The patterns of exhumation across Western Europe are inferred to be linked to the crustal architecture inherited from the evolution of rifted margins associated with the Neo-Tethys, Atlantic and Alpine Tethys opening. The marked topographic change detected at around 50 Ma, from the High Atlas to the Pyrenees, emphasizes the acceleration of orogenic exhumation in southern Europe synchronous with onset of extension in the West European Rift. We show this period of widespread orogenic growth was caused by the onset of accretion of more buoyant and thicker portions of rifted margins triggered by the kinematic reorganization related to opening of the North Atlantic and onset of the Icelandic plume.

Supplementary Material

Supplementary File S1. Thermal structure of continental lithosphere.
Supplementary File S2. This file contains latitude, longitude of samples and central ages of apatite fission-track analyses published in Herman *et al.* (2014) and from our own compilation from the OROGEN project.
Supplementary Material Figure S1. Density model after EPcrust (Molinari and Morelli, 2011) used to derive topography of Europe shown in Figures 4 and 5.
Supplementary Material Figure S2. Cooling histories from which periods of maximum cooling rates have been derived for a selection of orogenic belts where thermal modelling has been published and containing apatite fission-track analyses.

The Supplementary Material is available at http://www.bsgf.fr/10.1051/bsgf/2021040/olm.

Acknowledgments. This paper is a contribution of Orogen, a tripartite project funded by TOTAL, BRGM and CNRS. It benefited from discussions along the course of the project with the Orogen Community. Alexandra Robert is thanked for her help in handling with lithosphere thickness models. We are also grateful to Olivier Vanderhaeghe, Yoann Denèle and Michel Grégoire for discussions on an earlier version of the manuscript and their feedbacks regarding the evolution of the Variscan orogen and interpretation of xenoliths data. We gratefully acknowledge Laetitia Le Pourhiet and an anonymous reviewer for their careful reading, questions and comments that significantly improved the quality of the manuscript. Oliver Lacombe is thanked for his editorial handling and suggestions of improvements.

References

Abdelmalak MM, Planke S, Polteau S, Hartz EH, Faleide JI, Tegner C, *et al.* 2019. Breakup volcanism and plate tectonics in the NW Atlantic. *Tectonophysics* 760: 267–296. https://doi.org/10.1016/j.tecto.2018.08.002.

Advokaat EL, van Hinsbergen DJJ, Maffione M, Langereis CG, Vissers RLM, Cherchi A, *et al.* 2014. Eocene rotation of Sardinia, and the paleogeography of the Western Mediterranean Region. *Earth Planet. Sci. Lett.* 401: 183–195. https://doi.org/10.1016/j.epsl.2014.06.012.

Afonso JC, Fernàndez M, Ranalli G, Griffin WL, Connolly JAD. 2008. Integrated geophysical-petrological modeling of the lithosphere and sublithospheric upper mantle: Methodology and applications. *Geochem. Geophys. Geosyst.* 9: n/a–n/a. https://doi.org/10.1029/2007gc001834.

Afonso JC, Salajegheh F, Szwillus W, Ebbing J, Gaina C. 2019. A global reference model of the lithosphere and upper mantle from joint inversion and analysis of multiple data sets. *Geophys. J. Int.* 217: 1602–1628. https://doi.org/10.1093/gji/ggz094.

Agostinetti NP, Faccenna C. 2018. Deep structure of Northern Apennines Subduction Orogen (Italy) as revealed by a joint interpretation of passive and active seismic data. *Geophysical Research Letters* 45: 4017–4024. https://doi.org/10.1029/2018gl077640.

Allen PA, Bennett SD, Cunningham MJM, Carter A, Gallagher K, Lazzaretti E, *et al.* 2002. The post-Variscan thermal and denudational history of Ireland. *Geol. Soc. Lond. Special Publ.* 196: 371–399. https://doi.org/10.1144/gsl.sp.2002.196.01.20.

Amaru. 2007. Global travel time tomography with 3-D reference models. *Geologica Ultraiectina* 274: 174.

Angrand P, Mouthereau F. 2021. Evolution of the Alpine orogenic belts in the Western Mediterranean region as resolved by the kinematics of the Europe-Africa diffuse plate boundary. Revision sent for publication to *BSGF Earth Sciences Bulletin* 192: 42. https://doi.org/10.1051/bsgf/2021031.

Angrand P, Mouthereau F, Masini E, Asti R. 2020. A reconstruction of Iberia accounting for Western Tethys-North Atlantic kinematics since the Late-Permian-Triassic. *Solid Earth* 11: 1313–1332. https://doi.org/10.5194/se-11-1313-2020.

Arboleya ML, Teixell A, Charroud M, Julivert M. 2004. A structural transect through the High and Middle Atlas of Morocco. *Journal of African Earth Sciences* 39: 319–327. https://doi.org/10.1016/j.jafrearsci.2004.07.036.

Arche A, López-Gómez J. 2005. Sudden changes in fluvial style across the Permian–Triassic boundary in the eastern Iberian Ranges, Spain: Analysis of possible causes. *Palaeogeogr Palaeoclim Palaeoecol* 229: 104–126. https://doi.org/10.1016/j.palaeo.2005.06.033.

Argus DF, Gordon RG, DeMets C. 2011. Geologically current motion of 56 plates relative to the no-net-rotation reference frame. *Geochemistry, Geophysics, Geosystems* 12. https://doi.org/10.1029/2011gc003751.

ArRajehi A, McClusky S, Reilinger R, Daoud M, Alchalbi A, Ergintav S, *et al.* 2010. Geodetic constraints on present-day motion of the Arabian Plate: Implications for Red Sea and Gulf of Aden rifting. *Tectonics* 29: n/a–n/a. https://doi.org/10.1029/2009tc002482.

Artemieva IM, Mooney WD. 2001. Thermal thickness and evolution of Precambrian lithosphere: A global study. *Journal of Geophysical Research* 106: 16387–16414. https://doi.org/10.1029/2000jb900439.

Artemieva IM, Meissner R. 2012. Crustal thickness controlled by plate tectonics: A review of crust-mantle interaction processes illustrated by European examples. *Tectonophysics* 1–113. https://doi.org/10.1016/j.tecto.2011.12.037.

Audet P, Bürgmann R. 2011. Dominant role of tectonic inheritance in supercontinent cycles. *Nature Geoscience* 4: 184–187. https://doi.org/10.1038/ngeo1080.

Awdankiewicz M, Kryza R, Szczepara N. 2013. Timing of post-collisional volcanism in the eastern part of the Variscan Belt: Constraints from SHRIMP zircon dating of Permian rhyolites in the North-Sudetic Basin (SW Poland). *Geol. Mag.* 151: 611–628. https://doi.org/10.1017/s0016756813000678.

Babel Working Group. 1993. Deep seismic reflection/refraction interpretation of crustal structure along Babel profiles A and B in the Southern Baltic Sea. *Geophysical Journal International* 112: 325–343. https://doi.org/10.1111/j.1365-246x.1993.tb01173.x.

Balestrieri ML, Moratti G, Bigazzi G, Algouti A. 2009. Neogene exhumation of the Marrakech High Atlas (Morocco) recorded by apatite fission-track analysis. *Terra Nova* 21: 75–82. https://doi.org/10.1111/j.1365-3121.2008.00857.x.

Ballèvre M, Cataln JRM, Lpez-Carmona A, Pitra P, Abati J, Fernndez RD, *et al.* 2014. Correlation of the nappe stack in the Ibero-Armorican arc across the Bay of Biscay: A joint French–Spanish project. *Geol. Soc. Lond. Special Publ.* 405: 77–113. https://doi.org/10.1144/sp405.13.

Banks CJ, Warburton J. 1991. Mid-crustal detachment in the Betic system of southeast Spain. *Tectonophysics* 191: 275–289. https://doi.org/10.1016/0040-1951(91)90062-w.

Barbarand J, Lucazeau F, Pagel M, Séranne M. 2001. Burial and exhumation history of the south-eastern Massif Central (France) constrained by apatite fission-track thermochronology. *Tectonophysics* 335: 275–290.

Barbarand J, Quesnel F, Pagel M. 2013. Lower Paleogene denudation of Upper Cretaceous cover of the Morvan Massif and southeastern Paris Basin (France) revealed by AFT thermochronology and constrained by stratigraphy and paleosurfaces. *Tectonophysics* 608: 1310–1327. https://doi.org/10.1016/j.tecto.2013.06.011.

Barbarand J, Bour I, Pagel M, Quesnel F, Delcambre B, Dupuis C, *et al.* 2018. Post-Paleozoic evolution of the Northern Ardenne Massif constrained by apatite fission-track thermochronology and geological data. *Bulletin de la Société géologique de France* 189: 16. https://doi.org/10.1051/bsgf/2018015.

Barbarand J, Préhaud P, Baudin F, Missenard Y, Matray JM, François T, *et al.* 2020. Where are the limits of Mesozoic intracontinental sedimentary basins of southern France? *Mar. Petrol. Geol.* 121: 104589. https://doi.org/10.1016/j.marpetgeo.2020.104589.

Barbero L, Teixell A, Arboleya M-L, del Río P, Reiners PW, Bougadir B. 2007. Jurassic-to-present thermal history of the central High Atlas (Morocco) assessed by low-temperature thermochronology. *Terra Nova* 19: 58–64. https://doi.org/10.1111/j.1365-3121.2006.00715.x.

Barth S, Oberli F, Meier M, Blattner P, Bargossi GM, Battistini GD. 1993. The evolution of a calc-alkaline basic to silicic magma system: Geochemical and Rb-Sr, Sm-Nd, and isotopic evidence from the Late Hercynian Atesina-Cima d'Asta volcano-plutonic complex, Northern Italy. *Geochim. Cosmochim. Acta* 57: 4285–4300. https://doi.org/10.1016/0016-7037(93)90323-o.

Barth MG, Rudnick RL, Carlson RW, Horn I, McDonough WF. 2002. Re-Os and U-Pb geochronological constraints on the eclogite–tonalite connection in the Archean Man Shield, West Africa. *Precambrian Res* 118: 267–283. https://doi.org/10.1016/s0301-9268(02)00111-0.

Bayer U, Scheck M, Rabbel W, Krawczyk CM, Götze H-J, Stiller M, *et al.* 1999. An integrated study of the NE German Basin. *Tectonophysics* 314: 285–307. https://doi.org/10.1016/s0040-1951(99)00249-8.

Bea F, Montero P, Molina JF. 1999. Mafic Precursors, Peraluminous Granitoids, and Late Lamprophyres in the Avila Batholith: A model for the generation of Variscan Batholiths in Iberia. *J. Geol.* 107: 399–419. https://doi.org/10.1086/314356.

Beauchamp W, Allmendinger RW, Barazangi M, Demnati A, Alji ME, Dahmani M. 1999. Inversion tectonics and the evolution of the High Atlas Mountains, Morocco, based on a geological-geophysical transect. *Tectonics* 18: 163–184. https://doi.org/10.1029/1998tc900015.

Beccaluva L, Bianchini G, Natali C, Siena F. 2020. Plume-related Paranà-Etendeka igneous province: An evolution from plateau to continental rifting and breakup. *Lithos* 362-363: 105484. https://doi.org/10.1016/j.lithos.2020.105484.

Becker TW, Faccenna C. 2011. Mantle conveyor beneath the Tethyan collisional belt. *Earth Planet. Sci. Lett.* 310: 453–461. https://doi.org/10.1016/j.epsl.2011.08.021.

Bellahsen N, Mouthereau F, Boutoux A, Bellanger M, Lacombe O, Jolivet L, *et al.* 2014. Collision kinematics in the western external Alps. *Tectonics* 33: 1055–1088. https://doi.org/10.1002/2013tc003453.

Bensalah MK, Youbi N, Mata J, Madeira J, Martins L, Hachimi HE, *et al.* 2013. The Jurassic–Cretaceous basaltic magmatism of the Oued El-Abid syncline (High Atlas, Morocco): Physical volcanology, geochemistry and geodynamic implications. *J. Afr. Earth Sci.* 81: 60–81. https://doi.org/10.1016/j.jafrearsci.2013.01.004.

Berger J, Féménias O, Mercier J-CC, Demaiffe D. 2006. A Variscan slow-spreading ridge (MOR-LHOT) in Limousin (French Massif Central): Magmatic evolution and tectonic setting inferred from mineral chemistry. *Miner. Mag.* 70: 175–185. https://doi.org/10.1180/0026461067020322.

Berger J, Féménias O, Ohnenstetter D, Bruguier O, Plissart G, Mercier J-CC, *et al.* 2010. New occurrence of UHP eclogites in Limousin (French Massif Central): Age, tectonic setting and fluid–rock interactions. *Lithos* 118: 365–382. https://doi.org/10.1016/j.lithos.2010.05.013.

Bessière E, Jolivet L, Augier R, Scaillet S, Précigout J, Azañon J-M, *et al.* 2021. Lateral variations of pressure-temperature evolution in non-cylindrical orogens and 3-D subduction dynamics: The Betic-Rif Cordillera example. *BSGF – Earth Sci. Bull.* 192: 8. https://doi.org/10.1051/bsgf/2021007.

Beyer EE, Brueckner HK, Griffin WL, O'Reilly SY, Graham S. 2004. Archean mantle fragments in Proterozoic crust, Western Gneiss Region, Norway. *Geology* 32: 609–612. https://doi.org/10.1130/g20366.1.

Beyer EE, Griffin WL, O'Reilly SY. 2006. Transformation of Archaean lithospheric mantle by refertilization: Evidence from exposed peridotites in the Western Gneiss Region, Norway. *J. Petrol.* 47: 1611–1636. https://doi.org/10.1093/petrology/egl022.

Bezada MJ, Humphreys ED, Toomey DR, Harnafi M, Dávila JM, Gallart J. 2013. Evidence for slab rollback in westernmost Mediterranean from improved upper mantle imaging. *Earth and Planetary Science Letters* 368: 51–60. https://doi.org/10.1016/j.epsl.2013.02.024.

Bijwaard H, Spakman W, Engdahl ER. 1998. Closing the gap between regional and global travel time tomography. *J. Geophys. Res. Solid Earth* 103: 30055–30078. https://doi.org/10.1029/98jb02467.

Bingen B, Viola G, Möller C, Auwera JV, Laurent A, Yi K. 2020. The Sveconorwegian orogeny. *Gondwana Res.* 90: 273–313. https://doi.org/10.1016/j.gr.2020.10.014.

Bogdanova SV, Bingen B, Gorbatschev R, Kheraskova TN, Kozlov VI, Puchkov VN, *et al.* 2008. The East European Craton (Baltica) before and during the assembly of Rodinia. *Precambrian Research* 160: 23–45. https://doi.org/10.1016/j.precamres.2007.04.024.

Bois C, Party ES. 1990. Major geodynamic processes studied from the ECORS deep seismic profiles in France and adjacent areas. *Tectonophysics* 173: 397–410. https://doi.org/10.1016/0040-1951(90)90233-x.

Bosch D, Maury RC, Azzouzi ME, Bollinger C, Bellon H, Verdoux P. 2014. Lithospheric origin for Neogene–Quaternary Middle Atlas lavas (Morocco): Clues from trace elements and Sr–Nd–Pb–Hf isotopes. *Lithos* 205: 247–265. https://doi.org/10.1016/j.lithos.2014.07.009.

Bosch GV, Teixell A, Jolivet M, Labaume P, Stockli D, Domènech M, *et al.* 2016. Timing of Eocene-Miocene Thrust activity in the Western Axial Zone and Chaînons Béarnais (west-central Pyrenees) revealed by multi-method thermochronology. *C. R. Geosci.* 348: 246–256. https://doi.org/10.1016/j.crte.2016.01.001.

Botor D, Anczkiewicz AA, Dunkl I, Golonka J, Paszkowski M, Mazur S. 2018. Tectonothermal history of the Holy Cross Mountains (Poland) in the light of low-temperature thermochronology. *Terra Nova* 30: 270–278. https://doi.org/10.1111/ter.12336.

Botor D, Anczkiewicz AA, Mazur S, Siwecki T. 2019. Post-Variscan thermal history of the Intra-Sudetic Basin (Sudetes, Bohemian Massif) based on apatite fission track analysis. *Int. J. Earth Sci.* 108: 2561–2576. https://doi.org/10.1007/s00531-019-01777-9.

Bouabdellah M, Hoernle K, Kchit A, Duggen S, Hauff F, Klügel A, *et al.* 2010. Petrogenesis of the Eocene Tamazert Continental Carbonatites (Central High Atlas, Morocco): Implications for a common source for the Tamazert and Canary and Cape Verde Island Carbonatites. *J. Petrol.* 51: 1655–1686. https://doi.org/10.1093/petrology/egq033.

Bourquin S, Bercovici A, López-Gómez J, Diez JB, Broutin J, Ronchi A, *et al.* 2011. The Permian-Triassic transition and the onset of Mesozoic sedimentation at the northwestern peri-Tethyan domain scale: Palaeogeographic maps and geodynamic implications. *Palaeogeogr Palaeoclim Palaeoecol* 299: 265–280. https://doi.org/10.1016/j.palaeo.2010.11.007.

Braga JC, Martin JM, Quesada C. 2003. Patterns and average rates of Late Neogene–Recent uplift of the Betic Cordillera, SE Spain. *Geomorphology* 50: 3–26. https://doi.org/10.1016/s0169-555x(02)00205-2.

Brueckner HK, Carswell DA, Griffin WL. 2002. Paleozoic diamonds within a Precambrian peridotite lens in UHP gneisses of the Norwegian Caledonides. *Earth Planet. Sci. Lett.* 203: 805–816. https://doi.org/10.1016/s0012-821x(02)00919-6.

Bruguier O, Becq-Giraudon JF, Champenois M, Deloule E, Ludden J, Mangin D. 2003. Application of in situ zircon geochronology and accessory phase chemistry to constraining basin development during post-collisional extension: A case study from the French Massif Central. *Chem. Geol.* 201: 319–336. https://doi.org/10.1016/j.chemgeo.2003.08.005.

Brune S, Williams SE, Butterworth NP, Müller RD. 2016. Abrupt plate accelerations shape rifted continental margins. *Nature* 536: 201–204. https://doi.org/10.1038/nature18319.

Burke K, Steinberger B, Torsvik TH, Smethurst MA. 2008. Plume Generation Zones at the margins of Large Low Shear Velocity Provinces on the core-mantle boundary. *Earth Planet. Sci. Lett.* 265: 49–60. https://doi.org/10.1016/j.epsl.2007.09.042.

Burkhard M, Caritg S, Helg U, Robert-Charrue C, Soulaimani A. 2006. Tectonics of the Anti-Atlas of Morocco. *C. R. Geosci.* 338: 11–24. https://doi.org/10.1016/j.crte.2005.11.012.

Burov EB, Diament M. 1995. The effective elastic thickness (Te) of continental lithosphere: What does it really mean? *J. Geophys. Res. Solid Earth* 100: 3905–3927. https://doi.org/10.1029/94jb02770.

Burov EB, Watts AB. 2006. The long-term strength of continental lithosphere: "jelly sandwich" or "crème brûlée"? *GSA Today* 16: 4. https://doi.org/10.1130/1052-5173(2006)016<4:tltsoc>2.0.co;2.

Bussy F, Hernandez J, Raumer JV. 2000. Bimodal magmatism as a consequence of the post-collisional readjustment of the thickened Variscan continental lithosphere (Aiguilles Rouges-Mont Blanc Massifs, Western Alps). *Earth Environ. Sci. Trans. Royal Soc.* 91: 221–233. https://doi.org/10.1017/s0263593300007392.

Calais E, Camelbeeck T, Stein S, Liu M, Craig TJ. 2016. A new paradigm for large earthquakes in stable continental plate interiors: Large earthquakes in SCRS. *Geophys. Res. Lett.* 43: 10621–10637. https://doi.org/10.1002/2016gl070815.

Calvert A, Sandvol E, Seber D, Barazangi M, Roecker S, Mourabit T, *et al.* 2000. Geodynamic evolution of the lithosphere and upper mantle beneath the Alboran region of the western Mediterranean: Constraints from travel time tomography. *Journal of Geophysical Research: Solid Earth* 105: 10871–10898. https://doi.org/10.1029/2000jb900024.

Campanyà J, Ledo J, Queralt P, Marcuello A, Liesa M, Muñoz JA. 2011. Lithospheric characterization of the Central Pyrenees based on new magnetotelluric data. *Terra Nova* 23: 213–219. https://doi.org/10.1111/j.1365-3121.2011.01001.x.

Cande SC, Stegman DR. 2012. Indian and African plate motions driven by the push force of the Réunion plume head. *Nature* 475: 47–52. https://doi.org/10.1038/nature10174.

Candan O, Akal C, Koralay OE, Okay AI, Oberhänsli R, Prelević D, *et al.* 2016. Carboniferous granites on the northern margin of Gondwana, Anatolide-Tauride Block, Turkey – Evidence for southward subduction of Paleotethys. *Tectonophysics* 683: 349–366. https://doi.org/10.1016/j.tecto.2016.06.030.

Carbonell R, Simancas F, Juhlin C, Pous J, Pérez-Estaún A, Gonzalez-Lodeiro F, *et al.* 2004. Geophysical evidence of a mantle derived intrusion in SW Iberia: Evidence for a mafic intrusion complex. *Geophys. Res. Lett.* 31: n/a–n/a. https://doi.org/10.1029/2004gl019684.

Cardello GL, Mancktelow NS. 2014. Cretaceous syn-sedimentary faulting in the Wildhorn Nappe (SW Switzerland). *Swiss J. Geosci.* 107: 223–250. https://doi.org/10.1007/s00015-014-0166-8.

Carlson RW, Pearson DG, James DE. 2005. Physical, chemical, and chronological characteristics of continental mantle. *Reviews of Geophysics* 43: 1. https://doi.org/10.1029/2004rg000156.

Carola E, Muñoz JA, Roca E. 2015. The transition from thick-skinned to thin-skinned tectonics in the Basque-Cantabrian Pyrenees: The Burgalesa Platform and surroundings. *International Journal of Earth Sciences* 104: 2215–2239. https://doi.org/10.1007/s00531-015-1177-z.

Casado BO, Gebauer D, Schäfer HJ, Ibarguchi JIG, Peucat JJ. 2001. A single Devonian subduction event for the HP/HT metamorphism of the Cabo Ortegal complex within the Iberian Massif. *Tectonophysics* 332: 359–385. https://doi.org/10.1016/s0040-1951(00)00210-9.

Cassinis G, Perotti CR, Ronchi A. 2011. Permian continental basins in the Southern Alps (Italy) and peri-mediterranean correlations. *Int. J. Earth Sci.* 101: 129–157. https://doi.org/10.1007/s00531-011-0642-6.

Cavazza W, Roure F, Ziegler PA. 2004. The TRANSMED Atlas. The Mediterranean Region from crust to mantle, geological and geophysical framework of the Mediterranean and the surrounding areas, pp. 1–29. https://doi.org/10.1007/978-3-642-18919-7_1.

Cawood PA, Pisarevsky SA. 2017. Laurentia-Baltica-Amazonia relations during Rodinia assembly. *Precambrian Res.* 292: 386–397. https://doi.org/10.1016/j.precamres.2017.01.031.

Cawood PA, McCausland PJA, Dunning GR. 2001. Opening Iapetus: Constraints from the Laurentian margin in Newfoundland. *GSA Bulletin* 113: 443–453. https://doi.org/10.1130/0016-7606(2001)113<0443:oicftl>2.0.co;2.

Cebriá JM, López-Ruiz J, Doblas M, Martins LT, Munha J. 2003. Geochemistry of the Early Jurassic Messejana-Plasencia dyke (Portugal-Spain): Implications on the origin of the Central Atlantic Magmatic Province. *J. Petrol.* 4: 547–568. https://doi.org/10.1093/petrology/44.3.547.

Cederbom C, Larson SÅ, Tullborg E-L, Stiberg J-P. 2000. Fission track thermochronology applied to Phanerozoic thermotectonic events in Central and Southern Sweden. *Tectonophysics* 316: 153–167. https://doi.org/10.1016/s0040-1951(99)00230-9.

Čermák V, Bodri L. 1986. Two-dimensional temperature modelling along five East-European geotraverses. *J. Geodyn.* 5: 133–163. https://doi.org/10.1016/0264-3707(86)90003-7.

Chantraine J, Egal E, Thiéblemont D, Goff EL, Guerrot C, Ballèvre M, *et al.* 2001. The Cadomian active margin (North Armorican Massif, France): A segment of the North Atlantic Panafrican Belt. *Tectonophysics* 331: 1–18. https://doi.org/10.1016/s0040-1951(00)00233-x.

Chelle-Michou C, Laurent O, Moyen J-F, Block S, Paquette J-L, Couzinié S, *et al.* 2017. Pre-Cadomian to Late-Variscan odyssey of the eastern Massif Central, France: Formation of the West European crust in a nutshell. *Gondwana Res.* 46: 170–190. https://doi.org/10.1016/j.gr.2017.02.010.

Chenin P, Picazo S, Jammes S, Manatschal G, Müntener O, Karner G. 2018. Potential role of lithospheric mantle composition in the Wilson cycle: A North Atlantic perspective. *Geol. Soc. Lond. Special Publ.* 470: 157–172. https://doi.org/10.1144/sp470.10.

Chevrot S, Sylvander M, Diaz J, Martin R, Mouthereau F, Manatschal G, *et al.* 2018. The non-cylindrical crustal architecture of the Pyrenees. *Scientific Reports* 8: 9591. https://doi.org/10.1038/s41598-018-27889-x.

Chew DM, Strachan RA. 2014. The Laurentian Caledonides of Scotland and Ireland. *Geol. Soc. Lond. Special Publ.* 390: 45–91. https://doi.org/10.1144/sp390.16.

Chiarabba C, Giacomuzzi G, Bianchi I, Agostinetti NP, Park J. 2014. From underplating to delamination-retreat in the northern Apennines. *Earth and Planetary Science Letters* 403: 108–116. https://doi.org/10.1016/j.epsl.2014.06.041.

Cloetingh S, Ziegler PA. 2007. Treatise on geophysics. In: Schubert G, ed. *Treatise on Geophysics*. Elsevier, pp. 485–611. https://doi.org/10.1016/b978-044452748-6.00109-7.

Cogné N, Doepke D, Chew D, Stuart FM, Mark C. 2016. Measuring plume-related exhumation of the British Isles in Early Cenozoic times. *Earth Planet. Sci. Lett.* 456: 1–15. https://doi.org/10.1016/j.epsl.2016.09.053.

Coltice N, Phillips BR, Bertrand H, Ricard Y, Rey P. 2007. Global warming of the mantle at the origin of flood basalts over supercontinents. *Geology* 35: 391. https://doi.org/10.1130/g23240a.1.

Coltice N, Bertrand H, Rey P, Jourdan F, Phillips BR, Ricard Y. 2009. Global warming of the mantle beneath continents back to the Archaean. *Gondwana Res.* 15: 254–266. https://doi.org/10.1016/j.gr.2008.10.001.

Conway-Jones BW, Roberts GG, Fichtner A, Hoggard M. 2019. Neogene Epeirogeny of Iberia. *Geochem. Geophys. Geosyst.* 20: 1138–1163. https://doi.org/10.1029/2018gc007899.

Cook CA, Holdsworth RE, Styles MT, Pearce JA. 2000. Pre-emplacement structural history recorded by mantle peridotites: An example from the Lizard Complex, SW England. *J. Geol. Soc. Lond.* 157: 1049–1064. https://doi.org/10.1144/jgs.157.5.1049.

Corfu F, Andersen TB, Gasser D. 2014. The Scandinavian Caledonides: Main features, conceptual advances and critical questions. *Geol. Soc. Lond. Special Publ.* 390: 9–43. https://doi.org/10.1144/sp390.25.

Couzinié S, Laurent O, Poujol M, Mintrone M, Chelle-Michou C, Moyen J-F, *et al.* 2017. Cadomian S-type granites as basement rocks of the Variscan Belt (Massif Central, France): Implications for the crustal evolution of the North Gondwana margin. In: *Mantle Dynamics and Crust-Mantle Interactions in Collisional Orogens Topical Session* at the *Geological Society of America Annual Meeting, 2007*, 286-287: 16–34. https://doi.org/10.1016/j.lithos.2017.06.001.

Curry ME, van der Beek P, Huismans RS, Wolf SG, Muñoz J-A. 2019. Evolving paleotopography and lithospheric flexure of the Pyrenean Orogen from 3D flexural modeling and basin analysis. *Earth Planet. Sci. Lett.* 515: 26–37. https://doi.org/10.1016/j.epsl.2019.03.009.

Danišík M, Pfaff K, Evans NJ, Manoloukos C, Staude S, McDonald BJ, *et al.* 2010. Tectonothermal history of the Schwarzwald Ore District (Germany): An apatite triple dating approach. *Chem. Geol.* 278: 58–69. https://doi.org/10.1016/j.chemgeo.2010.08.022.

Danišík M, Štěpančíková P, Evans NJ. 2012. Constraining long-term denudation and faulting history in intraplate regions by multisystem thermochronology: An example of the Sudetic Marginal Fault (Bohemian Massif, Central Europe). *Tectonics* 31. https://doi.org/10.1029/2011tc003012.

Das P, Lin AT-S, Chen M-PP, Miramontes E, Liu C-S, Huang N-W, *et al.* 2021. Deep-sea submarine erosion by the Kuroshio Current in the Manila accretionary prism, offshore Southern Taiwan. *Tectonophysics* 807: 228813. https://doi.org/10.1016/j.tecto.2021.228813.

Daudet M, Mouthereau F, Brichau S, Crespo-Blanc A, Gautheron C, Angrand P. 2020. Tectono-stratigraphic and thermal evolution of the western Betic flysch: Implications for the geodynamics of South Iberian margin and Alboran Domain. *Tectonics* 39. https://doi.org/10.1029/2020tc006093.

Debon F, Zimmermann JL. 1993. Mafic dykes from some plutons of the western Pyrenean Axial Zone (France, Spain): Markers of the transition from Late-Hercynian to Early-Alpine events. *Schweizerische mineralogische und petrographische Mitteilunge* 73. https://doi.org/10.5169/seals-55585.

Dekorp Basin Research Group. 1999. Deep crustal structure of the Northeast German basin: New DEKORP-BASIN '96 deep-profiling results. *Geology* 27: 55–58. https://doi.org/10.1130/0091-7613(1999)027<0055:dcsotn>2.3.co;2.

DeMets C, Gordon RG, Argus DF. 2010. Geologically current plate motions. *Geophysical Journal International* 181: 1–80. https://doi.org/10.1111/j.1365-246x.2009.04491.x.

Denèle Y, Olivier P, Gleizes G, Barbey P. 2007. The Hospitalet gneiss dome (Pyrenees) revisited: Lateral flow during Variscan transpression in the middle crust. *Terra Nova* 19: 445–453. https://doi.org/10.1111/j.1365-3121.2007.00770.x.

Dewey JF, Pitman WC, Ryan WBF, Bonnin J. 1973. Plate tectonics and the evolution of the Alpine System. *GSA Bulletin* 84: 3137–3180. https://doi.org/10.1130/0016-7606(1973)84<3137:ptateo>2.0.co;2.

Dèzes P, Schmid SM, Ziegler PA. 2004. Evolution of the European Cenozoic Rift System: interaction of the Alpine and Pyrenean orogens with their foreland lithosphere. *Tectonophysics* 389: 1–33. https://doi.org/10.1016/j.tecto.2004.06.011.

Dias G, Leterrier J. 1994. The genesis of felsic-mafic plutonic associations: A Sr and Nd isotopic study of the Hercynian Braga Granitoid Massif (Northern Portugal). *Lithos* 32: 207–223. https://doi.org/10.1016/0024-4937(94)90040-x.

Dielforder A, Frasca G, Brune S, Ford M. 2019. Formation of the Iberian-European convergent plate boundary fault and its effect on intraplate deformation in Central Europe. *Geochem Geophys Geosyst* 20: 2395–2417. https://doi.org/10.1029/2018gc007840.

Dieni I, Massari F, Médus J. 2008. Age, depositional environment and stratigraphic value of the Cuccuru 'e Flores Conglomerate: Insight into the Palaeogene to Early Miocene geodynamic evolution of Sardinia. *Bulletin de la Société géologique de France* 179: 51–72. https://doi.org/10.2113/gssgfbull.179.1.51.

Dijkstra AH, Drury MR, Vissers RLM, Newman J. 2002. On the role of melt-rock reaction in mantle shear zone formation in the Othris Peridotite Massif (Greece). *J. Struct. Geol.* 24: 1431–1450. https://doi.org/10.1016/s0191-8141(01)00142-0.

Dijkstra AH, Dale CW, Oberthür T, Nowell GM, Pearson DG. 2016. Osmium isotope compositions of detrital Os-rich alloys from the Rhine River provide evidence for a global Late Mesoproterozoic mantle depletion event. *Earth Planet. Sci. Lett.* 452: 115–122. https://doi.org/10.1016/j.epsl.2016.07.047.

D'Lemos RS, Inglis JD, Samson SD. 2006. A newly discovered orogenic event in Morocco: Neoproterozic ages for supposed Eburnean basement of the Bou Azzer inlier, Anti-Atlas Mountains. *Precambrian Res.* 147: 65–78. https://doi.org/10.1016/j.precamres.2006.02.003.

Do Couto D, Gumiaux C, Augier R, Lebret N, Folcher N, Jouannic G, *et al.* 2014. Tectonic inversion of an asymmetric graben: Insights from a combined field and gravity survey in the Sorbas basin. *Tectonics* 33: 1360–1385. https://doi.org/10.1002/2013tc003458.

Do Couto D, Gorini C, Jolivet L, Lebret N, Augier R, Gumiaux C, *et al.* 2016. Tectonic and stratigraphic evolution of the Western Alboran Sea Basin in the last 25 Myrs. *Tectonophysics* 677-678: 280–311. https://doi.org/10.1016/j.tecto.2016.03.020.

Domeier M. 2016. A plate tectonic scenario for the Iapetus and Rheic Oceans. *Gondwana Res.* 36: 275–295. https://doi.org/10.1016/j.gr.2015.08.003.

Domeier M, Font E, Youbi N, Davies J, Nemkin S, der Voo RV, *et al.* 2020. On the Early Permian shape of Pangea from paleomagnetism at its core. *Gondwana Res.* 90: 171–198. https://doi.org/10.1016/j.gr.2020.11.005.

Dostal J, Keppie JD, Hamilton MA, Aarab EM, Lefort JP, Murphy JB. 2005. Crustal xenoliths in Triassic lamprophyre dykes in western Morocco: tectonic implications for the Rheic Ocean suture. *Geol. Mag.* 142: 159–172. https://doi.org/10.1017/s0016756805000440.

Dostal J, Murphy JB, Shellnutt JG. 2019. Secular isotopic variation in lithospheric mantle through the Variscan orogen: Neoproterozoic to Cenozoic magmatism in continental Europe. *Geology* 47: 637–640. https://doi.org/10.1130/g46067.1.

Dresmann H, Keulen N, Timar-Geng Z, Fügenschuh B, Wetzel A, Stünitz H. 2008. The south-western Black Forest and the Upper Rhine Graben Main Border Fault: thermal history and hydrothermal fluid flow. *Int. J. Earth Sci.* 99: 285–297. https://doi.org/10.1007/s00531-008-0391-3.

Drost K, Gerdes A, Jeffries T, Linnemann U, Storey C. 2011. Provenance of Neoproterozoic and Early Paleozoic siliciclastic rocks of the Teplá-Barrandian Unit (Bohemian Massif): Evidence

from U-Pb detrital zircon ages. *Gondwana Res.* 19: 213–231. https://doi.org/10.1016/j.gr.2010.05.003.

Ducoux M, Jolivet L, Callot J-P, Aubourg C, Masini E, Lahfid A, *et al.* 2019. The Nappe des Marbres Unit of the Basque-Cantabrian Basin: The tectono-thermal evolution of a fossil hyperextended rift basin. *Tectonics* 38: 3881–3915. https://doi.org/10.1029/2018tc005348.

Duggen S, Hoernle K, van den Bogaard P, Rüpke L, Morgan JP. 2003. Deep roots of the Messinian salinity crisis. *Nature* 422: 602–606. https://doi.org/10.1038/nature01553.

Duggen S, Hoernle K, van den Bogaard P, Harris C. 2004. Magmatic evolution of the Alboran region: The role of subduction in forming the western Mediterranean and causing the Messinian salinity crisis. *Earth and Planetary Science Letters* 218: 91–108. https://doi.org/10.1016/s0012-821x(03)00632-0.

Duggen S, Hoernle KA, Hauff F, Klügel A, Bouabdellah M, Thirlwall MF. 2009. Flow of Canary mantle plume material through a subcontinental lithospheric corridor beneath Africa to the Mediterranean. *Geology* 37: 283–286. https://doi.org/10.1130/g25426a.1.

Dusséaux C, Gébelin A, Ruffet G, Mulch A. 2021. Late Carboniferous paleoelevation of the Variscan Belt of Western Europe. *Earth Planet. Sci. Lett.* 569: 117064. https://doi.org/10.1016/j.epsl.2021.117064.

El-Sharkawy A, Meier T, Lebedev S, Behrmann JH, Hamada M, Cristiano L, *et al.* 2020. The slab puzzle of the Alpine-Mediterranean Region: Insights from a new, high-resolution, shear wave velocity model of the Upper Mantle. *Geochem. Geophys. Geosyst.* 21. https://doi.org/10.1029/2020gc008993.

Ennih N, Liégeois J-P. 2001. The Moroccan Anti-Atlas: The West African craton passive margin with limited Pan-African activity. Implications for the northern limit of the craton. *Precambrian Res.* 112: 289–302. https://doi.org/10.1016/s0301-9268(01)00195-4.

Ennih N, Liégeois J-P. 2008. The boundaries of the West African craton, with special reference to the basement of the Moroccan metacratonic Anti-Atlas Belt. *Geological Society, London, Special Publications* 297: 1–17. https://doi.org/10.1144/sp297.1.

Espurt N, Angrand P, Teixell A, Labaume P, Ford M, de Saint Blanquat M, *et al.* 2019. Crustal-scale balanced cross-section and restorations of the Central Pyrenean Belt (Nestes-Cinca transect): Highlighting the structural control of Variscan Belt and Permian-Mesozoic rift systems on mountain building. *Tectonophysics* 764: 25–45. https://doi.org/10.1016/j.tecto.2019.04.026.

Essaifi A, Samson S, Goodenough K. 2014. Geochemical and Sr-Nd isotopic constraints on the petrogenesis and geodynamic significance of the Jebilet magmatism (Variscan Belt, Morocco). *Geol. Mag.* 151: 666–691. https://doi.org/10.1017/s0016756813000654.

Esteban JJ, Aranguren A, Cuevas J, Hilario A, Tubía JM, Larionov A, *et al.* 2015. Is there a time lag between the metamorphism and emplacement of plutons in the Axial Zone of the Pyrenees? *Geol. Mag.* 152: 935–941. https://doi.org/10.1017/s001675681500014x.

Eynatten H. von, Dunkl I, Brix M, Hoffmann V-E, Raab M, Thomson SN, *et al.* 2019. Late Cretaceous exhumation and uplift of the Harz Mountains, Germany: A multi-method thermochronological approach. *Int. J. Earth Sci.* 108: 2097–2111. https://doi.org/10.1007/s00531-019-01751-5.

Fabries J, Lorand JP, Bodinier JL, Dupuy C. 1991. Evolution of the Upper Mantle beneath the Pyrenees: Evidence from Orogenic Spinel Lherzolite Massifs. *Journal of Petrology Special Volume* 55–76. https://doi.org/10.1093/petrology/special_volume.2.55.

Faccenna C, Becker TW. 2010. Shaping mobile belts by small-scale convection. *Nature* 465: 602–5. https://doi.org/10.1038/nature09064.

Faccenna C, Becker TW. 2020. Topographic expressions of mantle dynamics in the Mediterranean. *Earth-Sci. Rev.* 103327. https://doi.org/10.1016/j.earscirev.2020.103327.

Faccenna C, Becker TW, Lucente FP, Jolivet L, Rossetti F. 2001. History of subduction and back-arc extension in the Central Mediterranean. *Geophys. J. Int.* 145: 809–820. https://doi.org/10.1046/j.0956-540x.2001.01435.x.

Faccenna C, Becker TW, Lallemand S, Lagabrielle Y, Funiciello F, Piromallo C. 2010. Subduction-triggered magmatic pulses: A new class of plumes? *Earth Planet. Sci. Lett.* 299: 54–68. https://doi.org/10.1016/j.epsl.2010.08.012.

Faccenna C, Becker TW, Conrad CP, Husson L. 2013a. Mountain building and mantle dynamics: Mountain building and mantle dynamics. *Tectonics* 32: 80–93. https://doi.org/10.1029/2012tc003176.

Faccenna C, Becker TW, Jolivet L, Keskin M. 2013b. Mantle convection in the Middle East: Reconciling Afar upwelling, Arabia indentation and Aegean trench rollback. *Earth Planet. Sci. Lett.* 375: 254–269. https://doi.org/10.1016/j.epsl.2013.05.043.

Faccenna C, Becker TW, Auer L, Billi A, Boschi L, Brun JP, *et al.* 2014. Mantle dynamics in the Mediterranean. *Rev. Geophys.* 52: 283–332. https://doi.org/10.1002/2013rg000444.

Fauquette S, Suc J-P, Popescu S-M, Guillocheau F, Violette S, Jost A, *et al.* 2020. Pliocene uplift of the Massif Central (France) constrained by the palaeoelevation quantified from the pollen record of sediments preserved along the Cantal Stratovolcano (Murat area). *J. Geol. Soc. Lond.* jgs2020-010. https://doi.org/10.1144/jgs2020-010.

Faure M. 1995. Late orogenic carboniferous extensions in the Variscan French Massif Central. *Tectonics* 14: 132–153. https://doi.org/10.1029/94tc02021.

Féménias O, Coussaert N, Bingen B, Whitehouse M, Mercier J-CC, Demaiffe D. 2003. A Permian underplating event in late- to post-orogenic tectonic setting. Evidence from the mafic-ultramafic layered xenoliths from Beaunit (French Massif Central). *Chem. Geol.* 199: 293–315. https://doi.org/10.1016/s0009-2541(03)00124-4.

Fernández-Suárez J, Dunning GR, Jenner GA, Gutiérrez-alonso G. 2000. Variscan collisional magmatism and deformation in NW Iberia: constraints from U-Pb geochronology of granitoids. *J. Geol. Soc. Lond.* 157: 565–576. https://doi.org/10.1144/jgs.157.3.565.

Fillon C, van der Beek P. 2012. Post-orogenic evolution of the southern Pyrenees: Constraints from inverse thermo-kinematic modelling of low-temperature thermochronology data. *Basin Res.* 24: 418–436. https://doi.org/10.1111/j.1365-2117.2011.00533.x.

Fillon C, Gautheron C, van der Beek P. 2013. Oligocene–Miocene burial and exhumation of the Southern Pyrenean foreland quantified by low-temperature thermochronology. *Journal of the Geological Society* 170: 67–77. https://doi.org/10.1144/jgs2012-051.

Fillon C, Mouthereau F, Calassou S, Pik R, Bellahsen N, Gautheron C, *et al.* 2021. Post-orogenic exhumation in the western Pyrenees: Evidence for extension driven by pre-orogenic inheritance. *J. Geol. Soc. Lond.* 178: jgs2020-079. https://doi.org/10.1144/jgs2020-079.

Flinch JF, Soto JI. 2017. Chapter 19: Allochthonous Triassic and salt tectonic processes in the Betic-Rif Orogenic Arc. In: *Permo-Triassic Salt Provinces of Europe, North Africa and the Atlantic Margins*. Elsevier CY, pp. 417–446. https://doi.org/1016/B978-0-12-809417-4.00020-3.

Flinch JF, Bally AW, Wu S. 1996. Emplacement of a passive-margin evaporitic allochthon in the Betic Cordillera of Spain. *Geology* 24: 67. https://doi.org/10.1130/0091-7613(1996)024<0067:eoapme>2.3.co;2.

Fortey RA, Cocks LRM. 2003. Palaeontological evidence bearing on global Ordovician-Silurian continental reconstructions. *Earth-Sci. Rev.* 61: 245–307. https://doi.org/10.1016/s0012-8252(02)00115-0.

François T, Barbarand J, Wyns R. 2020. Lower Cretaceous inversion of the European Variscan basement: record from the Vendée and Limousin (France). *Int. J. Earth Sci.* https://doi.org/10.1007/s00531-020-01875-z.

Franke W, Cocks LRM, Torsvik TH. 2017. The Palaeozoic Variscan Oceans revisited. *Gondwana Res.* 48: 257–284. https://doi.org/10.1016/j.gr.2017.03.005.

Frizon de Lamotte D, Zizi M, Missenard Y, Hafid M, Azzouzi ME, Maury RC, *et al.* 2008. Continental evolution: The geology of Morocco, structure, stratigraphy, and tectonics of the Africa-Atlantic-Mediterranean Triple Junction. *Lect. Notes Earth Sci.* 133–202. https://doi.org/10.1007/978-3-540-77076-3_4.

Frizon de Lamotte D, Leturmy P, Missenard Y, Khomsi S, Ruiz G, Saddiqi O, *et al.* 2009. Mesozoic and Cenozoic vertical movements in the Atlas system (Algeria, Morocco, Tunisia): An overview. *Tectonophysics* 475: 9–28. https://doi.org/10.1016/j.tecto.2008.10.024.

Froitzheim N, Stets J, Wurster P. 1988. *Lecture Notes in Earth Sciences* 219–244. https://doi.org/10.1007/bfb0011595.

Fügenschuh B, Schmid SM. 2005. Age and significance of core complex formation in a very curved orogen: Evidence from fission track studies in the South Carpathians (Romania). *Tectonophysics* 404: 33–53. https://doi.org/10.1016/j.tecto.2005.03.019.

Gallagher K. 2012. Transdimensional inverse thermal history modeling for quantitative thermochronology. *Journal of Geophysical Research: Solid Earth (1978–2012)* 117: n/a–n/a. https://doi.org/10.1029/2011jb008825.

Gallagher K, Charvin K, Nielsen S, Sambridge M, Stephenson J. 2009. Markov chain Monte Carlo (MCMC) sampling methods to determine optimal models, model resolution and model choice for Earth Science problems. *Marine and Petroleum Geology* 26: 525–535. https://doi.org/10.1016/j.marpetgeo.2009.01.003.

Ganne J, Feng X, Rey P, Andrade VD. 2016. Statistical petrology reveals a link between supercontinents cycle and mantle global climate. *Am. Miner.* 101: 2768–2773. https://doi.org/10.2138/am-2016-5868.

Garcia-Castellanos D, Larrasoaña JC. 2015. Quantifying the post-tectonic topographic evolution of closed basins: The Ebro Basin (northeast Iberia). *Geology* 43: 663–666. https://doi.org/10.1130/g36673.1.

Garrido CJ, Bodinier J-L. 1999. Diversity of mafic rocks in the Ronda Peridotite: Evidence for Pervasive melt-rock reaction during heating of subcontinental lithosphere by upwelling asthenosphere. *Journal of Petrology* 40: 729–754. https://doi.org/10.1093/petroj/40.5.729.

Garrido CJ, Gueydan F, Booth-Rea G, Precigout J, Hidas K, Padrón-Navarta JA, *et al.* 2011. Garnet lherzolite and garnet-spinel mylonite in the Ronda peridotite: Vestiges of Oligocene backarc mantle lithospheric extension in the western Mediterranean. *Geology* 39: 927–930. https://doi.org/10.1130/g31760.1.

Gasquet D, Ennih N, Liégeois J-P, Soulaimani A, Michard A. 2008. Continental evolution: The geology of Morocco, structure, stratigraphy, and tectonics of the Africa-Atlantic-Mediterranean Triple Junction. *Lect. Notes Earth Sci.* 33–64. https://doi.org/10.1007/978-3-540-77076-3_2.

Geach MR, Viveen W, Mather AE, Telfer MW, Fletcher WJ, Stokes M, *et al.* 2015. An integrated field and numerical modelling study of controls on Late Quaternary fluvial landscape development (Tabernas, southeast Spain). *Earth Surf. Process.* 40: 1907–1926. https://doi.org/10.1002/esp.3768.

Geissler WH, Sodoudi F, Kind R. 2010. Thickness of the central and eastern European lithosphere as seen by S receiver functions. *Geophys. J. Int.* 181: 604–634. https://doi.org/10.1111/j.1365-246x.2010.04548.x.

Ghosh A, Holt WE, Wen L. 2013. Predicting the lithospheric stress field and plate motions by joint modeling of lithosphere and mantle dynamics. *J. Geophys. Res. Solid Earth* 118: 346–368. https://doi.org/10.1029/2012jb009516.

Giaconia F, Booth-Rea G, Martinez-Martinez JM, Azañón JM, Storti F, Artoni A. 2014. Heterogeneous extension and the role of transfer faults in the development of the southeastern Betic Basins (SE Spain). *Tectonics* 33: 2467–2489. https://doi.org/10.1002/2014tc003681.

Giamboni M, Ustaszewski K, Schmid SM, Schumacher ME, Wetzel A. 2004. Plio-Pleistocene transpressional reactivation of Paleozoic and Paleogene structures in the Rhine-Bresse transform zone (Northern Switzerland and Eastern France). *Int. J. Earth Sci.* 93: 207–223. https://doi.org/10.1007/s00531-003-0375-2.

Giletycz S, Loget N, Chang C-P, Mouthereau F. 2015. Transient fluvial landscape and preservation of low-relief terrains in an emerging orogen: Example from Hengchun Peninsula, Taiwan. *Geomorphology* 231: 169–181. https://doi.org/10.1016/j.geomorph.2014.11.026.

Gimeno-Vives O, Mohn G, Bosse V, Haissen F, Zaghloul MN, Atouabat A, *et al.* 2019. The Mesozoic Margin of the Maghrebian Tethys in the Rift Belt (Morocco): Evidence for Polyphase Rifting and related magmatic activity. *Tectonics* 38: 2894–2918. https://doi.org/10.1029/2019tc005508.

Gimeno-Vives O, Mohn G, Bosse V, Haissen F, Zaghloul MN, Atouabat A, *et al.* 2020. Reply to comment by Michard, et al. on "The Mesozoic Margin of the Maghrebian Tethys in the Rif Belt (Morocco): Evidence for Polyphase Rifting and related magmatic activity". *Tectonics* 39. https://doi.org/10.1029/2020tc006165.

Goes S, Govers R, Vacher P. 2000. Shallow mantle temperatures under Europe from P and S waves tomography. *J. Geophys. Res. Solid Earth* 105: 11153–11169. https://doi.org/10.1029/1999jb900300.

González-Jiménez JM, Villaseca C, Griffin WL, Belousova E, Konc Z, Ancochea E, *et al.* 2013. The architecture of the European-Mediterranean lithosphere: A synthesis of the Re-Os evidence. *Geology* 41: 547–550. https://doi.org/10.1130/g34003.1.

Goodenough KM, Millar I, Strachan RA, Krabbendam M, Evans JA. 2011. Timing of regional deformation and development of the Moine Thrust Zone in the Scottish Caledonides: Constraints from the U–Pb geochronology of alkaline intrusions. *J. Geol. Soc. Lond.* 168: 99–114. https://doi.org/10.1144/0016-76492010-020.

Gordon RG. 1998. The plate tectonic approximation: Plate nonrigidity, diffuse plate boundaries, and global plate reconstructions. *Annual Review of Earth and Planetary Sciences* 26: 615–642. https://doi.org/10.1146/annurev.earth.26.1.615.

Graciansky PC de, Lemoine M. 1988. Early Cretaceous extensional tectonics in the southwestern French Alps: A consequence of North-Atlantic rifting during Tethyan spreading. *Bulletin de la Société géologique de France* IV: 733–737. https://doi.org/10.2113/gssgfbull.iv.5.733.

Granet M, Wilson M, Achauer U. 1995. Imaging a mantle plume beneath the French Massif Central. *Earth Planet. Sci. Lett.* 136: 281–296. https://doi.org/10.1016/0012-821x(95)00174-b.

Green PF. 1989. Thermal and tectonic history of the East Midlands shelf (onshore UK) and surrounding regions assessed by apatite fission track analysis. *J. Geol. Soc. Lond.* 146: 755–773. https://doi.org/10.1144/gsjgs.146.5.0755.

Gretter N, Ronchi A, López-Gómez J, Arche A, La Horra RD, Barrenechea J, *et al.* 2015. The Late Palaeozoic-Early Mesozoic from the Catalan Pyrenees (Spain): 60 Myr of environmental evolution in the frame of the western peri-Tethyan palaeogeography. *Earth-Sci. Rev.* 150: 679–708. https://doi.org/10.1016/j.earscirev.2015.09.001.

Griffin WL, O'Reilly SY. 2007. Chapter 8.2: The earliest subcontinental lithospheric mantle. *Developments in Precambrian Geology* 15: 1013–1035. https://doi.org/10.1016/s0166-2635(07)15082-9.

Gröger HR, Fügenschuh B, Tischler M, Schmid SM, Foeken JPT. 2008. Tertiary cooling and exhumation history in the Maramures area (internal Eastern Carpathians, Northern Romania): Thermochronology and structural data. *Geol. Soc. Lond. Special Publ.* 298: 169–195. https://doi.org/10.1144/sp298.9.

Guimera J, Alvaro M. 1990. Structure et évolution de la compression alpine dans la Chaîne Iberique et la chaîne côtière catalane (Espagne). *Bulletin de la Société géologique de France* VI: 339–348. https://doi.org/10.2113/gssgfbull.vi.2.339.

Guiraud R, Bosworth W, Thierry J, Delplanque A. 2005. Phanerozoic geological evolution of Northern and Central Africa: An overview. *J. Afr. Earth Sci.* 43: 83–143. https://doi.org/10.1016/j.jafrearsci.2005.07.017.

Gunnell Y, Calvet M, Brichau S, Carter A, Aguilar JP, Zeyen H. 2009. Low long-term erosion rates in high-energy mountain belts: Insights from thermo- and biochronology in the Eastern Pyrenees. *Earth and Planetary Science Letters* 278: 208–218. https://doi.org/10.1016/j.epsl.2008.12.004.

Gutierrez-Alonso G, Murphy JB, Fernandez-Suárez J, Weil AB, Franco MP, Gonzalo JC. 2011. Lithospheric delamination in the core of Pangea: Sm-Nd insights from the Iberian mantle. *Geology* 39: 155–158. https://doi.org/10.1130/g31468.1.

Hacker BR, Gans PB. 2005. Continental collisions and the creation of ultrahigh-pressure terranes: Petrology and thermochronology of nappes in the central Scandinavian Caledonides. *GSA Bulletin* 117: 117–134. https://doi.org/10.1130/b25549.1.

Handy MR, Schmid SM, Bousquet R, Kissling E, Bernoulli D. 2010. Reconciling plate-tectonic reconstructions of Alpine Tethys with the geological–geophysical record of spreading and subduction in the Alps. *Earth-Science Reviews* 102: 121–158. https://doi.org/10.1016/j.earscirev.2010.06.002.

Handy MR, Ustaszewski K, Kissling E. 2015. Reconstructing the Alps-Carpathians-Dinarides as a key to understanding switches in subduction polarity, slab gaps and surface motion. *Int. J. Earth Sci.* 104: 1–26. https://doi.org/10.1007/s00531-014-1060-3.

Harmand C, Cantagrel JM. 1984. Le volcanisme alcalin tertiaire et quaternaire du moyen atlas (Maroc) : chronologie K/Ar et cadre géodynamique. *J. Afr. Earth Sci.* 2: 51–55. https://doi.org/10.1016/0899-5362(84)90019-8.

Harvey J, Gannoun A, Burton KW, Schiano P, Rogers NW, Alard O. 2010. Unravelling the effects of melt depletion and secondary infiltration on mantle Re–Os isotopes beneath the French Massif Central. *Geochim. Cosmochim. Acta* 74: 293–320. https://doi.org/10.1016/j.gca.2009.09.031.

Heeremans M, Larsen BT, Stel H. 1996. Paleostress reconstruction from kinematic indicators in the Oslo Graben, southern Norway: new constraints on the mode of rifting. *Tectonophysics* 266: 55–79. https://doi.org/10.1016/s0040-1951(96)00183-7.

Heidbach O, Rajabi M, Cui X, Fuchs K, Müller B, Reinecker J, *et al.* 2018. The World Stress Map database release 2016: Crustal stress pattern across scales. *Tectonophysics* 744: 484–498. https://doi.org/10.1016/j.tecto.2018.07.007.

Heinrichs T, Giese P, Bankwitz P, Bankwitz E. 1994. DEKORP 3/MVE-90(West) – Preliminary geological interpretation of a deep near-vertical reflection profile between the Rhenish and the Bohemian Massifs, Germany. *Z. G. Wiss* 22(6): 771–801.

Heit B, Mancilla F de L, Yuan X, Morales J, Stich D, Martín R, *et al.* 2017. Tearing of the mantle lithosphere along the intermediate-depth seismicity zone beneath the Gibraltar Arc: The onset of lithospheric delamination. *Geophys. Res. Lett.* 44: 4027–4035. https://doi.org/10.1002/2017gl073358.

Helg U, Burkhard M, Caritg S, Robert-Charrue C. 2004. Folding and inversion tectonics in the Anti-Atlas of Morocco. *Tectonics* 23, TC4006. https://doi.org/10.1029/2003tc001576.

Henry P, Azambre B, Montigny R, Rossy M, Stevenson RK. 1998. Late mantle evolution of the Pyrenean sub-continental lithospheric mantle in the light of new ^{40}Ar-^{39}Ar and Sm-Nd ages on pyroxenites and peridotites (Pyrenees, France). *Tectonophysics* 296: 103–123. https://doi.org/10.1016/s0040-1951(98)00139-5.

Herman F, Seward D, Valla PG, Carter A, Kohn B, Willett SD, *et al.* 2014. Worldwide acceleration of mountain erosion under a cooling climate. *Nature* 504: 423–426. https://doi.org/10.1038/nature12877.

Hermann J, Rubatto D. 2003. Relating zircon and monazite domains to garnet growth zones: Age and duration of granulite facies metamorphism in the Val Malenco lower crust: Relating zircon and monazite to garnet growth. *J. Metamorph. Geol.* 21: 833–852. https://doi.org/10.1046/j.1525-1314.2003.00484.x.

Heuer B, Geissler WH, Kind R, Kämpf H. 2006. Seismic evidence for asthenospheric updoming beneath the western Bohemian Massif, central Europe. *Geophysical Research Letters* 33. https://doi.org/10.1029/2005gl025158.

Hinsken S, Ustaszewski K, Wetzel A. 2007. Graben width controlling syn-rift sedimentation: The Palaeogene southern Upper Rhine Graben as an example. *Int. J. Earth Sci.* 96: 979–1002. https://doi.org/10.1007/s00531-006-0162-y.

Hodel F, Triantafyllou A, Berger J, Macouin M, Baele J-M, Mattielli N, *et al.* 2020. The Moroccan Anti-Atlas ophiolites: Timing and melting processes in an intra-oceanic arc-back-arc environment. *Gondwana Res.* 86: 182–202. https://doi.org/10.1016/j.gr.2020.05.014.

Hoepffner C, Houari MR, Bouabdelli M. 2006. Tectonics of the North African Variscides (Morocco, western Algeria): An outline. *C. R. Geosci.* 338: 25–40. https://doi.org/10.1016/j.crte.2005.11.003.

Hoggard MJ, Czarnota K, Richards FD, Huston DL, Jacques AL, Ghelichktan S. 2020. Global distribution of sediment-hosted metals controlled by craton edge stability. *Nat. Geosci.* 13: 504–510. https://doi.org/10.1038/s41561-020-0593-2.

Houari M-R, Hoepffner C. 2003. Late Carboniferous dextral wrench-dominated transpression along the North African craton margin (Eastern High-Atlas, Morocco). *J. Afr. Earth Sci.* 37: 11–24. https://doi.org/10.1016/s0899-5362(03)00085-x.

Huyghe D, Mouthereau F, Emmanuel L. 2012. Oxygen isotopes of marine mollusc shells record Eocene elevation change in the Pyrenees. *Earth and Planetary Science Letters* 345-348: 131–141. https://doi.org/10.1016/j.epsl.2012.06.035.

Huyghe D, Mouthereau F, Ségalen L, Furió M. 2020. Long-term dynamic topographic support during post-orogenic crustal thinning revealed by stable isotope (δ18O) paleo-altimetry in Eastern Pyrenees. *Sci. Rep.-UK* 10: 2267. https://doi.org/10.1038/s41598-020-58903-w.

Inglis JD, MacLean JS, Samson SD, D'Lemos RS, Admou H, Hefferan K. 2004. A precise U–Pb zircon age for the Bleïda granodiorite, Anti-Atlas, Morocco: implications for the timing of deformation and terrane assembly in the eastern Anti-Atlas. *J. Afr. Earth Sci.* 39: 277–283. https://doi.org/10.1016/j.jafrearsci.2004.07.041.

Izquierdo-Llavall E, Menant A, Aubourg C, Callot J, Hoareau G, Camps P, *et al.* 2020. Preorogenic Folds and Syn-Orogenic Basement Tilts in an Inverted Hyperextended Margin: The Northern Pyrenees Case Study. *Tectonics* 39. https://doi.org/10.1029/2019tc005719.

Janowski M, Loget N, Gautheron C, Barbarand J, Bellahsen N, Driessche JV den, *et al.* 2017. Neogene exhumation and relief

evolution in the eastern Betics (SE Spain): Insights from the Sierra de Gador. *Terra Nova* 29: 91–97. https://doi.org/10.1111/ter.12252.
Jaupart C, Labrosse S, Lucazeau F, Mareschal J-C. 2015. Treatise on geophysics (2nd ed.), pp. 223–270. https://doi:10.1016/b978-0-444-53802-4.00126-3.
Jolivet L. 2003. Subduction tectonics and exhumation of high-pressure metamorphic rocks in the Mediterranean orogens. *Am. J. Sci.* 303: 353–409. https://doi.org/10.2475/ajs.303.5.353.
Jolivet L, Faccenna C. 2000. Mediterranean extension and the Africa-Eurasia collision. *Tectonics* 19: 1095–1106. https://doi.org/10.1029/2000tc900018.
Jolivet L, Augier R, Faccenna C, Negro F, Rimmele G, Agard P, *et al.* 2008. Subduction, convergence and the mode of backarc extension in the Mediterranean Region. *Bulletin de la Société géologique de France* 179: 525–550. https://doi.org/10.2113/gssgfbull.179.6.525.
Jolivet L, Faccenna C, Agard P, Frizon de Lamotte D, Menant A, Sternai P, *et al.* 2016. Neo-Tethys geodynamics and mantle convection: From extension to compression in Africa and a conceptual model for obduction. *Can. J. Earth Sci.* 53: 1190–1204. https://doi.org/10.1139/cjes-2015-0118.
Jolivet L, Baudin T, Bitri A, Calassou S, Ford M, Issautier B, *et al.* 2021. Geodynamic evolution of a wide plate boundary in the Western Mediterranean, near-field versus far-field interactions. *BSGF Earth Sci. Bull.* 192: 48. https://doi.org/10.1051/bsgf/2021043.
Jordan TH. 1978. Composition and development of the continental tectosphere. *Nature* 274: 544–548. https://doi.org/10.1038/274544a0.
Jourdan F, Féraud G, Bertrand H, Kampunzu AB, Tshoso G, Watkeys MK, *et al.* 2005. Karoo large igneous province: Brevity, origin, and relation to mass extinction questioned by new $^{40}Ar/^{39}Ar$ age data. *Geology* 33: 745–748. https://doi.org/10.1130/g21632.1.
Jourdon A, Pourhiet LL, Mouthereau F, Masini E. 2019. Role of rift maturity on the architecture and shortening distribution in mountain belts. *Earth and Planetary Science Letters* 512: 89–99. https://doi.org/10.1016/j.epsl.2019.01.057.
Jourdon A, Mouthereau F, Pourhiet LL, Callot J. 2020a. Topographic and tectonic evolution of mountain belts controlled by salt thickness and rift architecture. *Tectonics* 39. https://doi.org/10.1029/2019tc005903.
Jourdon A, Pourhiet LL, Mouthereau F, May D. 2020b. Modes of Propagation of Continental Breakup and Associated Oblique Rift Structures. *J. Geophys. Res. Solid Earth* 125. https://doi.org/10.1029/2020jb019906.
Juez-Larré J, Andriessen PAM. 2006. Tectonothermal evolution of the northeastern margin of Iberia since the break-up of Pangea to present, revealed by low-temperature fission-track and (U-Th)/He thermochronology: A case history of the Catalan Coastal Ranges. *Earth and Planetary Science Letters* 243: 159–180. https://doi.org/10.1016/j.epsl.2005.12.026.
Kaczmarek M-A, Müntener O. 2008. Juxtaposition of melt impregnation and high-temperature shear zones in the Upper Mantle: Field and petrological constraints from the Lanzo Peridotite (Northern Italy). *J. Petrol.* 49: 2187–2220. https://doi.org/10.1093/petrology/egn065.
Kaczmarek M-A, Müntener O, Rubatto D. 2007. Trace element chemistry and U-Pb dating of zircons from oceanic gabbros and their relationship with whole rock composition (Lanzo, Italian Alps). *Contrib. Miner. Petrol.* 155: 295–312. https://doi.org/10.1007/s00410-007-0243-3.
Kaislaniemi L, van Hunen J. 2014. Dynamics of lithospheric thinning and mantle melting by edge-driven convection: Application to Moroccan Atlas mountains. *Geochemistry, Geophysics, Geosystems* 15: n/a–n/a. https://doi.org/10.1002/2014gc005414.
Keller J, Kramel M, Henjes-Kunst F. 2002. $^{40}Ar/^{39}Ar$ single crystal laser dating of early volcanism in the Upper Rhine Graben and tectonic implications. *Schweiz Miner. Petrogr. Mitt.* 82: 1–10.
Ketcham RA. 2005. Forward and inverse modeling of low-temperature thermochronometry data. *Reviews in Mineralogy and Geochemistry* 58: 275–314. https://doi.org/10.2138/rmg.2005.58.11.
Kilzi MA, Grégoire M, Bosse V, Benoît M, Driouch Y, de Saint Blanquat M, *et al.* 2016. Geochemistry and zircon U–Pb geochronology of the ultramafic and mafic rocks emplaced within the anatectic series of the Variscan Pyrenees: The example of the Gavarnie–Heas dome (France). *C. R. Geosci.* 348: 107–115. https://doi.org/10.1016/j.crte.2015.06.014.
King SD, Anderson DL. 1998. Edge-driven convection. *Earth Planet. Sci. Lett.* 160: 289–296. https://doi.org/10.1016/s0012-821x(98)00089-2.
Kley J, Voigt T. 2008. Late Cretaceous intraplate thrusting in central Europe: Effect of Africa-Iberia-Europe convergence, not Alpine collision. *Geology* 36: 839–842. https://doi.org/10.1130/g24930a.1.
Kohn BP, Lorencak M, Gleadow AJW, Kohlmann F, Raza A, Osadetz KG, *et al.* 2009. A reappraisal of low-temperature thermochronology of the eastern Fennoscandia Shield and radiation-enhanced apatite fission-track annealing. *Geol. Soc. Lond. Special Publ.* 324: 193–216. https://doi.org/10.1144/sp324.15.
Koulali A, Ouazar D, Tahayt A, King RW, Vernant P, Reilinger RE, *et al.* 2011. New GPS constraints on active deformation along the Africa-Iberia plate boundary. *Earth Planet. Sci. Lett.* 308: 211–217. https://doi.org/10.1016/j.epsl.2011.05.048.
Kreemer C, Blewitt G, Davis PM. 2020. Geodetic evidence for a buoyant mantle plume beneath the Eifel volcanic area, NW Europe. *Geophys. J. Int.* 222: 1316–1332. https://doi.org/10.1093/gji/ggaa227.
Kroner U, Romer RL. 2013. Two plates – Many subduction zones: The Variscan orogeny reconsidered. *Gondwana Research* 24: 298–329. https://doi.org/10.1016/j.gr.2013.03.001.
Kukkonen IT, Peltonen P. 1999. Xenolith-controlled geotherm for the central Fennoscandian Shield: implications for lithosphere-asthenosphere relations. *Tectonophysics* 304: 301–315. https://doi.org/10.1016/s0040-1951(99)00031-1.
Kylander-Clark ARC, Hacker BR, Johnson CM, Beard BL, Mahlen NJ, Lapen TJ. 2007. Coupled Lu–Hf and Sm–Nd geochronology constrains prograde and exhumation histories of high- and ultrahigh-pressure eclogites from western Norway. *Chem. Geol.* 242: 137–154. https://doi.org/10.1016/j.chemgeo.2007.03.006.
Labails C, Olivet J-L, Aslanian D, Roest WR. 2010. An alternative early opening scenario for the Central Atlantic Ocean. *Earth and Planetary Science Letters* 297: 355–368. https://doi.org/10.1016/j.epsl.2010.06.024.
Lachenbruch AH, Morgan P. 1990. Continental extension, magmatism and elevation: Formal relations and rules of thumb. *Tectonophysics* 174: 39–62. https://doi.org/10.1016/0040-1951(90)90383-J.
Lacombe O, Mouthereau F. 2002. Basement-involved shortening and deep detachment tectonics in forelands of orogens: Insights from recent collision belts (Taiwan, Western Alps, Pyrenees). *Tectonics* 21: 12-1-12-22. https://doi.org/10.1029/2001tc901018.
Lago M, Arranz E, Pocoví A, Gale C, Gil-Imaz A. 2004a. Permian magmatism and basin dynamics in the southern Pyrenees: a record of the transition from Late Variscan transtension to Early Alpine extension. *Geological Society, London, Special Publications* 223: 439–464.
Lago M, Arranz E, Pocoví A, Gale C, Gil-Imaz A. 2004b. Permian magmatism and basin dynamics in the southern Pyrenees: A record of the transition from Late Variscan transtension to Early Alpine extension. *Geological Society, London, Special Publications* 223: 439–464. https://doi.org/10.1144/gsl.sp.2004.223.01.19.

Lahtinen R, Korja A, Nironen M. 2005. Chapter 11: Paleoproterozoic tectonic evolution. *Developments in Precambrian Geology* 14: 481–531. https://doi.org/10.1016/s0166-2635(05)80012-x.

Lapen TJ, Medaris LG, Johnson CM, Beard BL. 2005. Archean to Middle Proterozoic evolution of Baltica subcontinental lithosphere: Evidence from combined Sm–Nd and Lu–Hf isotope analyses of the Sandvik ultramafic body, Norway. *Contrib. Miner. Petrol.* 150: 131–145. https://doi.org/10.1007/s00410-005-0021-z.

Lapen TJ, Medaris LG, Beard BL, Johnson CM. 2009. The Sandvik peridotite, Gurskøy, Norway: Three billion years of mantle evolution in the Baltica lithosphere. *Lithos* 109: 145–154. https://doi.org/10.1016/j.lithos.2008.08.007.

Lardeaux J-M. 2014. Deciphering orogeny: A metamorphic perspective Examples from European Alpine and Variscan Belts. *Bulletin de la Société géologique de France* 185: 281–310. https://doi.org/10.2113/gssgfbull.185.5.281.

Larrey M. 2020. Processus d'amincissement et fluides carbonatés en contexte post-orogénique : exemple de la marge Nord Alboran dans l'Est des Cordillères Bétiques (région d'Almería). PhD Thesis, Toulouse, France, 287 pp.

Larrey M, Mouthereau F, Masini E, Huyghe D, Gaucher EC, Virgone A, *et al.* 2020. Quaternary tectonic and climate changes at the origin of travertine and calcrete in the eastern Betics (Almería region, SE Spain). *J. Geol. Soc. Lond.* jgs2020-025. https://doi.org/10.1144/jgs2020-025.

Laske G, Masters G, Ma Z, Pasyanos M. 2013. Update on CRUST1.0 – A 1-degree Global Model of Earth's Crust. *Geophys. Res. Abstr.* 15, Abstract EGU2013-2658.

Laurent O, Couzinié S, Zeh A, Vanderhaeghe O, Moyen J-F, Villaros A, *et al.* 2017. Protracted, coeval crust and mantle melting during Variscan late-orogenic evolution: U–Pb dating in the eastern French Massif Central. *Int. J. Earth Sci.* 106: 421–451. https://doi.org/10.1007/s00531-016-1434-9.

Le Breton E, Handy MR, Molli G, Ustaszewski K. 2017. Post-20 Ma motion of the Adriatic plate – New constraints from surrounding orogens and implications for crust-mantle decoupling. *Tectonics* n/a–n/a. https://doi.org/10.1002/2016tc004443.

Le Pichon XL. 1968. Sea-floor spreading and continental drift. *J. Geophys. Res.* 73: 3661–3697. https://doi.org/10.1029/jb073i012p03661.

Lee C-T, Yin Q, Rudnick RL, Jacobsen SB. 2001. Preservation of ancient and fertile lithospheric mantle beneath the southwestern United States. *Nature* 411: 69–73. https://doi.org/10.1038/35075048.

Lee C-TA, Luffi P, Chin EJ. 2011. Building and destroying continental Mantle. *Annual Review of Earth and Planetary Sciences* 39: 59–90. https://doi.org/10.1146/annurev-earth-040610-133505.

Lefranc J Ph, Guiraud R. 1990. The continental intercalaire of northwestern Sahara and its equivalents in the neighbouring regions. *J. Afr. Earth Sci. Middle East* 10: 27–77. https://doi.org/10.1016/0899-5362(90)90047-i.

Legendre CP, Meier T, Lebedev S, Friederich W, Viereck-Götte L. 2012. A shear wave velocity model of the European upper mantle from automated inversion of seismic shear and surface waveforms: S-velocity model of the European upper mantle. *Geophys. J. Int.* 191: 282–304. https://doi.org/10.1111/j.1365-246x.2012.05613.x.

Leprêtre R, Barbarand J, Missenard Y, Leparmentier F, Frizon de Lamotte D. 2014. Vertical movements along the northern border of the West African Craton: The Reguibat Shield and adjacent basins. *Geol. Mag.* 151: 885–898. https://doi.org/10.1017/s0016756813000939.

Leprêtre R, Missenard Y, Barbarand J, Gautheron C, Saddiqi O, Jamme RP. 2015. Postrift history of the eastern central Atlantic passive margin: Insights from the Saharan region of South Morocco. *Journal of Geophysical Research: Solid Earth* 120: 4645–4666. https://doi.org/10.1002/2014jb011549.

Leprêtre R, Barbarand J, Missenard Y, Gautheron C, Pinna-Jamme R, Saddiqi O. 2017. Mesozoic evolution of NW Africa: Implications for the Central Atlantic Ocean dynamics. *J. Geol. Soc. Lond.* 174: 817–835. https://doi.org/10.1144/jgs2016-100.

Leprêtre R, Frizon de Lamotte D, Combier V, Gimeno-Vives O, Mohn G, Eschard R. 2018. The Tell-Rif orogenic system (Morocco, Algeria, Tunisia) and the structural heritage of the southern Tethys margin. *Bulletin de la Société géologique de France* 189: 10. https://doi.org/10.1051/bsgf/2018009.

Leprêtre R, Missenard Y, Barbarand J, Gautheron C, Jouvie I, Saddiqi O. 2018. Polyphased Inversions of an Intracontinental Rift: Case study of the Marrakech High Atlas, Morocco. *Tectonics* 37: 818–841. https://doi.org/10.1002/2017tc004693.

Leroy S, Gente P, Fournier M, d'Acremont E, Patriat P, Beslier M-O, *et al.* 2004. From rifting to spreading in the eastern Gulf of Aden: a geophysical survey of a young oceanic basin from margin to margin. *Terra Nova* 16: 185–192. https://doi.org/10.1111/j.1365-3121.2004.00550.x.

Lettéron A, Hamon Y, Fournier F, Séranne M, Pellenard P, Joseph P. 2018. Reconstruction of a saline, lacustrine carbonate system (Priabonian, St-Chaptes Basin, SE France): Depositional models, paleogeographic and paleoclimatic implications. *Sediment. Geol.* 367: 20–47. https://doi.org/10.1016/j.sedgeo.2017.12.023.

Li ZX, Bogdanova SV, Collins AS, Davidson A, Waele BD, Ernst RE, *et al.* 2008. Assembly, configuration, and break-up history of Rodinia: A synthesis. *Precambrian Res.* 160: 179–210. https://doi.org/10.1016/j.precamres.2007.04.021.

Liégeois J-P, Abdelsalam MG, Ennih N, Ouabadi A. 2013. Metacraton: Nature, genesis and behavior. *Gondwana Res.* 23: 220–237. https://doi.org/10.1016/j.gr.2012.02.016.

Linnemann U, Nance RD, Kraft P, Zulauf G, Gerdes A, Drost K, *et al.* 2007. The evolution of the Rheic Ocean: From Avalonian-Cadomian active margin to Alleghenian-Variscan collision. https://doi.org/10.1130/2007.2423(03).

Linnemann U, Herbosch A, Liégeois J-P, Pin C, Gärtner A, Hofmann M. 2012. The Cambrian to Devonian odyssey of the Brabant Massif within Avalonia: A review with new zircon ages, geochemistry, Sm-Nd isotopes, stratigraphy and palaeogeography. *Earth-Sci. Rev.* 112: 126–154. https://doi.org/10.1016/j.earscirev.2012.02.007.

Lustrino M, Morra V, Fedele L, Franciosi L. 2009. Beginning of the Apennine subduction system in central western Mediterranean: Constraints from Cenozoic "orogenic" magmatic activity of Sardinia, Italy: Beginning of apennine subduction. *Tectonics* 28: n/a–n/a. https://doi.org/10.1029/2008tc002419.

Macchiavelli C, Vergés J, Schettino A, Fernàndez M, Turco E, Casciello E, *et al.* 2017. A new southern North Atlantic isochron map: Insights into the drift of the Iberian Plate since the Late Cretaceous. *J. Geophys. Res. Solid Earth* 122: 9603–9626. https://doi.org/10.1002/2017jb014769.

Malarkey J, Wittig N, Pearson DG, Davidson JP. 2011. Characterising modal metasomatic processes in young continental lithospheric mantle: A microsampling isotopic and trace element study on xenoliths from the Middle Atlas Mountains, Morocco. *Contrib. Miner. Petrol.* 162: 289–302. https://doi.org/10.1007/s00410-010-0597-9.

Malusà MG, Polino R, Feroni AC, Ellero A, Ottria G, Baidder L, *et al.* 2007. Post-Variscan tectonics in eastern Anti-Atlas (Morocco). *Terra Nova* 19: 481–489. https://doi.org/10.1111/j.1365-3121.2007.00775.x.

Malusà MG, Danišík M, Kuhlemann J. 2016. Tracking the Adriatic-slab travel beneath the Tethyan margin of Corsica-Sardinia by low-temperature thermochronometry. *Gondwana Research* 31: 135–149. https://doi.org/10.1016/j.gr.2014.12.011.

Mancilla F de L, Booth-Rea G, Stich D, Pérez-Peña JV, Morales J, Azañón JM, *et al.* 2015a. Slab rupture and delamination under the Betics and Rif constrained from receiver functions. *Tectonophysics*. https://doi.org/10.1016/j.tecto.2015.06.028.

Mancilla F de L, Stich D, Morales J, Martin R, Diaz J, Pazos A, *et al.* 2015b. Crustal thickness and images of the lithospheric discontinuities in the Gibraltar arc and surrounding areas. *Geophysical Journal International* 203: 1804–1820. https://doi.org/10.1093/gji/ggv390.

Marchand E, Séranne M, Bruguier O, Vinches M. 2021. LA-ICP-MS dating of detrital zircon grains from the Cretaceous allochthonous bauxites of Languedoc (south of France): Provenance and geodynamic consequences. *Basin Res.* 33: 270–290. https://doi.org/10.1111/bre.12465.

Marchesi C, Griffin WL, Garrido CJ, Bodinier J-L, O'Reilly SY, Pearson NJ. 2010. Persistence of mantle lithospheric Re-Os signature during asthenospherization of the subcontinental lithospheric mantle: Insights from in situ isotopic analysis of sulfides from the Ronda peridotite (Southern Spain). *Contributions to Mineralogy and Petrology* 159: 315–330. https://doi.org/10.1007/s00410-009-0429-y.

Martin LAJ, Rubatto D, Brovarone AV, Hermann J. 2011. Late Eocene lawsonite-eclogite facies metasomatism of a granulite sliver associated to ophiolites in Alpine Corsica. *Lithos* 125: 620–640. https://doi.org/10.1016/j.lithos.2011.03.015.

Martínez Catalán JR, Arenas R, García FD, Cuadra PG, Gómez-Barreiro J, Abati J, *et al.* 2007. 4-D framework of continental crust. *Geol. Soc. Am. Mem.* 403–423. https://doi.org/10.1130/2007.1200(21).

Martínez-García P, Comas M, Lonergan L, Watts AB. 2017. From extension to shortening: Tectonic inversion distributed in time and space in the Alboran Sea, Western Mediterranean: Tectonic inversion in the Alboran Sea. *Tectonics* 36: 2777–2805. https://doi.org/10.1002/2017tc004489.

Martínez-Garzón P, Heidbach O, Bohnhoff M. 2019. Contemporary stress and strain field in the Mediterranean from stress inversion of focal mechanisms and GPS data. *Tectonophysics* 774: 228286. https://doi.org/10.1016/j.tecto.2019.228286.

Marzoli A, Melluso L, Morra V, Renne PR, Sgrosso I, D'Antonio M, *et al.* 1999a. Geochronology and petrology of Cretaceous basaltic magmatism in the Kwanza Basin (Western Angola), and relationships with the Paranà-Etendeka continental flood basalt province. *J. Geodyn.* 28: 341–356. https://doi.org/10.1016/s0264-3707(99)00014-9.

Marzoli A, Renne PR, Piccirillo EM, Ernesto M, Bellieni G, Min AD. 1999b. Extensive 200-million-year-old continental flood basalts of the Central Atlantic Magmatic Province. *Geophys. J. Int.* 284: 616–618.

Marzoli A, Bertrand H, Knight KB, Cirilli S, Buratti N, Verati C, *et al.* 2004. Synchrony of the Central Atlantic magmatic province and the Triassic-Jurassic boundary climatic and biotic crisis. *Geology* 32: 973–976. https://doi.org/10.1130/g20652.1.

Marzoli A, Bertrand H, Youbi N, Callegaro S, Merle R, Reisberg L, *et al.* 2019. The Central Atlantic Magmatic Province (CAMP) in Morocco. *J. Petrol.* 60: 945–996. https://doi.org/10.1093/petrology/egz021.

Mattauer M, Proust F, Tapponnier P. 1972. Major strike-slip fault of Late Hercynian Age in Morocco. *Nature* 237: 160–162. https://doi.org/10.1038/237160b0.

Matte P. 2001. The Variscan collage and orogeny (480–290 Ma) and the tectonic definition of the Armorica microplate: A review. *Terra Nova* 13: 122–128. https://doi.org/10.1046/j.1365-3121.2001.00327.x.

Maurel O, Respaut JP, Monié P, Arnaud N, Brunel M. 2004. U-Pb emplacement and Ar-40/Ar-39 cooling ages of the Eastern Mont-Louis Granite Massif (Eastern Pyrenees, France). *Comptes Rendus Geoscience* 336: 1091–1098. https://doi.org/10.1016/j.crte.2004.04.005.

Mazur S, Scheck-Wenderoth M, Krzywiec P. 2005. Different modes of the Late Cretaceous–Early Tertiary inversion in the North German and Polish Basins. *Int. J. Earth Sci.* 94: 782–798. https://doi.org/10.1007/s00531-005-0016-z.

McCann T, Pascal C, Timmerman MJ, Krzywiec P, López-Gómez J, Wetzel L, *et al.* 2006. Post-Variscan (end Carboniferous-Early Permian) Basin evolution in Western and Central Europe. *Geol. Soc. Lond. Mem.* 32: 355–388. https://doi.org/10.1144/gsl.mem.2006.032.01.22.

McCarthy A, Müntener O. 2015. Ancient depletion and mantle heterogeneity: Revisiting the Permian-Jurassic paradox of Alpine peridotites. *Geology* 43: 255–258. https://doi.org/10.1130/g36340.1.

McCarthy A, Tugend J, Mohn G, Candioti L, Chelle-Michou C, Arculus R, *et al.* 2020. A case of Ampferer-type subduction and consequences for the Alps and the Pyrenees. *Am. J. Sci.* 320: 313–372. https://doi.org/10.2475/04.2020.01.

McCulloch AA. 1993. Apatite fission track results from Ireland and the Porcupine Basin and their significance for the evolution of the North Atlantic. *Mar. Petrol. Geol.* 10: 572–590. https://doi.org/10.1016/0264-8172(93)90060-6.

McHone JG. 2000. Non-plume magmatism and rifting during the opening of the central Atlantic Ocean. *Tectonophysics* 316: 287–296. https://doi.org/10.1016/s0040-1951(99)00260-7.

McQuarrie N, Stock JM, Verdel C, Wernicke BP. 2003. Cenozoic evolution of Neotethys and implications for the causes of plate motions. *Geophysical Research Letters* 30. https://doi.org/10.1029/2003gl017992.

Meer DG van der, van Hinsbergen DJJ, Spakman W. 2018. Atlas of the underworld: Slab remnants in the mantle, their sinking history, and a new outlook on lower mantle viscosity. *Tectonophysics* 723: 309–448. https://doi.org/10.1016/j.tecto.2017.10.004.

Meier T, Soomro RA, Viereck L, Lebedev S, Behrmann JH, Weidle C, *et al.* 2016. Mesozoic and Cenozoic evolution of the Central European lithosphere. *Tectonophysics* 692: 58–73. https://doi.org/10.1016/j.tecto.2016.09.016.

Melleton J, Cocherie A, Faure M, Rossi P. 2010. Precambrian protoliths and Early Paleozoic magmatism in the French Massif Central: U-Pb data and the North Gondwana connection in the west European Variscan Belt. *Gondwana Res.* 17: 13–25. https://doi.org/10.1016/j.gr.2009.05.007.

Ménard G, Molnar P. 2004. Collapse of a Hercynian Tibetan Plateau into a Late Palaeozoic European Basin and Range province. *Nature* 334: 235–237. https://doi.org/10.1038/334235a0.

Mesalles L, Mouthereau F, Bernet M, Chang C-P, Lin AT-S, Fillon C, *et al.* 2014. From submarine continental accretion to arc-continent orogenic evolution: The thermal record in southern Taiwan. *Geology* 42: 907–910. https://doi.org/10.1130/g35854.1.

Michalski I, Soom M. 1990. The Alpine thermo-tectonic evolution of the Aar and Gotthard Massifs, Central Switzerland: Fission track ages on zircon and apatite and K-Ar mica ages. *Schweizerische mineralogische und petrographische Mitteilungen* 373–387. https://doi.org/10.5169/seals-53628.

Michard A, Soulaimani A, Hoepffner C, Ouanaimi H, Baidder L, Rjimati EC, *et al.* 2010. The south-western branch of the Variscan

Belt: Evidence from Morocco. *Tectonophysics* 492: 1–24. https://doi.org/10.1016/j.tecto.2010.05.021.

Michard A, Saddiqi O, Chalouan A, Chabou MC, Lach P, Rossi P, *et al.* 2020. Comment on "The Mesozoic Margin of the Maghrebian Tethys in the Rif Belt (Morocco): Evidence for Polyphase Rifting and Related Magmatic Activity" by Gimeno-Vives *et al. Tectonics* 39. https://doi.org/10.1029/2019tc006004.

Michard-Vitrac A, Albarede F, Dupuis C, Taylor HP. 1980. The genesis of Variscan (Hercynian) plutonic rocks: Inferences from Sr, Pb, and O studies on the Maladeta igneous complex, central Pyrenees (Spain). *Contrib. Miner. Petrol.* 72: 57–72. https://doi.org/10.1007/bf00375568.

Michel LA, Tabor NJ, Montañez IP, Schmitz MD, Davydov VI. 2015. Chronostratigraphy and Paleoclimatology of the Lodève Basin, France: Evidence for a pan-tropical aridification event across the Carboniferous-Permian boundary. *Palaeogeogr Palaeoclim Palaeoecol* 430: 118–131. https://doi.org/10.1016/j.palaeo.2015.03.020.

Michon L, Merle O. 2001. The evolution of the Massif Central Rift; spatio-temporal distribution of the volcanism. *Bulletin de la Société géologique de France* 172: 201–211. https://doi.org/10.2113/172.2.201.

Missenard Y, Cadoux A. 2012. Can Moroccan Atlas lithospheric thinning and volcanism be induced by Edge-Driven Convection? *Terra Nova* 24: 27–33. https://doi.org/10.1111/j.1365-3121.2011.01033.x.

Missenard Y, Zeyen H, Frizon de Lamotte D, Leturmy P, Petit C, Sébrier M, *et al.* 2006. Crustal versus asthenospheric origin of relief of the Atlas Mountains of Morocco. *Journal of Geophysical Research* 111: B03401. https://doi.org/10.1029/2005jb003708.

Molina-Aguilera A, Mancilla F de L, Morales J, Stich D, Yuan X, Heit B. 2019. Connection between the Jurassic oceanic lithosphere of the Gulf of Cádiz and the Alboran slab imaged by Sp receiver functions. *Geology* 47: 227–230. https://doi.org/10.1130/g45654.1.

Molinari I, Morelli A. 2011. EPcrust: A reference crustal model for the European Plate. *Geophysical Journal International* 185: 352–364. https://doi.org/10.1111/j.1365-246x.2011.04940.x.

Molnar P. 1988. Continental tectonics in the aftermath of plate tectonics. *Nature* 335: 131–137. https://doi.org/10.1038/335131a0.

Monié P, Chopin C. 1991. $^{40}Ar/^{39}Ar$ dating in coesite-bearing and associated units of the Dora Maira Massif, Western Alps. *Eur. J. Miner.* 3: 239–262. https://doi.org/10.1127/ejm/3/2/0239.

Mondy LS, Rey PF, Duclaux G, Moresi L. 2017 The role of asthenospheric flow during rift propagation and breakup. *Geology* 46: 103–106. https://doi.org/10.1130/g39674.1.

Moore NB, Hassan R, Müller RD, Williams SE, Flament N. 2017. Dynamic topography and eustasy controlled the paleogeographic evolution of northern Africa since the mid-Cretaceous. *Tectonics* 36: 929–944. https://doi.org/10.1002/2016tc004280.

Morgan WJ. 1968. Rises, trenches, great faults, and crustal blocks. *J. Geophys. Res.* 73: 1959–1982. https://doi.org/10.1029/jb073i006p01959.

Mosar J, Lewis G, Torsvik TH. 2002. North Atlantic sea-floor spreading rates: implications for the Tertiary development of inversion structures of the Norwegian–Greenland Sea. *J. Geol. Soc. Lond.* 159: 503–515. https://doi.org/10.1144/0016-764901-135.

Moucha R, Forte AM. 2011. Changes in African topography driven by mantle convection. *Nat. Geosci.* 4: 707–712. https://doi.org/10.1038/ngeo1235.

Mouthereau F, Lacombe O, Vergés J. 2012. Building the Zagros collisional orogen: Timing, strain distribution and the dynamics of Arabia/Eurasia plate convergence. *Tectonophysics* 532-535: 27–60. https://doi.org/10.1016/j.tecto.2012.01.022.

Mouthereau F, Watts AB, Burov E. 2013. Structure of orogenic belts controlled by lithosphere age. *Nat. Geosci.* 6: 785–789. https://doi.org/10.1038/ngeo1902.

Mouthereau F, Filleaudeau P-Y, Vacherat A, Pik R, Lacombe O, Fellin MG, *et al.* 2014. Placing limits to shortening evolution in the Pyrenees: Role of margin architecture and implications for the Iberia/Europe convergence. *Tectonics* 33: 2283–2314. https://doi.org/10.1002/2014tc003663.

Müller RD, Zahirovic S, Williams SE, Cannon J, Seton M, Bower DJ, *et al.* 2019. A global plate model including lithospheric deformation along major rifts and orogens since the Triassic. *Tectonics* 38: 1884–1907. https://doi.org/10.1029/2018tc005462.

Müntener O, Piccardo GB. 2003. Melt migration in ophiolitic peridotites: the message from Alpine-Apennine peridotites and implications for embryonic ocean basins. *Geological Society, London, Special Publications* 218: 69–89. https://doi.org/10.1144/gsl.sp.2003.218.01.05.

Müntener O, Hermann J, Trommsdorff V. 2000. Cooling history and exhumation of lower-crustal granulite and upper mantle (Malenco, Eastern Central Alps). *Journal of Petrology* 41: 175–200.

Murphy JB, Dostal J. 2007. Continental mafic magmatism of different ages in the same terrane: Constraints on the evolution of an enriched mantle source. *Geology* 35: 335–338. https://doi.org/10.1130/g23072a.1.

Murphy JB, Strachan RA, Nance RD, Parker KD, Fowler MB. 2000. Proto-Avalonia: A 1.2–1.0 Ga tectonothermal event and constraints for the evolution of Rodinia. *Geology* 28: 1071. https://doi.org/10.1130/0091-7613(2000)28<1071:pagtea>2.0.co;2.

Murphy JB, Gutierrez-Alonso G, Nance RD, Fernandez-Suárez J, Keppie JD, Quesada C, *et al.* 2006. Origin of the Rheic Ocean: Rifting along a Neoproterozoic suture? *Geology* 34: 325–328. https://doi.org/10.1130/g22068.1.

Murphy JB, Gutiérrez-Alonso G, Fernández-Suárez J, Braid JA. 2008. Probing crustal and mantle lithosphere origin through Ordovician volcanic rocks along the Iberian passive margin of Gondwana. *Tectonophysics* 461: 166–180. https://doi.org/10.1016/j.tecto.2008.03.013.

Murphy JB, Gutiérrez-Alonso G, Nance RD, Fernández-Suárez J, Keppie JD, Quesada C, *et al.* 2009. Rheic Ocean mafic complexes: Overview and synthesis. *Geol. Soc. Lond. Special Publ.* 327: 343–369. https://doi.org/10.1144/sp327.15.

Najih A, Montero P, Verati C, Chabou MC, Fekkak A, Baidder L, *et al.* 2019. Initial Pangean rifting north of the West African Craton: Insights from Late Permian U-Pb and $^{40}Ar/^{39}Ar$ dating of alkaline magmatism from the Eastern Anti-Atlas (Morocco). *J. Geodyn.* 132: 101670. https://doi.org/10.1016/j.jog.2019.101670.

Nance RD, Murphy JB, Keppie JD. 2002. A Cordilleran model for the evolution of Avalonia. *Tectonophysics* 352: 11–31. https://doi.org/10.1016/s0040-1951(02)00187-7.

Neumann E-R, Dunworth EA, Sundvoll BA, Tollefsrud JI. 2002. B1 basaltic lavas in Vestfold-Jeløya area, central Oslo rift: Derivation from initial melts formed by progressive partial melting of an enriched mantle source. *Lithos* 61: 21–53. https://doi.org/10.1016/s0024-4937(02)00068-3.

Neumann E-R, Wilson M, Heeremans M, Spencer EA, Obst K, Timmerman MJ, *et al.* 2004. Carboniferous-Permian rifting and magmatism in southern Scandinavia, the North Sea and northern Germany: A review. *Geol. Soc. Lond. Special Publ.* 223: 11–40. https://doi.org/10.1144/gsl.sp.2004.223.01.02.

Nocquet J-M. 2012. Present-day kinematics of the Mediterranean: A comprehensive overview of GPS results. *Tectonophysics* 579: 220–242. https://doi.org/10.1016/j.tecto.2012.03.037.

Olivetti V, Godard V, Bellier O, Team ASTER. 2016. Cenozoic rejuvenation events of Massif Central topography (France): Insights from cosmogenic denudation rates and river profiles. *Earth Planet. Sci. Lett.* 444: 179–191. https://doi.org/10.1016/j.epsl.2016.03.049.

Olivetti V, Balestrieri ML, Godard V, Bellier O, Gautheron C, Valla PG, *et al.* 2020. Cretaceous and Late Cenozoic uplift of a Variscan Massif: The case of the French Massif Central studied through low-temperature thermochronometry. *Lithosphere*. https://doi.org/10.1130/l1142.1.

Olyphant JR, Johnson RA, Hughes AN. 2017. Evolution of the Southern Guinea Plateau: Implications on Guinea-Demerara Plateau formation using insights from seismic, subsidence, and gravity data. *Tectonophysics* 717: 358–371. https://doi.org/10.1016/j.tecto.2017.08.036.

Oncken O, Winterfeld C. von, Dittmar U. 1999. Accretion of a rifted passive margin: The Late Paleozoic Rhenohercynian Fold and Thrust Belt (Middle European Variscides). *Tectonics* 18: 75–91. https://doi.org/10.1029/98tc02763.

Orejana D, Villaseca C, Billström K, Paterson BA. 2008. Petrogenesis of Permian alkaline lamprophyres and diabases from the Spanish Central System and their geodynamic context within western Europe. *Contrib. Miner. Petrol.* 156: 477–500. https://doi.org/10.1007/s00410-008-0297-x.

Orejana D, Villaseca C, Pérez-Soba C, López-García JA, Billström K. 2009. The Variscan gabbros from the Spanish Central System: A case for crustal recycling in the sub-continental lithospheric mantle? *Lithos* 110: 262–276. https://doi.org/10.1016/j.lithos.2009.01.003.

Orejana D, Villaseca C, Kristoffersen M. 2020. Geochemistry and geochronology of mafic rocks from the Spanish Central System: Constraints on the mantle evolution beneath Central Spain. *Geosci. Front.* 11: 1651–1667. https://doi.org/10.1016/j.gsf.2020.01.002.

Ouabid M, Garrido CJ, Ouali H, Harvey J, Hidas K, Marchesi C, *et al.* 2020. Late Cadomian rifting of the NW Gondwana margin and the reworking of Precambrian crust – Evidence from bimodal magmatism in the Early Paleozoic Moroccan Meseta. *Int. Geol. Rev.* 1–24. https://doi.org/10.1080/00206814.2020.1818301.

Oukassou M, Saddiqi O, Barbarand J, Sebti S, Baidder L, Michard A. 2013. Post-Variscan exhumation of the Central Anti-Atlas (Morocco) constrained by zircon and apatite fission-track thermochronology. *Terra Nova* 25: 151–159. https://doi.org/10.1111/ter.12019.

Palano M, González PJ, Fernández J. 2015. The diffuse plate boundary of Nubia and Iberia in the Western Mediterranean: Crustal deformation evidence for viscous coupling and fragmented lithosphere. *Earth and Planetary Science Letters* 430: 439–447. https://doi.org/10.1016/j.epsl.2015.08.040.

Palomeras I, Villaseñor A, Thurner S, Levander A, Gallart J, Harnafi M. 2017. Lithospheric structure of Iberia and Morocco using finite-frequency Rayleigh wave tomography from earthquakes and seismic ambient noise. *Geochemistry, Geophysics, Geosystems* 18: 1824–1840. https://doi.org/10.1002/2016gc006657.

Paquette J-L, Ménot R-P, Pin C, Orsini J-B. 2003. Episodic and short-lived granitic pulses in a post-collisional setting: evidence from precise U–Pb zircon dating through a crustal cross-section in Corsica. *Chem. Geol.* 198: 1–20. https://doi.org/10.1016/s0009-2541(02)00401-1.

Pasyanos ME, Masters TG, Laske G, Ma Z. 2014. LIT HO1. 0: An updated crust and lithospheric model of the Earth. *Journal of Geophysical Research: Solid Earth* 119: 2153–2173. https://doi.org/10.1002/2013jb010626.

Peace AL, Phethean JJJ, Franke D, Foulger GR, Schiffer C, Welford JK, *et al.* 2019. A review of Pangaea dispersal and Large Igneous Provinces – In search of a causative mechanism. *Earth Science Reviews* 102902. https://doi.org/10.1016/j.earscirev.2019.102902.

Pearson DG, Nowell GM. 2004. Re-Os and Lu-Hf Isotope Constraints on the Origin and Age of Pyroxenites from the Beni Bousera Peridotite Massif: Implications for Mixed Peridotite-Pyroxenite Mantle Sources. *J. Petrol.* 45: 439–455. https://doi.org/10.1093/petrology/egg102.

Pedrera A, García-Senz J, Peropadre C, Robador A, López-Mir B, Díaz-Alvarado J, Rodríguez-Fernández LR. 2020a. The Getxo crustal-scale cross-section: Testing tectonic models in the Bay of Biscay-Pyrenean rift system. *Earth-Sci. Rev.* 212: 103429. https://doi.org/10.1016/j.earscirev.2020.103429.

Pedrera A, Ruiz-Constán A, García-Senz J, Azor A, Marín-Lechado C, Ayala C, *et al.* 2020b. Evolution of the South-Iberian paleomargin: From hyperextension to continental subduction. *J. Struct. Geol.* 138: 104122. https://doi.org/10.1016/j.jsg.2020.104122.

Peltonen P, Brügmann G. 2006. Origin of layered continental mantle (Karelian craton, Finland): Geochemical and Re-Os isotope constraints. *Lithos* 89: 405–423. https://doi.org/10.1016/j.lithos.2005.12.013.

Pérez-Gussinyé M, Lowry AR, Watts AB, Velicogna I. 2004. On the recovery of effective elastic thickness using spectral methods: Examples from synthetic data and from the Fennoscandian Shield. *Journal of Geophysical Research* 109: B10409. https://doi.org/10.1029/2003jb002788.

Petit C, Le Pourhiet L, Scalabrino B, Corsini M, Bonnin M, Romagny A. 2015. Crustal structure and gravity anomalies beneath the Rif, northern Morocco: Implications for the current tectonics of the Alboran Region. *Geophys. J. Int.* 202: 640–652. https://doi.org/10.1093/gji/ggv169.

Petri B, Mohn G, Štípská P, Schulmann K, Manatschal G. 2016. The Sondalo gabbro contact aureole (Campo Unit, Eastern Alps): Implications for mid-crustal mafic magma emplacement. *Contrib. Miner. Petrol.* 171: 52. https://doi.org/10.1007/s00410-016-1263-7.

Peyaud J-B, Barbarand J, Carter A, Pagel M. 2005. Mid-Cretaceous uplift and erosion on the northern margin of the Ligurian Tethys deduced from thermal history reconstruction. *Int. J. Earth Sci.* 94: 462–474. https://doi.org/10.1007/s00531-005-0486-z.

Picazo S, Müntener O, Manatschal G, Bauville A, Karner G, Johnson C. 2016. Mapping the nature of mantle domains in Western and Central Europe based on clinopyroxene and spinel chemistry: Evidence for mantle modification during an extensional cycle. *Lithos* 266: 233–263. https://doi.org/10.1016/j.lithos.2016.08.029.

Piccardo GB, Müntener O, Zanetti A, Pettke T. 2004. Ophiolitic peridotites of the Alpine-Apennine System: Mantle processes and geodynamic relevance. *Int. Geol. Rev.* 46: 1119–1159. https://doi.org/10.2747/0020-6814.46.12.1119.

Piromallo C, Morelli A. 2003. P wave tomography of the mantle under the Alpine-Mediterranean area. *J. Geophys. Res. Solid Earth 1978–2012* 108: 2065. https://doi.org/10.1029/2002jb001757.

Platt JP, Whitehouse MJ, Kelley SP, Carter A, Hollick L. 2003. Simultaneous extensional exhumation across the Alboran Basin: Implications for the causes of late orogenic extension. *Geology* 31: 251–254. https://doi.org/10.1130/0091-7613(2003)031<0251:seeata>2.0.co;2.

Potrel A, Peucat JJ, Fanning CM. 1998. Archean crustal evolution of the West African Craton: Example of the Amsaga Area (Reguibat Rise). U–Pb and Sm–Nd evidence for crustal growth and recycling. *Precambrian Res.* 90: 107–117. https://doi.org/10.1016/s0301-9268(98)00044-8.

Poudjom Djomani YH, O'Reilly SY, Griffin WL, Morgan P. 2001. The density structure of subcontinental lithosphere through time. *Earth Planet. Sci. Lett.* 184: 605–621. https://doi.org/10.1016/s0012-821x(00)00362-9.

Priestley K, McKenzie D. 2013. The relationship between shear wave velocity, temperature, attenuation and viscosity in the shallow part of the mantle. *Earth Planet. Sci. Lett.* 381: 78–91. https://10.1016/j.epsl.2013.08.022.

Precigout J, Gueydan F, Gapais D, Garrido CJ, Essaifi A. 2007. Strain localisation in the subcontinental mantle – A ductile alternative to the brittle mantle. *Tectonophysics* 445: 318–336. https://doi.org/10.1016/j.tecto.2007.09.002.

Raffone N, Chazot G, Pin C, Vannucci R, Zanetti A. 2009. Metasomatism in the Lithospheric Mantle beneath Middle Atlas (Morocco) and the Origin of Fe- and Mg-rich Wehrlites. *J. Petrol.* 50: 197–249. https://doi.org/10.1093/petrology/egn069.

Rampone E, Hofmann AW, Piccardo GB, Vannucci R, Bottazzi P, Ottolini L. 1995. Petrology, Mineral and Isotope Geochemistry of the External Liguride Peridotites (Northern Apennines, Italy). *J. Petrol.* 36: 81–105. https://doi.org/10.1093/petrology/36.1.81.

Rampone E, Hofmann AW, Piccardo GB, Vannucci R, Bottazzi P, Ottolini L. 1996. Trace element and isotope geochemistry of depleted peridotites from an N-MORB type ophiolite (Internal Liguride, N. Italy). *Contrib. Miner. Petrol.* 123: 61–76. https://doi.org/10.1007/s004100050143.

Rampone E, Hofmann AW, Raczek I. 2009. Isotopic equilibrium between mantle peridotite and melt: Evidence from the Corsica ophiolite. *Earth Planet. Sci. Lett.* 288: 601–610. https://doi.org/10.1016/j.epsl.2009.10.024.

Rat P. 1988. The Basque-Cantabrian Basin between the Iberian and European Plates some facts but still many problems. *Revista de la Sociedad Geológica de España* 1: 327–348.

Rat J, Mouthereau F, Brichau S, Crémades A, Bernet M, Balvay M, *et al.* 2019. Tectonothermal evolution of the Cameros Basin: Implications for tectonics of North Iberia. *Tectonics* 40: 327. https://doi.org/10.1029/2018tc005294.

Raumer JF von, Finger F, Veselá P, Stampfli GM. 2013. Durbachites-Vaugnerites – A geodynamic marker in the central European Variscan orogen. *Terra Nova* 26: 85–95. https://doi.org/10.1111/ter.12071.

Reilinger R, McClusky S. 2011. Nubia-Arabia-Eurasia plate motions and the dynamics of Mediterranean and Middle East tectonics. *Geophysical Journal International* 186: 971–979. https://doi.org/10.1111/j.1365-246x.2011.05133.x.

Reisberg L, Lorand J-P. 1995. Longevity of sub-continental mantle lithosphere from osmium isotope systematics in orogenic peridotite massifs. *Nature* 376: 159–162. https://doi.org/10.1038/376159a0.

Reisberg L, Zindler A, Jagoutz E. 1989. Further Sr and Nd isotopic results from peridotites of the Ronda Ultramafic Complex. *Earth Planet. Sci. Lett.* 96: 161–180. https://doi.org/10.1016/0012-821x(89)90130-1.

Río PD, Barbero L, Stuart FM. 2009. Exhumation of the Sierra de Cameros (Iberian Range, Spain): constraints from low-temperature thermochronology. *Geol. Soc. Lond. Special Publ.* 324: 153–166. https://doi.org/10.1144/sp324.12.

Ritter JRR, Jordan M, Christensen UR, Achauer U. 2001. A mantle plume below the Eifel volcanic fields, Germany. *Earth Planet Sc Lett* 186: 7–14. https://doi.org/10.1016/s0012-821x(01)00226-6.

Roberts D. 2003. The Scandinavian Caledonides: event chronology, palaeogeographic settings and likely modern analogues. *Tectonophysics* 365: 283–299. https://doi.org/10.1016/s0040-1951(03)00026-x.

Roca E, Ferrer O, Rowan MG, Muñoz JA, Butillé M, Giles KA, *et al.* 2020. Salt tectonics and controls on halokinetic-sequence development of an exposed deepwater diapir: The Bakio Diapir, Basque-Cantabrian Basin, Pyrenees. *Mar. Petrol. Geol.* 123: 104770. https://doi.org/10.1016/j.marpetgeo.2020.104770.

Rodriguez M, Arnould M, Coltice N, Soret M. 2021. Long-term evolution of a plume-induced subduction in the Neotethys realm. *Earth Planet. Sci. Lett.* 561. 116798. https://doi.org/10.1016/j.epsl.2021.116798.

Rodríguez-Méndez L, Cuevas J, Tubía JM. 2016. Post-Variscan Basin evolution in the Central Pyrenees: Insights from the Stephanian-Permian Anayet Basin. *C. R. Geosci.* 348: 333–341. https://doi.org/10.1016/j.crte.2015.11.006.

Romagny A, Münch P, Cornée JJ, Corsini M, Azdimousa A, Melinte-Dobrinescu MC, *et al.* 2014. Late Miocene to present-day exhumation and uplift of the Internal Zone of the Rif chain: Insights from low temperature thermochronometry and basin analysis. *Journal of Geodynamics* 77: 39–55. https://doi.org/10.1016/j.jog.2014.01.006.

Romagny A, Jolivet L, Menant A, Bessière E, Maillard A, Canva A, *et al.* 2020. Detailed tectonic reconstructions of the Western Mediterranean region for the last 35 Ma, insights on driving mechanisms. *BSGF – Earth Sci Bulletin* 191: 37. https://doi.org/10.1051/bsgf/2020040.

Romer RL, Förster H-J, Breitkreuz C. 2001. Intracontinental extensional magmatism with a subduction fingerprint: The Late Carboniferous Halle Volcanic Complex (Germany). *Contrib. Miner. Petrol.* 141: 201–221. https://doi.org/10.1007/s004100000231.

Roscher M, Schneider JW. 2006. Permo-Carboniferous climate: Early Pennsylvanian to Late Permian climate development of Central Europe in a regional and global context. *Geol. Soc. Lond. Special Publ.* 265: 95–136. https://doi.org/10.1144/gsl.sp.2006.265.01.05.

Rossetti F, Lucci F, Theye T, Bouybaouenne M, Gerdes A, Opitz J, *et al.* 2020. Hercynian anatexis in the envelope of the Beni Bousera peridotites (Alboran Domain, Morocco): Implications for the tectono-metamorphic evolution of the deep crustal roots of the Mediterranean Region. *Gondwana Res.* 83: 157–182. https://doi.org/10.1016/j.gr.2020.01.020.

Roure F, Casero P, Addoum B. 2012. Alpine inversion of the North African margin and delamination of its continental lithosphere. *Tectonics* 31: n/a–n/a. https://doi.org/10.1029/2011tc002989.

Roux VL, Bodinier JL, Tommasi A, Alard O, Dautria JM, Vauchez A, *et al.* 2007. The Lherz spinel lherzolite: Refertilized rather than pristine mantle. *Earth and Planetary Science Letters* 259: 599–612. https://doi.org/10.1016/j.epsl.2007.05.026.

Royden L, Faccenna C. 2018. Subduction Orogeny and the Late Cenozoic evolution of the Mediterranean Arcs. *Annual Review of Earth and Planetary Sciences* 46: 261–289. https://doi.org/10.1146/annurev-earth-060115-012419.

Ruiz GMH, Sebti S, Negro F, Saddiqi O, Frizon de Lamotte D, Stockli D, *et al.* 2011. From central Atlantic continental rift to Neogene uplift – Western Anti-Atlas (Morocco): From central Atlantic continental rift to Neogene uplift. *Terra Nova* 23: 35–41. https://doi.org/10.1111/j.1365-3121.2010.00980.x.

Rutanen H, Andersson UB, Väisänen M, Johansson Å, Fröjdö S, Lahaye Y, *et al.* 2011. 1.8 Ga magmatism in southern Finland: strongly enriched mantle and juvenile crustal sources in a post-collisional setting. *Int. Geol. Rev.* 53: 1622–1683. https://doi.org/10.1080/00206814.2010.496241.

Samson SD, D'Lemos RS. 1998. U-Pb geochronology and Sm-Nd isotopic composition of Proterozoic gneisses,Channel Islands, UK. *J.*

Geol. Soc. Lond. 155: 609–618. https://doi.org/10.1144/gsjgs.155.4.0609.

Samson SD, Inglis JD, D'Lemos RS, Admou H, Blichert-Toft J, Hefferan K. 2004. Geochronological, geochemical, and Nd–Hf isotopic constraints on the origin of Neoproterozoic plagiogranites in the Tasriwine ophiolite, Anti-Atlas orogen, Morocco. *Precambrian Res.* 135: 133–147. https://doi.org/10.1016/j.precamres.2004.08.003.

Sánchez-Rodríguez L, Gebauer D. 2000. Mesozoic formation of pyroxenites and gabbros in the Ronda area (Southern Spain), followed by Early Miocene subduction metamorphism and emplacement into the middle crust: U-Pb sensitive high-resolution ion microprobe dating of zircon. *Tectonophysics* 316: 19–44. https://doi.org/10.1016/s0040-1951(99)00256-5.

Schaeffer AJ, Lebedev S. 2013. Global shear speed structure of the upper mantle and transition zone. *Geophysical Journal International* 194: ggt095-449. https://doi.org/10.1093/gji/ggt095.

Schaltegger U, Brack P. 2007. Crustal-scale magmatic systems during intracontinental strike-slip tectonics: U, Pb and Hf isotopic constraints from Permian magmatic rocks of the Southern Alps. *Int. J. Earth Sci.* 96: 1131–1151. https://doi.org/10.1007/s00531-006-0165-8.

Schmincke H-U. 2007. Mantle plumes: A multidisciplinary approach, pp. 241–322. https://doi.org/10.1007/978-3-540-68046-8_8.

Schuster R, Stüwe K. 2008. Permian metamorphic event in the Alps. *Geology* 36: 603. https://doi.org/10.1130/g24703a.1.

Seber D, Barazangi M, Ibenbrahim A, Demnati A. 1996. Geophysical evidence for lithospheric delamination beneath the Alboran Sea and Rif–Betic mountains. *Nature* 379: 785–790. https://doi.org/10.1038/379785a0.

Seghedi A. 2012. Palaeozoic Formations from Dobrogea and Pre-Dobrogea – An overview. *Turkish Journal of Earth Sciences*. https://doi.org/10.3906/yer-1101-20.

Sehrt M, Glasmacher UA, Stockli DF, Jabour H, Kluth O. 2017. Meso-/Cenozoic long-term landscape evolution at the southern Moroccan passive continental margin, Tarfaya Basin, recorded by low-temperature thermochronology. *Tectonophysics* 717: 499–518. https://doi.org/10.1016/j.tecto.2017.08.028.

Sehrt M, Glasmacher UA, Stockli DF, Jabour H, Kluth O. 2018. The southern Moroccan passive continental margin: An example of differentiated long-term landscape evolution in Gondwana. *Gondwana Res.* 53: 129–144. https://doi.org/10.1016/j.gr.2017.03.013.

Serpelloni E, Faccenna C, Spada G, Dong D, Williams SDP. 2013. Vertical GPS ground motion rates in the Euro-Mediterranean region: New evidence of velocity gradients at different spatial scales along the Nubia-Eurasia plate boundary. *J Geophys Res Solid Earth* 118: 6003–6024. https://doi.org/10.1002/2013jb010102.

Séverine C, Martin B, Romain D, Urs H, Lionel K, Christian S. 2004. Fold interference patterns in the Late Palaeozoic Anti-Atlas Belt of Morocco. *Terra Nova* 16: 27–37. https://doi.org/10.1111/j.1365-3121.2003.00525.x.

Simancas JF, Carbonell R, González-Lodeiro F, Perez-Estaun A, Juhlin C, Ayarza P, *et al.* 2003. Crustal structure of the transpressional Variscan orogen of SW Iberia: SW Iberia deep seismic reflection profile (IBERSEIS). *Tectonics* 22: n/a–n/a. https://doi.org/10.1029/2002tc001479.

Sobczyk A, Sobel ER, Georgieva V. 2020. Meso–Cenozoic cooling and exhumation history of the Orlica-Śnieżnik Dome (Sudetes, NE Bohemian Massif, Central Europe): Insights from apatite fission-track thermochronometry. *Terra Nova* 32: 122–133. https://doi.org/10.1111/ter.12449.

Soder CG, Romer RL. 2018. Post-collisional potassic-ultrapotassic magmatism of the Variscan Orogen: Implications for Mantle Metasomatism during Continental Subduction. *J. Petrol.* 59: 1007–1034. https://doi.org/10.1093/petrology/egy053.

Söderlund U, Möller C, Andersson J, Johansson L, Whitehouse M. 2002. Zircon geochronology in polymetamorphic gneisses in the Sveconorwegian orogen, SW Sweden: ion microprobe evidence for 1.46–1.42 and 0.98–0.96 Ga reworking. *Precambrian Res.* 113: 193–225. https://doi.org/10.1016/s0301-9268(01)00206-6.

Söderlund U, Isachsen CE, Bylund G, Heaman LM, Patchett PJ, Vervoort JD, *et al.* 2005. U–Pb baddeleyite ages and Hf, Nd isotope chemistry constraining repeated mafic magmatism in the Fennoscandian Shield from 1.6 to 0.9 Ga. *Contrib. Miner. Petrol.* 150: 174. https://doi.org/10.1007/s00410-005-0011-1.

Soomro RA, Weidle C, Cristiano L, Lebedev S, Meier T, Group PW. 2015. Phase velocities of Rayleigh and Love waves in central and northern Europe from automated, broad-band, interstation measurements. *Geophys. J. Int.* 204: 517–534. https://doi.org/10.1093/gji/ggv462.

Spakman W. 1990. Tomographic images of the upper mantle below central Europe and the Mediterranean. *Terra Nova* 2: 542–553. https://doi.org/10.1111/j.1365-3121.1990.tb00119.x.

Spakman W, Wortel R. 2004. The TRANSMED Atlas. The Mediterranean Region from crust to mantle, pp. 31–52. https://doi.org/10.1007/978-3-642-18919-7_2.

Spakman W, Chertova MV, van den Berg A, van Hinsbergen DJJ. 2018. Puzzling features of western Mediterranean tectonics explained by slab dragging. *Nat. Geosci.* 11. https://doi.org/10.1038/s41561-018-0066-z.

Steinberger B, Becker TW. 2016. A comparison of lithospheric thickness models. *Tectonophysics* 746: 325–338. https://doi.org/10.1016/j.tecto.2016.08.001.

Suc J-P, Fauquette S. 2012. The use of pollen floras as a tool to estimate palaeoaltitude of mountains: The eastern Pyrenees in the Late Neogene, a case study. *Palaeogeogr. Palaeoclim. Palaeoecol.* 321-322: 41–54. https://doi.org/10.1016/j.palaeo.2012.01.014.

Svenningsen OM. 2001. Onset of seafloor spreading in the Iapetus Ocean at 608 Ma: precise age of the Sarek Dyke Swarm, northern Swedish Caledonides. *Precambrian Res.* 110: 241–254. https://doi.org/10.1016/s0301-9268(01)00189-9.

Tavani S, Bertok C, Granado P, Piana F, Salas R, Vigna B, *et al.* 2018. The Iberia-Eurasia plate boundary east of the Pyrenees. *Earth Science Reviews* 187: 314–337. https://doi.org/10.1016/j.earscirev.2018.10.008.

Tegner C, Andersen TB, Kjøll HJ, Brown EL, Hagen-Peter G, Corfu F, *et al.* 2019a. A Mantle Plume Origin for the Scandinavian Dyke Complex: A "Piercing Point" for 615 Ma Plate Reconstruction of Baltica? *Geochem. Geophys. Geosyst.* 20: 1075–1094. https://doi.org/10.1029/2018gc007941.

Tegner C, Michelis SAT, McDonald I, Brown EL, Youbi N, Callegaro S, *et al.* 2019b. Mantle dynamics of the Central Atlantic Magmatic Province (CAMP): Constraints from Platinum Group, Gold and lithophile elements in flood basalts of Morocco. *J. Petrol.* 60: 1621–1652. https://doi.org/10.1093/petrology/egz041.

Teixell A, Arboleya M-L, Julivert M, Charroud M. 2003. Tectonic shortening and topography in the Central High Atlas (Morocco): Tectonic shortening in Morocco. *Tectonics* 22: n/a–n/a. https://doi.org/10.1029/2002tc001460.

Ternois S, Mouthereau F, Jourdon A. 2021. Decoding low-temperature thermochronology signals in mountain belts: modelling the role of rift thermal imprint into continental collision. *BSGF Earth Sci. Bull.* 192: 38. https://doi.org/10.1051/bsgf/2021028.

Thiry M, Quesnel F, Yans J, Wyns R, Vergari A, Theveniaut H, *et al.* 2006. Continental France and Belgium during the Early

Cretaceous: Paleoweatherings and paleolandforms. *Bulletin de la Société géologique de France* 177: 155–175. https://doi.org/10.2113/gssgfbull.177.3.155.

Thomas RJ, Chevallier LP, Gresse PG, Harmer RE, Eglington BM, Armstrong RA, *et al.* 2002. Precambrian evolution of the Sirwa Window, Anti-Atlas Orogen, Morocco. *Precambrian Res.* 118: 1–57. https://doi.org/10.1016/s0301-9268(02)00075-x.

Thomas RJ, Fekkak A, Ennih N, Errami E, Loughlin SC, Gresse PG, *et al.* 2004. A new lithostratigraphic framework for the Anti-Atlas Orogen, Morocco. *J. Afr. Earth Sci.* 39: 217–226. https://doi.org/10.1016/j.jafrearsci.2004.07.046.

Thomson SN, Zeh A. 2000. Fission-track thermochronology of the Ruhla Crystalline Complex: new constraints on the post-Variscan thermal evolution of the NW Saxo-Bohemian Massif. *Tectonophysics* 324: 17–35. https://doi.org/10.1016/s0040-1951(00)00113-x.

Thurner S, Palomeras I, Levander A, Carbonell R, Lee C-T. 2014. Ongoing lithospheric removal in the western Mediterranean: Evidence from Ps receiver functions and thermobarometry of Neogene basalts (PICASSO project). *Geochemistry, Geophysics, Geosystems* 15: 1113–1127. https://doi.org/10.1002/2013gc005124.

Tilhac R, Ceuleneer G, Griffin WL, O'Reilly SY, Pearson NJ, Benoit M, *et al.* 2016. Primitive arc magmatism and delamination: Petrology and geochemistry of pyroxenites from the Cabo Ortegal Complex, Spain. *J. Petrol.* 57: 1921–1954. https://doi.org/10.1093/petrology/egw064.

Tilhac R, Grégoire M, O'Reilly SY, Griffin WL, Henry H, Ceuleneer G. 2017. Sources and timing of pyroxenite formation in the sub-arc mantle: Case study of the Cabo Ortegal Complex, Spain. *Earth Planet. Sci. Lett.* 474: 490–502. https://doi.org/10.1016/j.epsl.2017.07.017.

Timar-Geng Z, Fügenschuh B, Wetzel A, Dresmann H. 2005. Low-temperature thermochronology of the flanks of the southern Upper Rhine Graben. *Int. J. Earth Sci.* 95: 685–702. https://doi.org/10.1007/s00531-005-0059-1.

Timmerman MJ. 2004. Timing, geodynamic setting and character of Permo-Carboniferous magmatism in the foreland of the Variscan Orogen, NW Europe. *Geol. Soc. Lond. Special Publ.* 223: 41–74. https://doi.org/10.1144/gsl.sp.2004.223.01.03.

Torsvik TH, Rehnström EF. 2003. The Tornquist Sea and Baltica-Avalonia docking. *Tectonophysics* 362: 67–82. https://doi.org/10.1016/s0040-1951(02)00631-5.

Torsvik TH, Smethurst MA, Meert JG, Voo RV der, McKerrow WS, Brasier MD, *et al.* 1996. Continental break-up and collision in the Neoproterozoic and Palaeozoic – A tale of Baltica and Laurentia. *Earth Science Reviews* 40: 229–258. https://doi.org/http://dx.doi.org/10.1016/0012-8252(96)00008-6.

Torsvik TH, Tucker RD, Ashwal LD, Carter LM, Jamtveit B, Vidyadharan KT, *et al.* 2000. Late Cretaceous India-Madagascar fit and timing of break-up related magmatism. *Terra Nova* 12: 220–224. https://doi.org/10.1046/j.1365-3121.2000.00300.x.

Torsvik TH, Smethurst MA, Burke K, Steinberger B. 2006. Large igneous provinces generated from the margins of the large low-velocity provinces in the deep mantle. *Geophys. J. Int.* 167: 1447–1460. https://doi.org/10.1111/j.1365-246x.2006.03158.x.

Torsvik TH, Voo RV der, Doubrovine PV, Burke K, Steinberger B, Ashwal LD, *et al.* 2014. Deep mantle structure as a reference frame for movements in and on the Earth. *Proceedings of the National Academy of Sciences of the United States of America* 111: 8735–8740. https://doi.org/10.1073/pnas.1318135111.

Triantafyllou A, Berger J, Baele J-M, Bruguier O, Diot H, Ennih N, *et al.* 2018. Intra-oceanic arc growth driven by magmatic and tectonic processes recorded in the Neoproterozoic Bougmane arc complex (Anti-Atlas, Morocco). *Precambrian Res.* 304: 39–63. https://doi.org/10.1016/j.precamres.2017.10.022.

Triantafyllou A, Berger J, Baele J-M, Mattielli N, Ducea MN, Sterckx S, *et al.* 2020. Episodic magmatism during the growth of a Neoproterozoic oceanic arc (Anti-Atlas, Morocco). *Precambrian Res.* 339: 105610. https://doi.org/10.1016/j.precamres.2020.105610.

Turland M, Marteau P, Jouval J, Monciardini C. 1994. Discovery of an Early Oligocene marine interval in the Palaeogene lacustrine to fluviatile series of the Le Puy-en-Velay Basin. *Géologie de la France* 4: 63–66.

Ulrych J, Dostal J, Hegner E, Balogh K, Ackerman L. 2008. Late Cretaceous to Paleocene melilitic rocks of the Ohře/Eger Rift in northern Bohemia, Czech Republic: Insights into the initial stages of continental rifting. *Lithos* 101: 141–161. https://doi.org/10.1016/j.lithos.2007.07.012.

Ulrych J, Dostal J, Adamovič J, Jelínek E, Špaček P, Hegner E, *et al.* 2011. Recurrent Cenozoic volcanic activity in the Bohemian Massif (Czech Republic). *Lithos* 123: 133–144. https://doi.org/10.1016/j.lithos.2010.12.008.

Vacherat A, Mouthereau F, Pik R, Bernet M, Gautheron C, Masini E, *et al.* 2014. Thermal imprint of rift-related processes in orogens as recorded in the Pyrenees. *Earth Planet Sc Lett* 408: 296–306. https://doi.org/10.1016/j.epsl.2014.10.014.

Vacherat A, Mouthereau F, Pik R, Bellahsen N, Gautheron C, Bernet M, *et al.* 2016. Rift-to-collision transition recorded by tectono-thermal evolution of the northern Pyrenees: cooling history of the northern Pyrenees. *Tectonics* 35: 907–933. https://doi.org/10.1002/2015tc004016.

Vacherat A, Mouthereau F, Pik R, Huyghe D, Paquette J-L, Christophoul F, *et al.* 2017. Rift-to-collision sediment routing in the Pyrenees: A synthesis from sedimentological, geochronological and kinematic constraints. *Earth-sci Rev* 172: 43–74. https://doi.org/10.1016/j.earscirev.2017.07.004.

Vanderhaeghe O, Laurent O, Gardien V, Moyen JF, Gébelin A, Chelle-Michou C, *et al.* 2020. Flow of partially molten crust controlling construction, growth and collapse of the Variscan orogenic belt: the geologic record of the French Massif Central. *BSGF – Earth Sci Bulletin* 191: 25. https://doi.org/10.1051/bsgf/2020013.

van Hinsbergen DJJ, Steinberger B, Doubrovine PV, Gassmöller R. 2011. Acceleration and deceleration of India-Asia convergence since the Cretaceous: Roles of mantle plumes and continental collision. *J Geophys Res Solid Earth 1978–2012* 116: B06101. https://doi.org/10.1029/2010jb008051.

van Hinsbergen DJJ, Lippert PC, Li S, Huang W, Advokaat EL, Spakman W. 2019a. Reconstructing Greater India: Paleogeographic, kinematic, and geodynamic perspectives. *Tectonophysics* 760: 69–94. https://doi.org/10.1016/j.tecto.2018.04.006.

van Hinsbergen DJJ, Torsvik TH, Schmid SM, Maţenco LC, Maffione M, Vissers RLM, *et al.* 2019b. Orogenic architecture of the Mediterranean region and kinematic reconstruction of its tectonic evolution since the Triassic. *Gondwana Res* 81: 79–229. https://doi.org/10.1016/j.gr.2019.07.009.

Varas-Reus MI, Garrido CJ, Marchesi C, Bodinier J-L, Frets E, Bosch D, *et al.* 2017. Refertilization Processes in the Subcontinental Lithospheric Mantle: the Record of the Beni Bousera Orogenic Peridotite (Rif Belt, Northern Morocco). *J. Petrol.* 57: 2251–2270. https://doi.org/10.1093/petrology/egx003.

Vavra G, Schmid R, Gebauer D. 1999. Internal morphology, habit and U-Th-Pb microanalysis of amphibolite-to-granulite facies zircons: geochronology of the Ivrea Zone (Southern Alps). *Contrib. Miner. Petrol.* 134: 380–404. https://doi.org/10.1007/s004100050492.

Vázquez M, Jabaloy A, Barbero L, Stuart FM. 2011. Deciphering tectonic- and erosion-driven exhumation of the Nevado-Filábride

Complex (Betic Cordillera, Southern Spain) by low temperature thermochronology: Deciphering tectonic- and erosion-driven exhumation. *Terra Nova* 23: 257–263. https://doi.org/10.1111/j.1365-3121.2011.01007.x.

Ventura B, Lisker F, Kopp J. 2009. Thermal and denudation history of the Lusatian Block (NE Bohemian Massif, Germany) as indicated by apatite fission-track data. *Geol. Soc. Lond. Special Publ.* 324: 181–192. https://doi.org/10.1144/sp324.14.

Villaseca C, Belousova EA, Barfod DN, González-Jiménez JM. 2018. Dating metasomatic events in the lithospheric mantle beneath the Calatrava volcanic field (central Spain). *Lithosphere US* 11: 192–208. https://doi.org/10.1130/l1030.1.

Villasenor A, Chevrot S, Harnafi M, Gallart J, Pazos A, Serrano I, *et al.* 2015. Subduction and volcanism in the Iberia–North Africa collision zone from tomographic images of the upper mantle. *Tectonophysics*. https://doi.org/10.1016/j.tecto.2015.08.042.

Voigt T, Wiese F, Eynatten H von, Franzke H-J, Gaupp R. 2006. Facies evolution of syntectonic Upper Cretaceous deposits in the Subhercynian Cretaceous Basin and adjoining areas (Germany) [Faziesentwicklung syntektonischer Sedimente der Oberkreide im Subherzynen Kreidebecken und benachbarten Gebieten]. *Zeitschrift Der Deutschen Gesellschaft Für Geowissenschaften* 157: 203–243. https://doi.org/10.1127/1860-1804/2006/0157-0203.

Voshage H, Hofmann AW, Mazzucchelli M, Rivalenti G, Sinigoi S, Raczek I, *et al.* 1990. Isotopic evidence from the Ivrea Zone for a hybrid lower crust formed by magmatic underplating. *Nature* 347: 731–736. https://doi.org/10.1038/347731a0.

Wal DV der, Vissers RLM. 1993. Uplift and emplacement of upper mantle rocks in the western Mediterranean. *Geology* 21: 1119–1122. https://doi.org/10.1130/0091-7613(1993)021<1119:uaeoum>2.3.co;2.

Waldner M, Bellahsen N, Mouthereau F, Bernet M, Pik R, Rosenberg CL, *et al.* 2021. Central Pyrenees Mountain Building: Constraints from new LT thermochronological data from the Axial Zone. *Tectonics* 40. https://doi.org/10.1029/2020tc006614.

Wang X, Holt WE, Ghosh A. 2015. Joint modeling of lithosphere and mantle dynamics: Evaluation of constraints from global tomography models. *J Geophys Res Solid Earth* 120: 8633–655. https://doi.org/10.1002/2015jb012188.

Wang Y, Chevrot S, Monteiller V, Komatitsch D, Mouthereau F, Manatschal G, *et al.* 2016. The deep roots of the western Pyrenees revealed by full waveform inversion of teleseismic P waves. *Geology* 44: 475–478. https://doi.org/10.1130/g37812.1.

Wang X, Holt WE, Ghosh A. 2019. Joint modeling of lithosphere and mantle dynamics: Sensitivity to viscosities within the lithosphere, asthenosphere, transition zone, and D layers. *Phys. Earth Planet. Int.* 293: 106263. https://doi.org/10.1016/j.pepi.2019.05.006.

Weijermars R, Roep TB, Eeckhout B van den, Postma G, Kleverlaan K. 2007. Uplift history of a Betic fold nappe inferred from Neogene-Quaternary sedimentation and tectonics (in the Sierra Alhamilla and Almeria, Sorbas and Tabernas Basins of the Betic Cordilleras, SE Spain). *Netherlands Journal of Geosciences / Geologie en Mijnbouw. Igitur.*

Whitchurch AL, Carter A, Sinclair HD, Duller RA, Whittaker AC, Allen PA. 2011. Sediment routing system evolution within a diachronously uplifting orogen: insights from detrital zircon thermochronological analyses from the south-central pyrenees. *American Journal of Science* 311: 442–482. https://doi.org/10.2475/05.2011.03.

Wilson JT. 1966. Did Atlantic close and then re-open. *Nature* 211: 676. https://doi.org/10.1038/211676a0.

Wilson M. 1997. Thermal evolution of the Central Atlantic passive margins: Continental break-up above a Mesozoic super-plume. *Journal of the Geological Society* 154: 491–495.

Wilson M, Downes H. 1992. Mafic alkaline magmatism associated with the European Cenozoic rift system. *Tectonophysics* 208: 173–182. https://doi.org/10.1016/0040-1951(92)90343-5.

Wilson M, Neumann E-R, Davies GR, Timmerman MJ, Heeremans M, Larsen BT. 2004. Permo-Carboniferous magmatism and rifting in Europe: Introduction. *Geol. Soc. Lond. Special Publ.* 223: 1–10. https://doi.org/10.1144/gsl.sp.2004.223.01.01.

Wittig N, Baker JA, Downes H. 2006. Dating the mantle roots of young continental crust. *Geology* 34: 237–240. https://doi.org/10.1130/g22135.1.

Wittig N, Pearson DG, Baker JA, Duggen S, Hoernle K. 2010a. A major element, PGE and Re–Os isotope study of Middle Atlas (Morocco) peridotite xenoliths: Evidence for coupled introduction of metasomatic sulphides and clinopyroxene. *Lithos* 115: 15–26. https://doi.org/10.1016/j.lithos.2009.11.003.

Wittig N, Pearson DG, Duggen S, Baker JA, Hoernle K. 2010b. Tracing the metasomatic and magmatic evolution of continental mantle roots with Sr, Nd, Hf and and Pb isotopes: A case study of Middle Atlas (Morocco) peridotite xenoliths. *Geochim. Cosmochim. Acta* 74: 1417–1435. https://doi.org/10.1016/j.gca.2009.10.048.

Youbi N, Kouyaté D, Söderlund U, Ernst RE, Soulaimani A, Hafid A, *et al.* 2013. The 1750 Ma Magmatic Event of the West African Craton (Anti-Atlas, Morocco). *Precambrian Res.* 236: 106–123. https://doi.org/10.1016/j.precamres.2013.07.003.

Zelaźniewicz A, Oberc-Dziedzic T, Fanning CM, Protas A, Muszyński A. 2016. Late Carboniferous–Early Permian events in the Trans-European Suture Zone: Tectonic and acid magmatic evidence from Poland. *Tectonophysics* 675: 227–243. https://doi.org/10.1016/j.tecto.2016.02.040.

Ziegler PA, Cloetingh S, Wees J-D van. 1995. Dynamics of intra-plate compressional deformation: the Alpine foreland and other examples. *Tectonophysics* 252: 7–59. https://doi.org/10.1016/0040-1951(95)00102-6.

Ziegler PA, Wees J-D van, Cloetingh S. 1998. Mechanical controls on collision-related compressional intraplate deformation. *Tectonophysics* 300: 103–129. https://doi.org/10.1016/s0040-1951(98)00236-4.

Zulauf G, Dörr W, Fisher-Spurlock SC, Gerdes A, Chatzaras V, Xypolias P. 2015. Closure of the Paleotethys in the External Hellenides: Constraints from U-Pb ages of magmatic and detrital zircons (Crete). *Gondwana Research* 28: 642–667. https://doi.org/10.1016/j.gr.2014.06.011.

Cite this article as: Mouthereau F, Angrand P, Jourdon A, Ternois S, Fillon C, Calassou S, Chevrot S, Ford M, Jolivet L, Manatschal G, Masini E, Thinon I, Vidal O, Baudin T. 2021. Cenozoic mountain building and topographic evolution in Western Europe: impact of billions of years of lithosphere evolution and plate kinematics, *BSGF - Earth Sciences Bulletin* 192: 56.